原子分子基准动力学参数及其在大气物理、天体物理中的应用

朱林繁

中国科学技术大学近代物理系

合肥微尺度物质科学国家研究中心

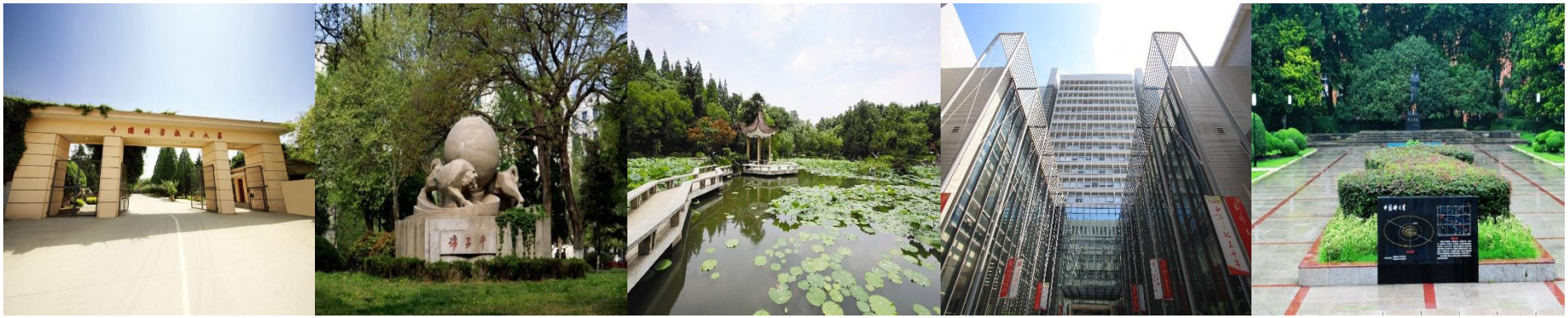

主要内容

- 背景
- 实验方法
- 现状
- 展望

主要内容

- 背景
- 实验方法
- 现状
- 展望

HD 124314

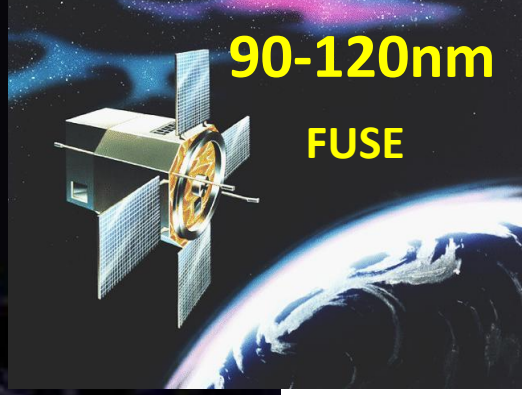

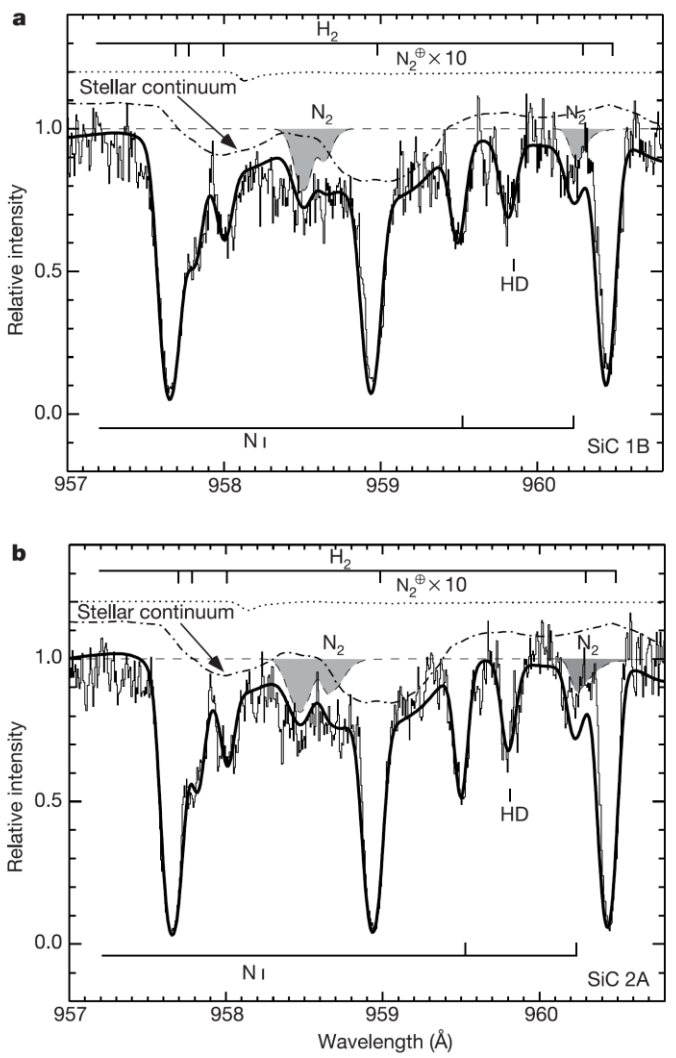

The normalized FUSE spectra of HD 124314

D. C. Knauth et al., Nature 429, 636(2004)

HD 124314

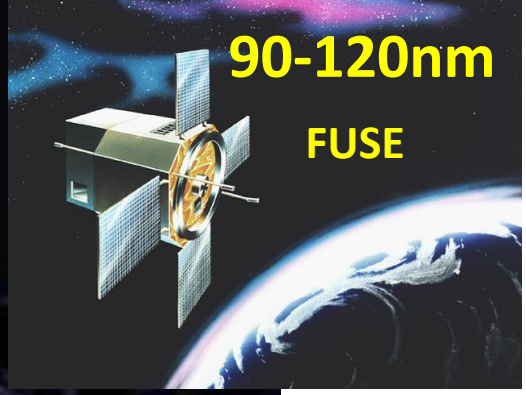

原子分子精确的能级结构、光吸收截面/光学振子强度数据是极端重要的！

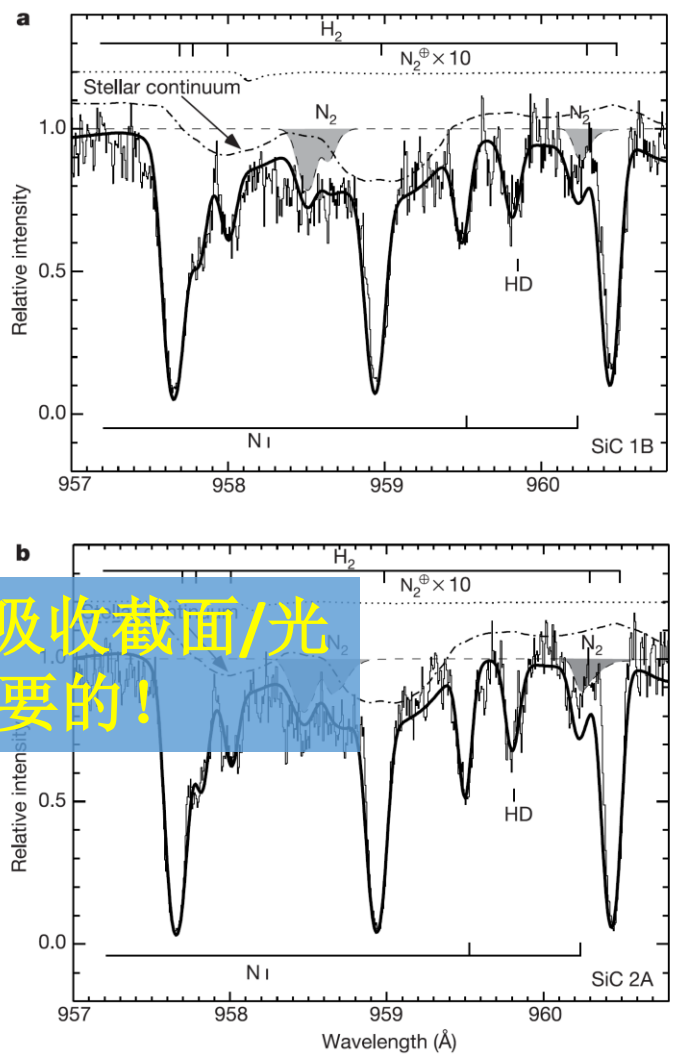

$N(N_2)=(4.6\pm0.8)\times10^{13}cm^{-2}$

The normalized FUSE spectra of HD 124314

- for dense cloud model, two orders of magnitude lower than expected
- for diffuse cloud model, two orders of magnitude larger than expected

D. C. Knauth et al., Nature 429, 636(2004)

TABLE I. Identified interstellar and circumstellar molecules. [Most molecules have been detected at radio and millimeter wavelengths, unless otherwise indicated (IR, VIS, or UV). Species labeled with a question mark await confirmation.]

Simple hydrides, oxides, sulfides, halogens				
H_2 (IR, UV)	CO	NH_3	CS	HCl
O_2	H_2O_2	PO	CO_2 (IR)	NaCl[a]
H_2O	SO_2	OCS	H_2S	KCl[a]
PN	SiO	SiH_4[a] (IR)	SiS	AlCl[a]
N_2O	CH_4 (IR)	HSCN	HF	AlF[a]
HONC	HNCO	AlOH		
Nitriles and acetylene derivatives				
C_2 (IR)	HCN	CH_3CN	HNC	C_2H_4[a] (IR)
C_3 (IR,UV)	HC_3N	CH_3C_3N	HNCO	C_2H_2 (IR)
C_5[a] (IR)	HC_5N	CH_3C_5N	HNCS	C_6H_2 (IR)
C_3O	HC_7N	CH_3C_2H	HNCCC	C_3H_6
C_3S	HC_9N	CH_3C_4H	CH_3NC	C_3H_7CN
C_4Si[a]	$HC_{11}N$	CH_3C_6H	HCCNC	
H_2C_4	HC_2CHO	CH_2CHCN	CH_2CCHCN	
Aldehydes, alcohols, ethers, ketones, amides				
H_2CO	CH_3OH	HCOOH	HCOCN	CH_3CH_2CN
CH_3CHO	CH_3CH_2OH	$HCOOCH_3$	CH_3NH_2	NH_2CH_2CN
CH_3CH_2CHO	CH_2CCHOH	CH_3COOH	CH_3CONH_2	NH_2CN
NH_2CHO	$(CH_2OH)_2$	$(CH_3)_2O$	H_2CCO	CH_2CHCN
CH_2OHCHO	$(CH_3)_2CO$	H_2CS		
C_2H_5OCHO		CH_3SH		
Cyclic molecules				
C_3H_2	SiC_2	*c*-C_3H	CH_2OCH_2	C_6H_6 (IR) ?
c-SiC_3	H_2C_3O	C_2H_4O		
Molecular cations				
CH^+	CO^+	$HCNH^+$	OH^+	HN_2^+
CH_3^+	HCO^+	HC_3NH^+	H_2O^+	H_3^+ (IR)
HS^+	HOC^+	H_2COH^+	H_3O^+	SO^+
HCS^+	$HOCO^+$	CF^+	HCl^+	H_2Cl^+
Molecular antions				
C_4H^-	C_6H^-	C_8H^-		
CN^-	C_3N^-	C_5N^-		
Radicals				
OH	C_2H	CN	C_2O	C_2S
CH	C_3H	C_3N	NO	NS
CH_2	C_4H	HCCN[a]	SO	SiC[a]
NH (UV)	C_5H	CH_2CN	HCO	SiN[a]
NH_2	C_6H	CH_2N	C_5N[a]	CP[a]
SH	C_7H	NaCN	KCN	MgCN
C_3H_2	C_8H	MgNC	FeCN	
C_4H_2	HNO	H_2CN	HNC_3	HO_2
C_6H_2	AlNC	SiNC	C_4Si	SiCN
HCP	CCP	AlO		
Fullerenes				
C_{60} (IR)	C_{70}[a] (IR)	C_{60}^+ (VIS) ?		

[a]These species have been detected only in the circumstellar envelope of carbon-rich stars.

TABLE II. The composition of diffuse clouds and molecular clouds. The entries in parentheses should be read as $a\ (-b) = a \times 10^{-b}$.

Species	Diffuse clouds[a]	Molecular cloud[b]
H	1.2	
H_2	1	1
HD	5 (−7)	
H_3^+	5 (−8)[e]	
O	1.6 (−4)	
OH	1.0 (−7)	3.0 (−7)
H_2O		5 (−9)[i]
OH^+	1 (−8)[f]	
H_2O^+	2 (−9)[f]	
H_3O^+	1.5 (−9)[f]	
O_2		5 (−8)[h]
C^+	2.6 (−4)	
C	7.0 (−6)	
C_2	3.3 (−8)	
C_3	3.5 (−9)	
CH	5 (−8)	
CH^+	6.3 (−8)	
C_2H	3 (−8)	5 (−8)
C_3H_2	1 (−9)	
CO	5 (−6)	5 (−5)
HCO^+	5 (−10)	8 (−9)
N	2.5 (−5)	
N_2	3 (−7)[c]	3 (−5)[d]
NH	2 (−9)	3 (−10)[g]
NH_2	2.0 (−9)	6 (−11)[g]
NH_3	2.0 (−9)	2 (−8)[g]
N_2H^+		5 (−10)
CN	5 (−8)	3 (−10)
HCN	3 (−9)	2 (−8)
HNC	6 (−10)	2 (−8)
HC_5N	<2 (−11)	1 (−10)
CS	3 (−9)	
SO	2 (−9)	
H_2CO	4.0 (−9)	2 (−8)
CH_3OH	<7 (−11)	2 (−9)
HCl	2 (−10)	

A. G. G. M. Tielens, Rev. Mod. Phys. 85,1021 (2013)

美丽的极光

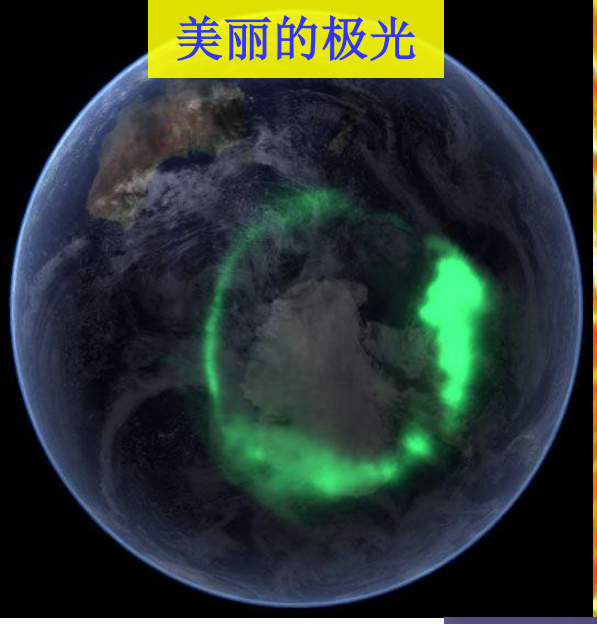

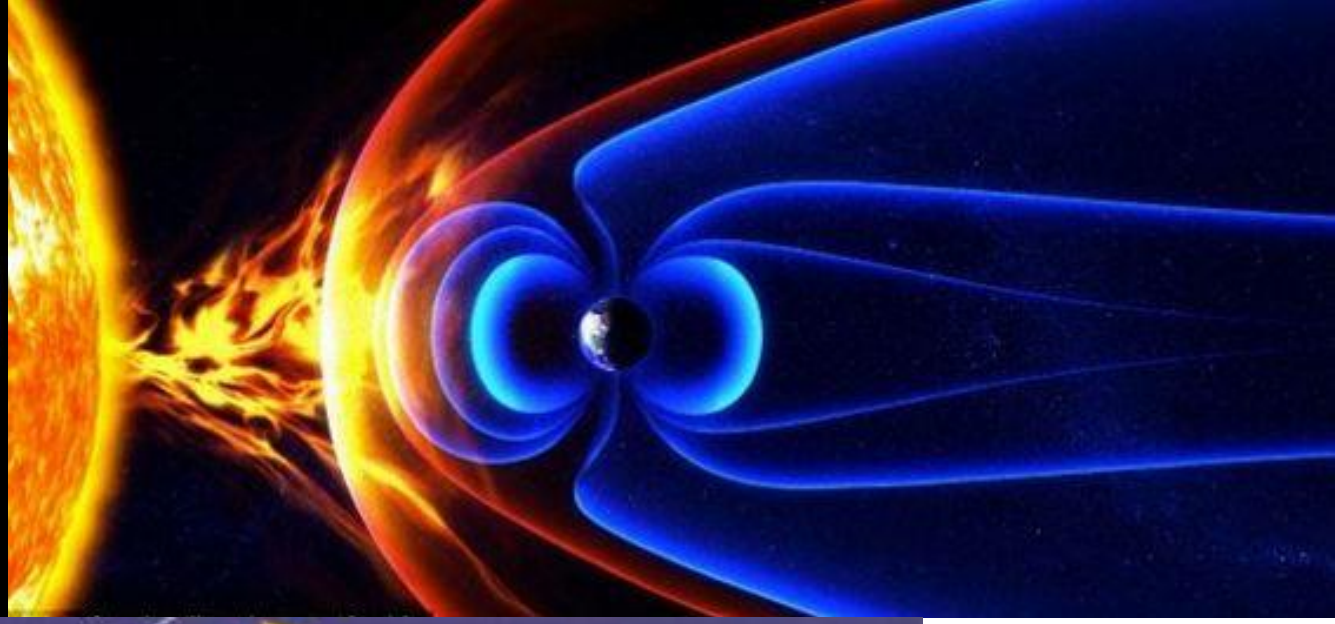

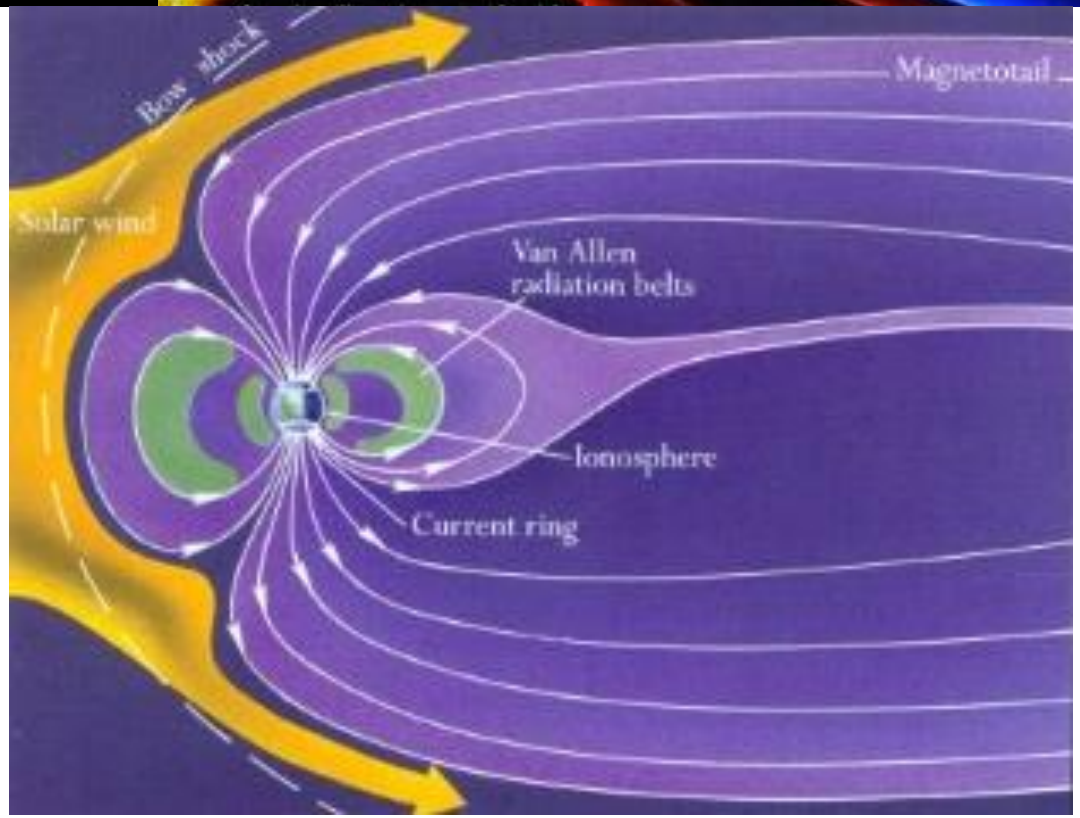
Bow shock
Magnetotail
Solar wind
Van Allen
radiation belts
Ionosphere
Current ring

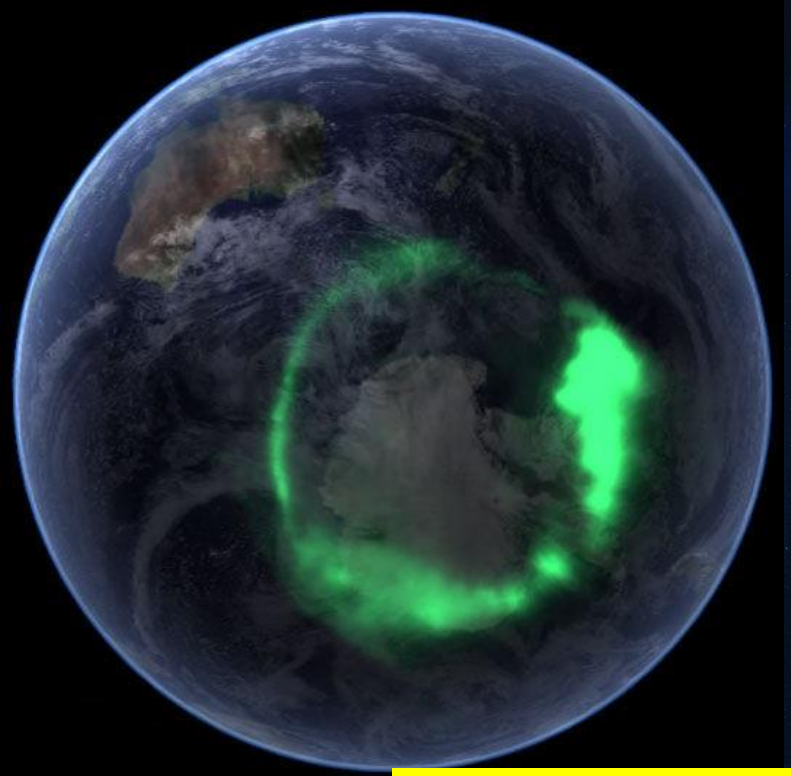

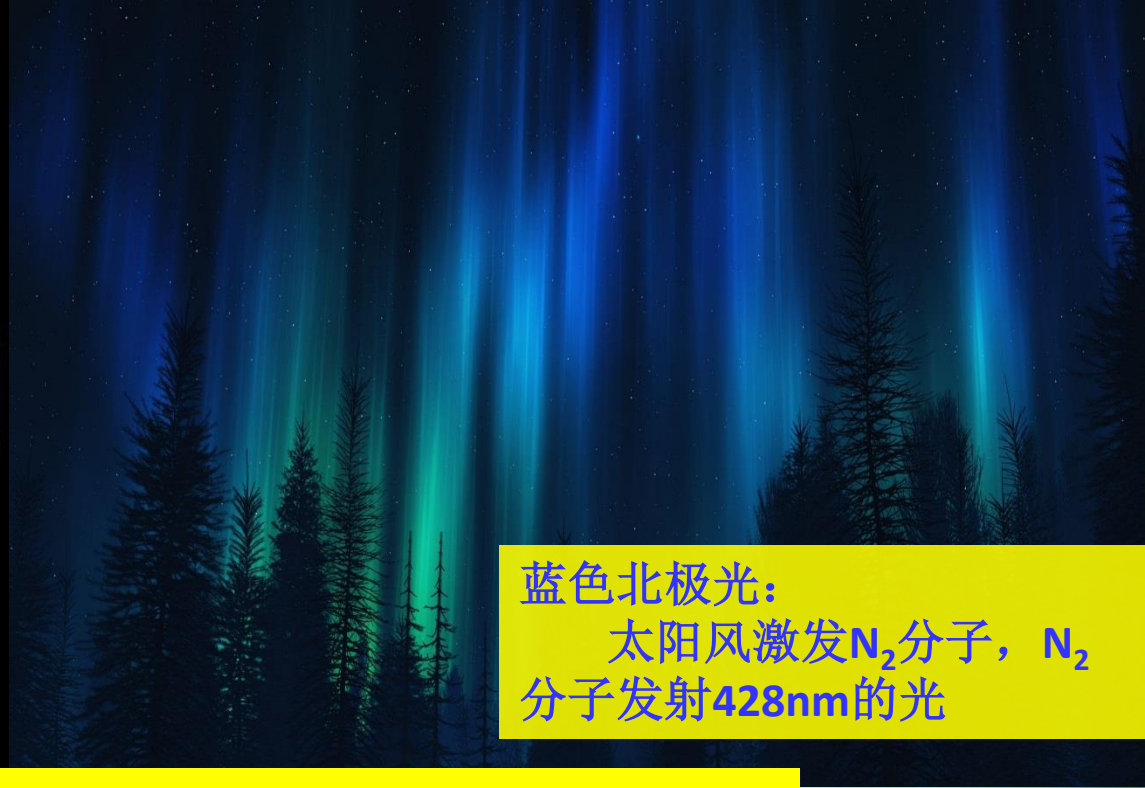

蓝色北极光：
太阳风激发N_2分子，N_2分子发射428nm的光

原子分子与电子、离子碰撞截面必不可少！

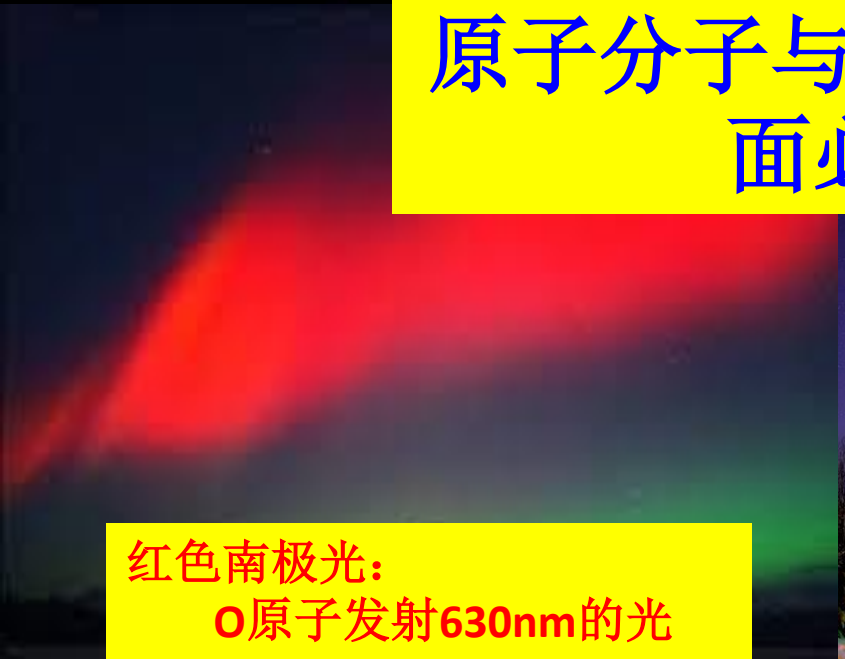

红色南极光：
O原子发射630nm的光

绿色北极光：
太阳风激发N_2分子，N_2分子传能给O原子，O原子发射557.7nm的光

金星[D]/[H]比值是地球和其他行星的100倍

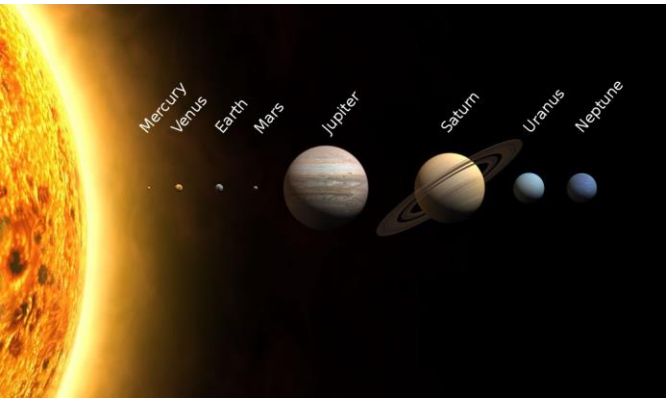

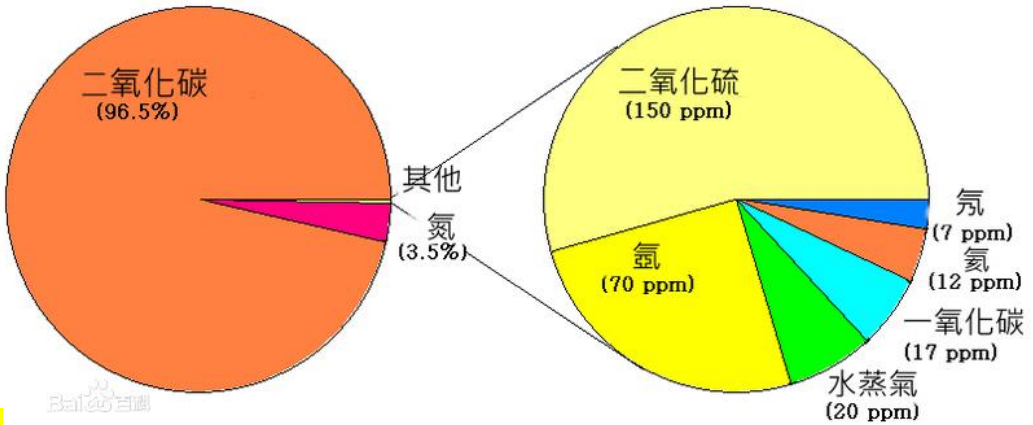

表面压力：92atm
温　　度：740K（467°C）

1966.6-1966.7

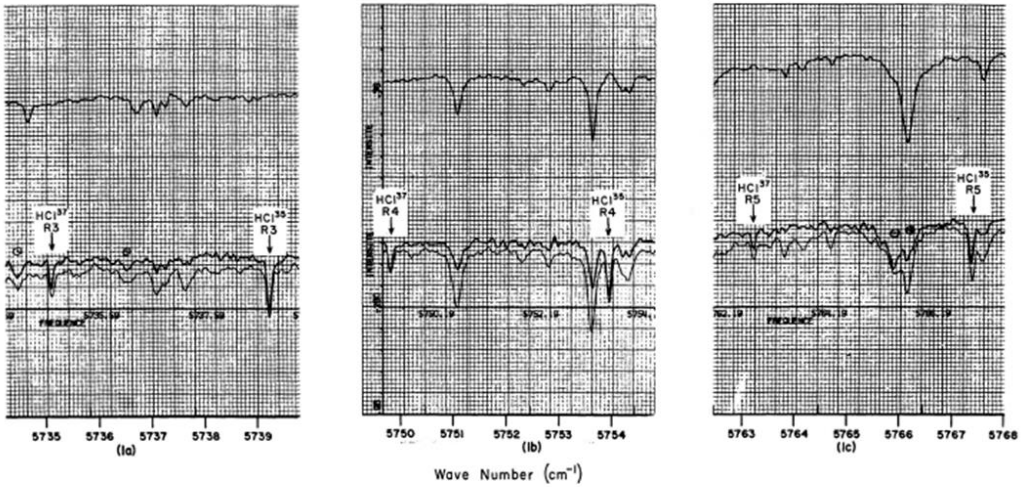

FIG. 1.—Interferometer spectra, 5733–5768 cm^{-1}. *Upper trace:* Sun, average of 2 spectra, July 2 and 4, 1966, mean sec $Z = 1.25$. *Middle trace:* Venus I, average of 4 spectra, June 6 to July 7, mean sec $Z = 1.14$. *Lower trace:* Venus II, average of 5 spectra, June 6 to July 7, mean sec $Z = 1.66$. In this last case the variation in sec Z during recording is quite large and the mean sec Z given merely as an order of magnitude indication. The wavenumber scale is in vacuum cm^{-1}. The slight shift between the positions of the HCl lines on the two traces is due to differences in Doppler effect. Also note the Doppler shifting of Fraunhofer lines (marked ⊙) on segment (*a*) and the greater breadth of telluric H_2O lines (marked ⊕) compared with HCl on segment (*b*).

Haute-Provence Observatory
（上普罗旺斯天文台）

CONNES. P, CONNES. J, BENEDICT. WS, ASTROPHYS J, 147:1230-1237 (1967)

U. von Zahn, V.I. Moroz, Composition of the Venus atmosphere below 100 km altitude. Adv. Space Res. **5**,173–195 (1985).

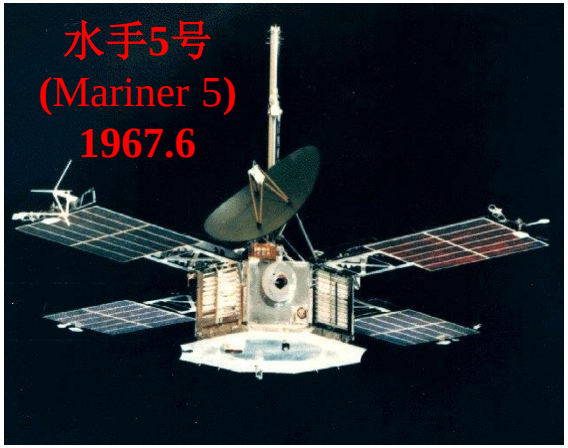

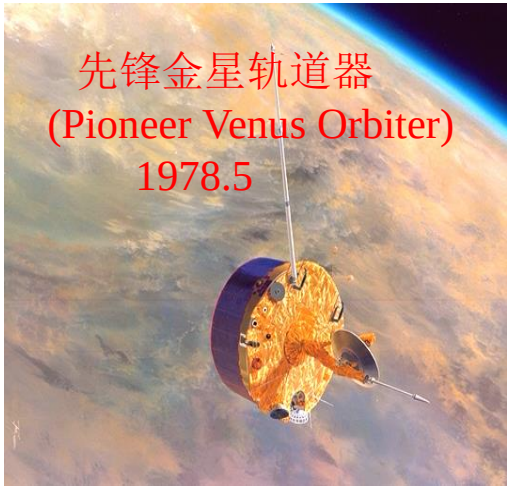

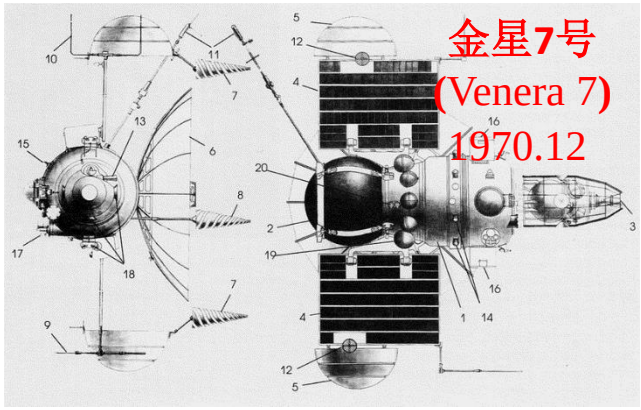

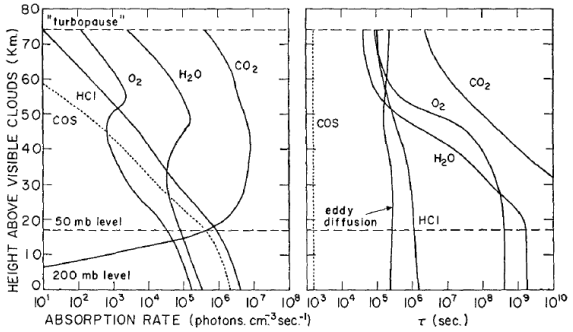

FIG. 1. Rates of absorption by CO_2, H_2O, O_2, HCl and COS (see Section 4) at various heights above the visible cloud deck on Venus (defined as the 200-mb level). Also given are the photodissociation lifetimes for these various molecules, which can be compared to the eddy diffusion time constant, obtained by assuming the eddy diffusion coefficient is 10^6 cm^2 sec^{-1}. The "turbopause" refers to the level where the CO_2 number density is 10^{12} cm^{-3}.

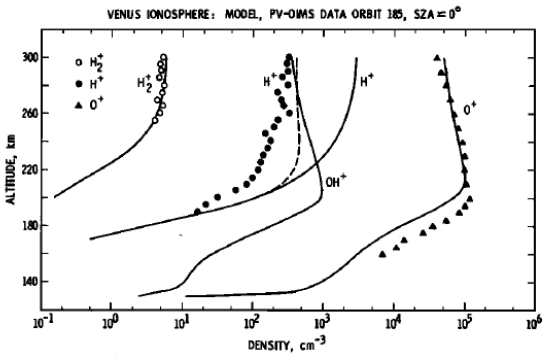

Fig. 2. O^+, H^+, H_2^+, and OH^+ ion distributions in the topside ionosphere of Venus. Model calculations are compared to the Pioneer Venus Ion Mass Spectrometer data of Taylor et al. [1980] with the exception of OH^+ for which no data are available. The dashed curve for H^+ is for ion escape velocity of 600 m/s.

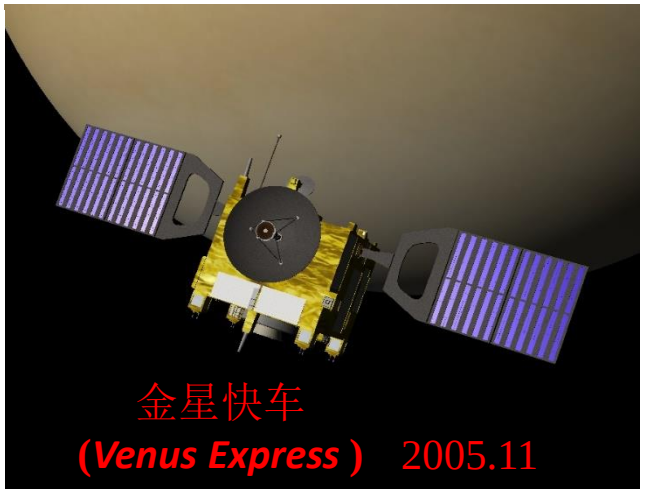

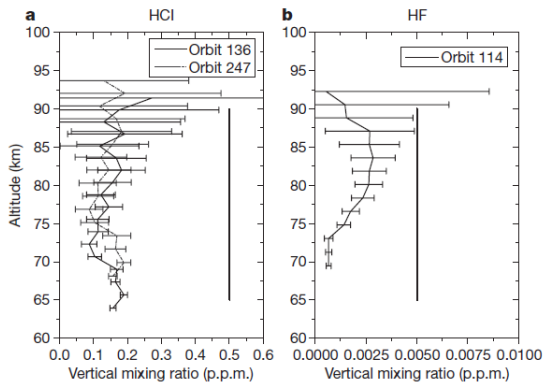

S. Kumar, D. M. Hunten, Geophys. Res. Lett. 8, 237 (1981)

J. L. Bertaux, A. C. Vandaele, Oleg Korablev, Nature, 05974(2007)

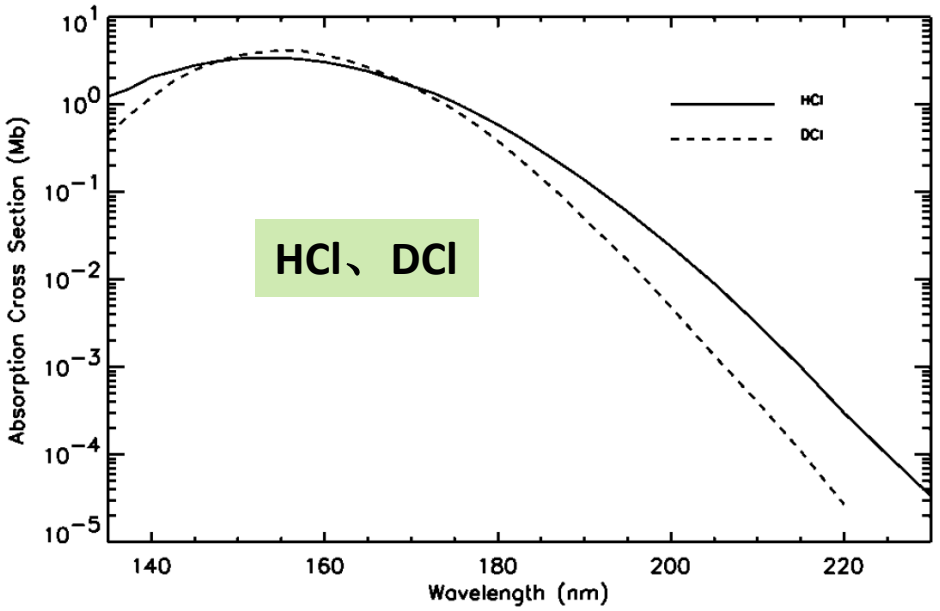
HCl、DCl
Absorption Cross Section (Mb)
Wavelength (nm)
HCl
DCl

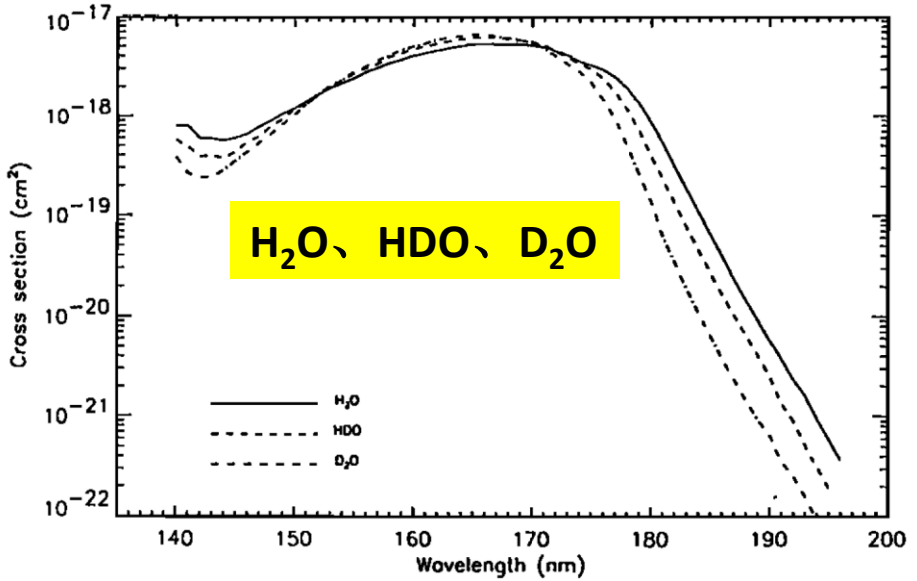
H_2O、HDO、D_2O
Cross section (cm^2)
Wavelength (nm)
H_2O
HDO
D_2O

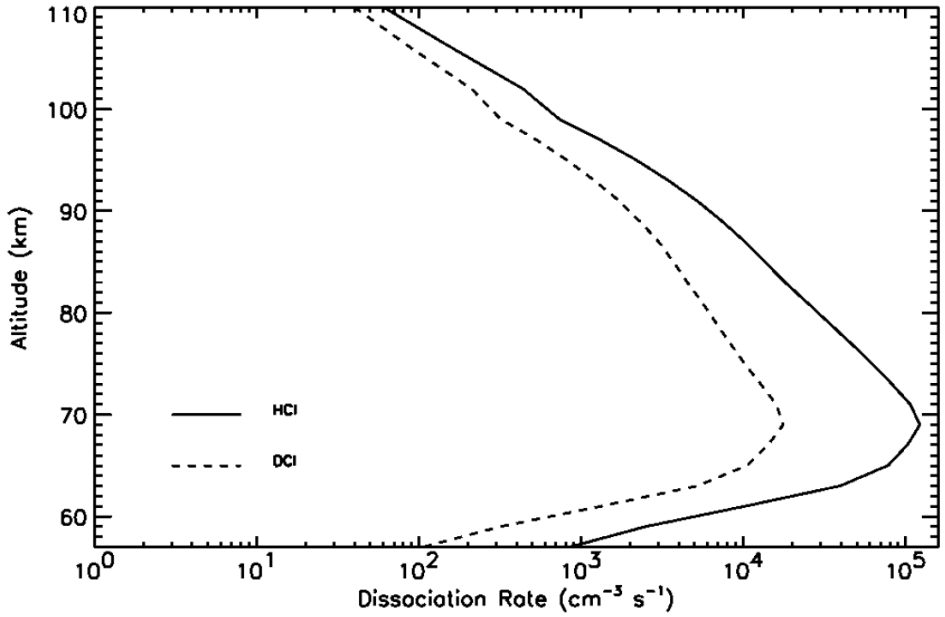
Altitude (km)
Dissociation Rate (cm^{-3} s^{-1})
HCl
DCl

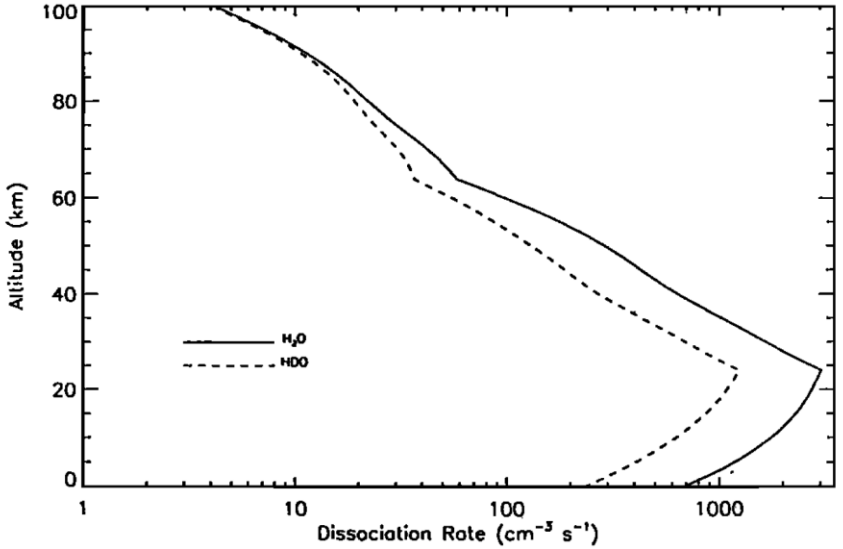
Altitude (km)
Dissociation Rate (cm^{-3} s^{-1})
H_2O
HDO

原子分子精确的能级结构及动力学参数是众多学科的基础和支撑！

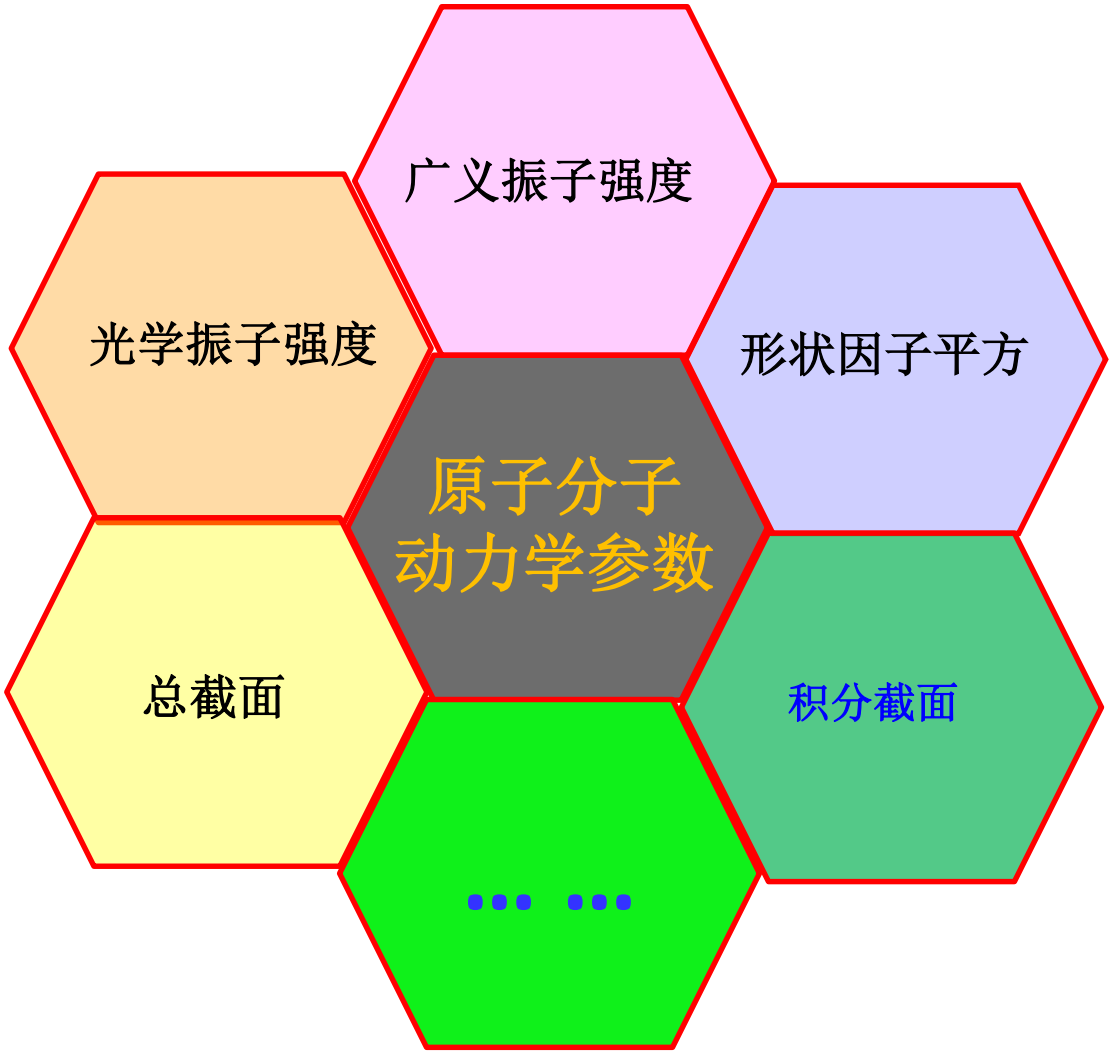
广义振子强度
光学振子强度
形状因子平方
原子分子
动力学参数
总截面
积分截面
… …

主要内容

- 背景
- 实验方法
- 现状
- 展望

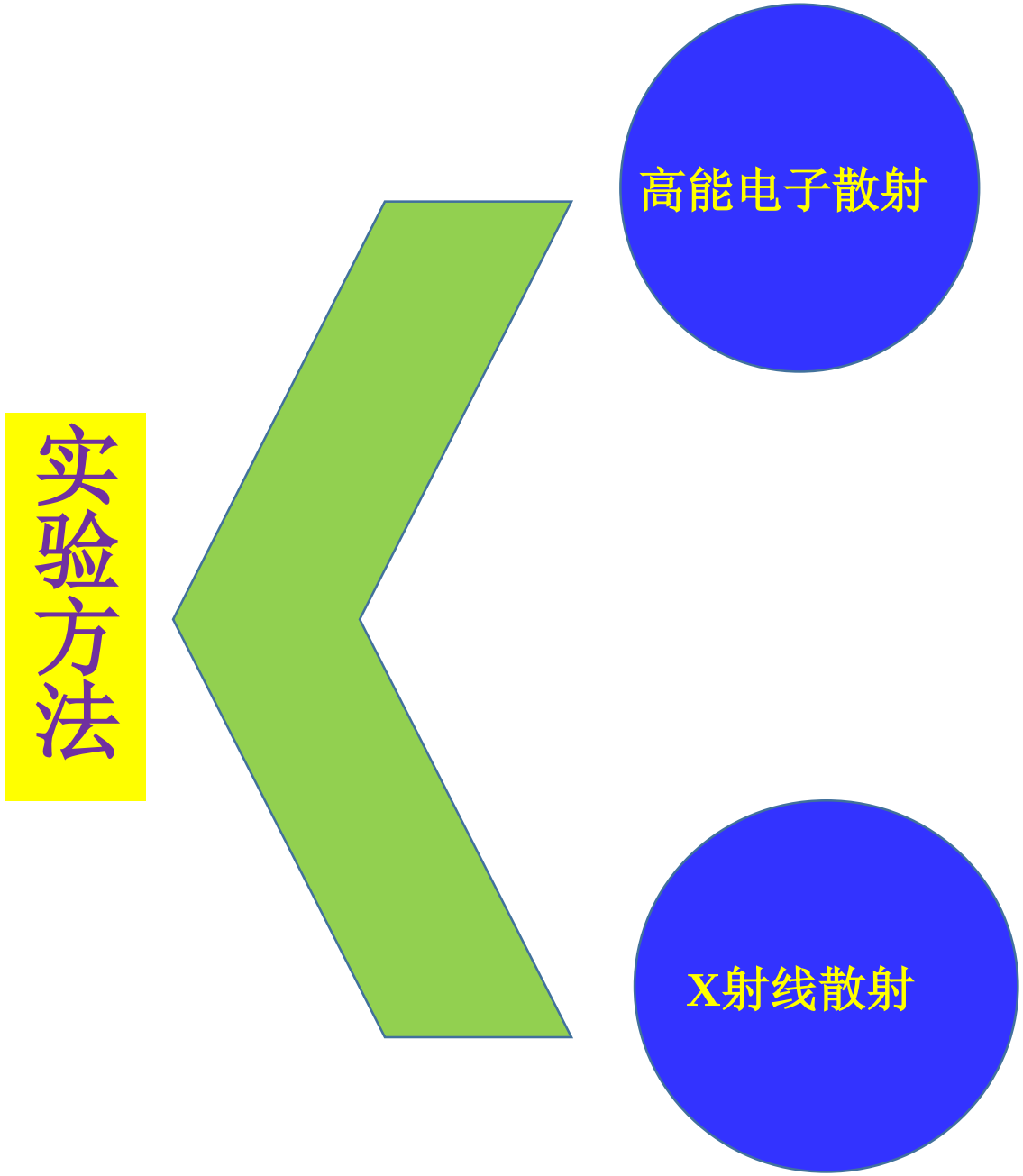
实验方法
高能电子散射
X射线散射

I. 高能电子散射

$$E_n = E_0 - E_a$$

$$K^2 = p_0^2 + p_a^2 - 2p_0 p_a \cos\theta$$

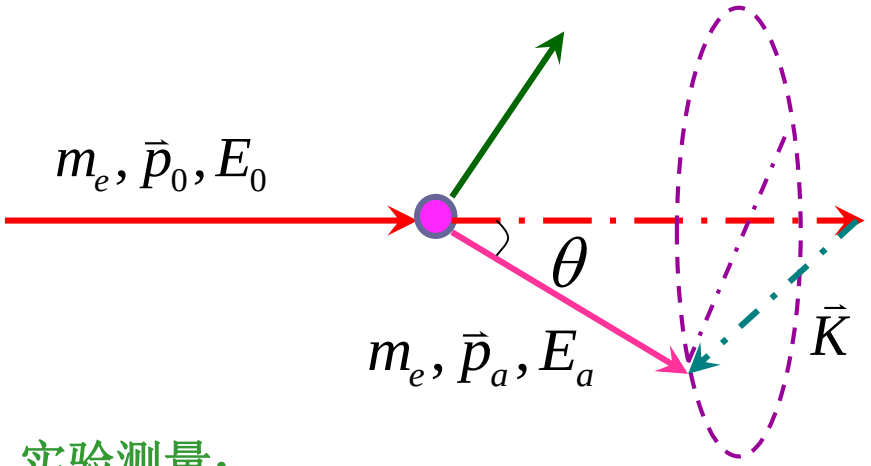

$$\frac{d\sigma_n^e(\theta)}{d\Omega} = \frac{4}{K^4}\frac{p_a}{p_0}\left|\left\langle \Psi_n \left| \sum_{j=1}^{N} e^{i\vec{K}\cdot\vec{r}_j} \right| \Psi_0 \right\rangle\right|^2$$

实验测量：

$$\frac{d\sigma_n^e(\theta)}{d\Omega} = \frac{dn(\theta)/d\Omega}{n_0 Nt}$$

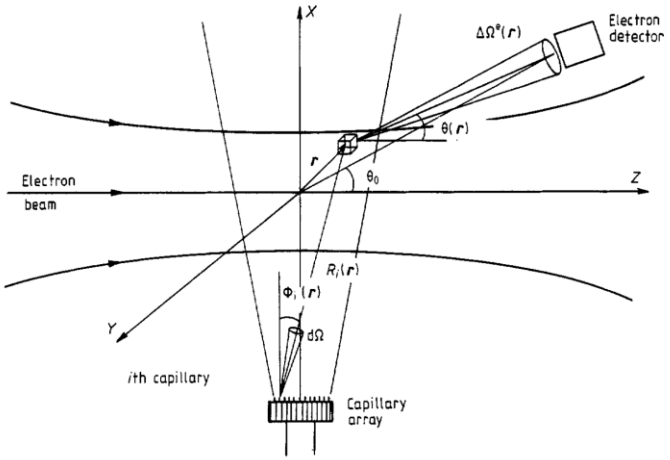

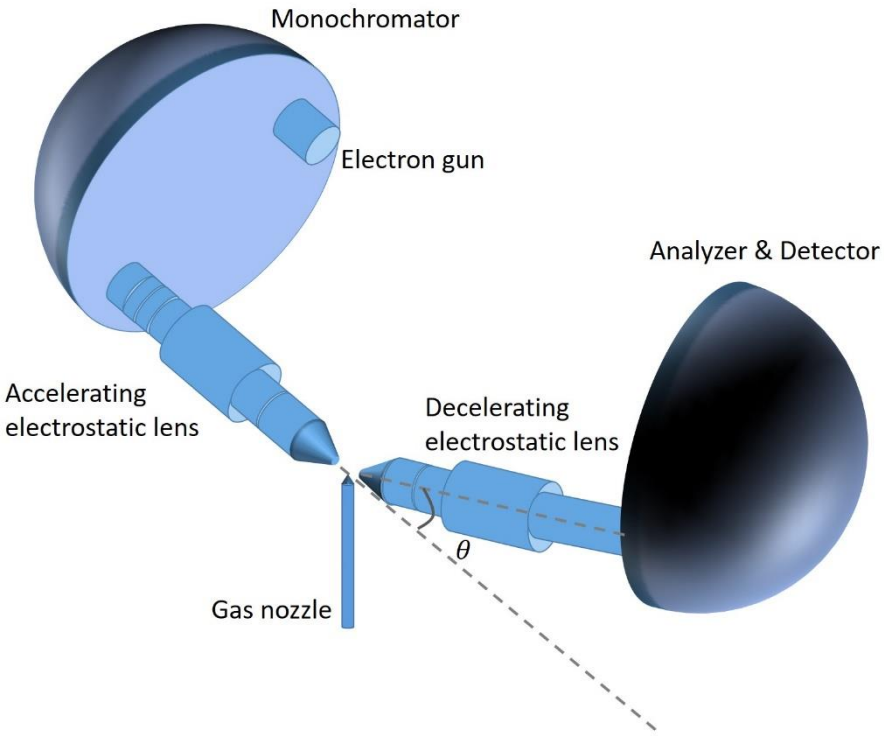

X. J. Liu, *et al.*, Rev. Sci. Instrum., 72, 3357(2001)

M. Inokuti, Rev. Mod. Phys. 43, 297(1971)

相对流量技术:

$$\frac{d\sigma_n^e(\theta)}{d\Omega} = \frac{dn(\theta)/d\Omega}{n_0 Nt}$$

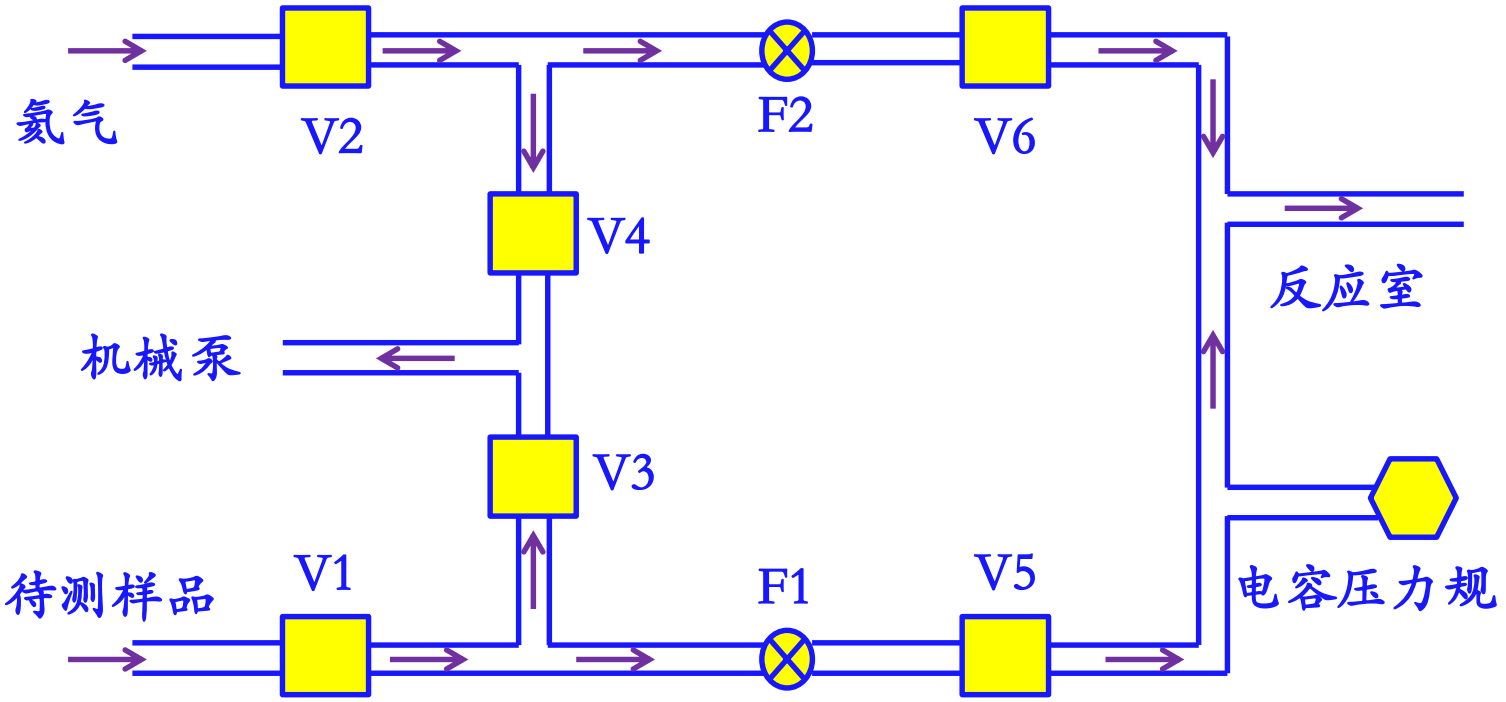

Y.W. Liu, L.Q. Xu *et al.* **J. Geophys. Res. 122** 3459 (2017);

$$N(E_0, E_j, \theta) = I(t) N_0 C(E_0, E_j, \theta) V_{eff}(\theta) \frac{d\sigma(E_0, E_j, \theta)}{d\Omega}$$

$$\frac{N^T(E_0, E_j, \theta)}{N^S(E_0, E_{j'}, \theta)} = \frac{I(t_1) N_0^T C(E_0, E_j, \theta) V_{eff}{}^T(\theta) d\sigma^T(E_0, E_j, \theta)/d\Omega}{I(t_2) N_0^S C(E_0, E_{j'}, \theta) V_{eff}{}^S(\theta) d\sigma^S(E_0, E_{j'}, \theta)/d\Omega}$$

$$\frac{d\sigma^T(E_0, E_j, \theta)}{d\Omega} = \frac{N^T(E_0, E_j, \theta)}{N^S(E_0, E_{j'}, \theta)} \frac{N_0^S}{N_0^T} \frac{d\sigma^S(E_0, E_{j'}, \theta)}{d\Omega}$$

$$\frac{N_0^S}{N_0^T} = \frac{\dot{n}_T}{\dot{n}_S} \sqrt{\frac{M_T}{M_S}}$$

$$\frac{d\sigma^T(E_0}{d\Omega} \quad \frac{d\sigma^S(E_0, E_{j'}, \theta)}{d\Omega}$$

相对流量技术的优点：

统一实验的绝对化标准

提高实验结果的精度

Y.W. Liu, L.Q. Xu *et al.* **J. Geop**

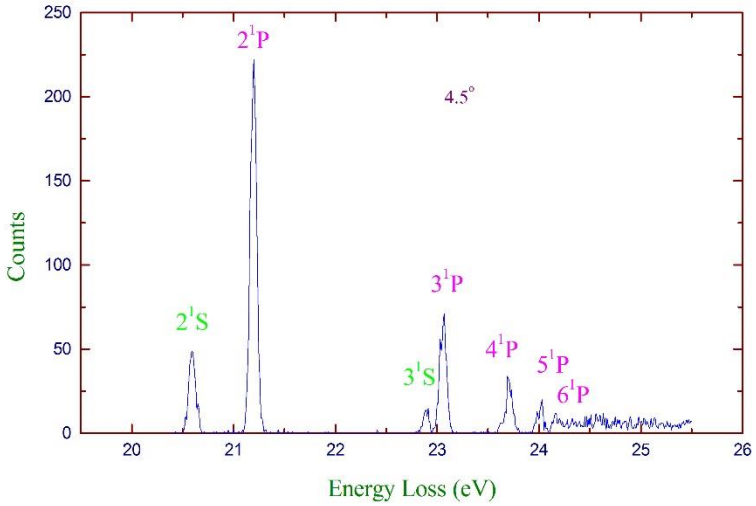

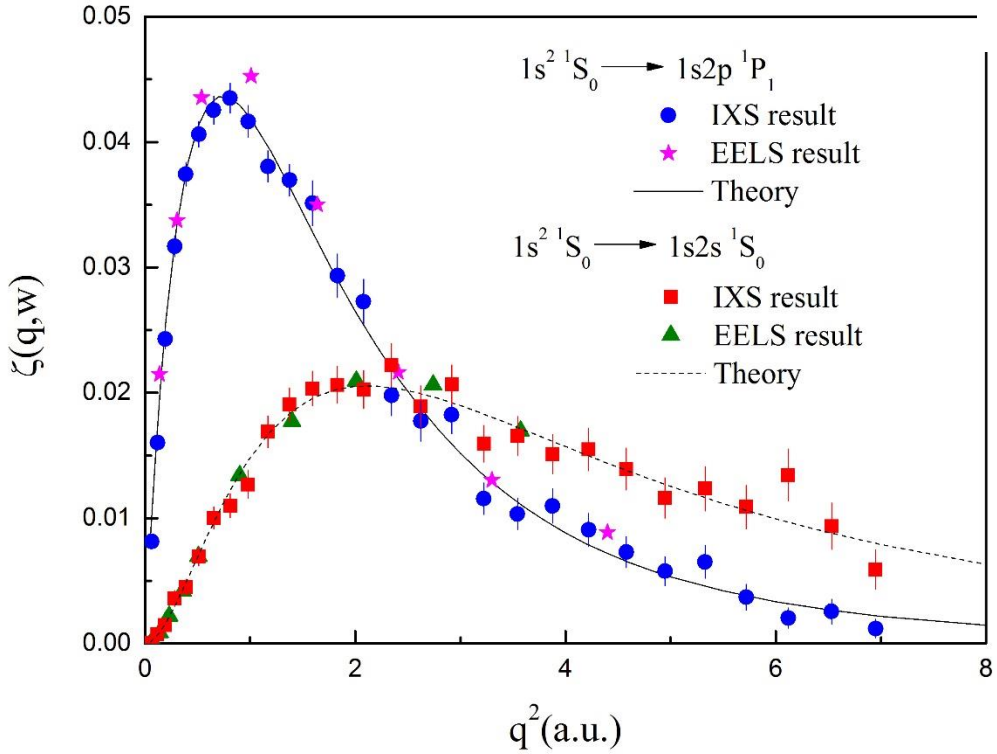

$$\zeta(\vec{q},\omega_n) = \left| \left\langle \Psi_n \left| \sum_{j=1}^{N} e^{i\vec{q}\cdot\vec{r}_j} \right| \Psi_0 \right\rangle \right|^2$$

B. P. Xie, L. F. Zhu,* K. Yang, B. Zhou, N. Hiraoka, Y. Q. Cai, Y. Yao, C. Q. Wu, E. L. Wang and D. L. Feng,* Phys. Rev. A 82, 032501(2010)

II. X射线散射

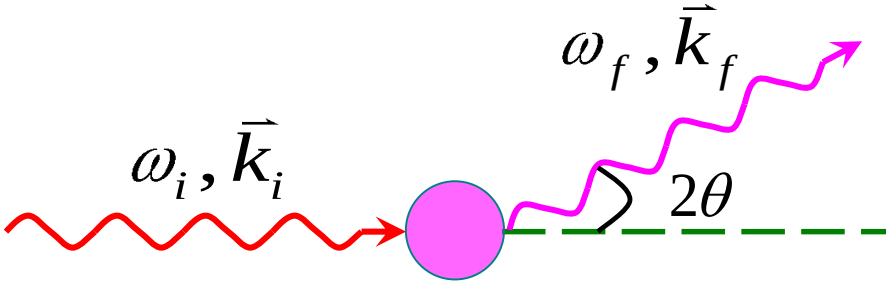

Schematics of IXS

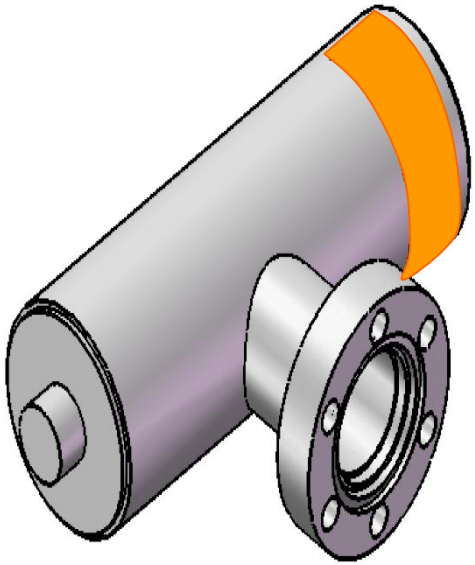

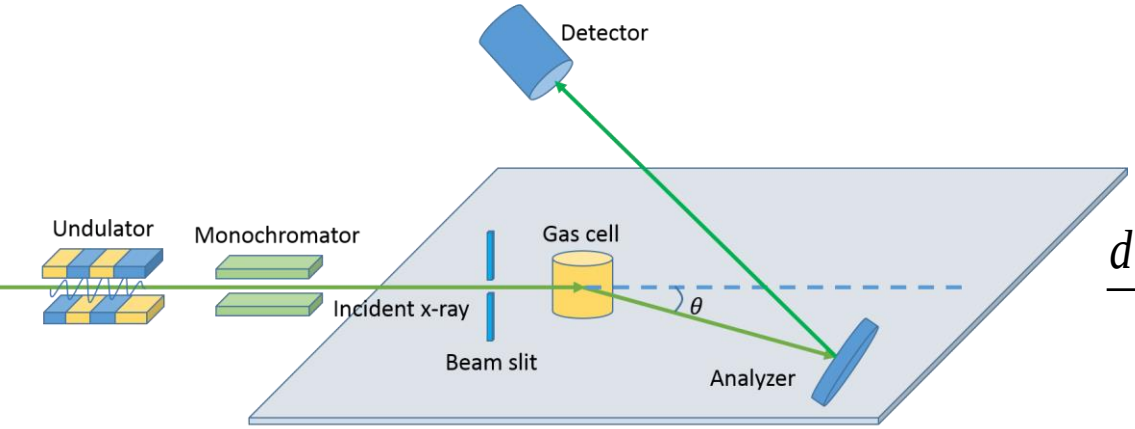

$$E_n = \hbar\omega_i - \hbar\omega_f$$

$$q^2 = k_i^2 + k_f^{\ 2} - 2k_i k_f \cos 2\theta$$

$$\frac{d\sigma_n^{\gamma}(2\theta)}{d\Omega} = r_0^2 \frac{\omega_f}{\omega_i} \left| \vec{\varepsilon}_i \cdot \vec{\varepsilon}_f^{\,*} \right|^2 \left| \left\langle \Psi_n \left| \sum_{j=1}^{N} e^{i\vec{q}\cdot\vec{r}_j} \right| \Psi_0 \right\rangle \right|^2$$

$$\zeta(\mathbf{q}, \omega_n) = \left| \left\langle \Psi_n \left| \sum_{j=1}^{N} e^{i\vec{q}\cdot\vec{r}_j} \right| \Psi_0 \right\rangle \right|^2$$

P. M. Platzman *et al.*, Phys. Rev. 139, A410 (1965)

日本 Spring-8


理化学研究所 播磨研究所
SACLA
X線自由電子レーザー施設
SPring-8
大型放射光施設
公益財団法人 高輝度光科学研究センター
兵庫県放射光ナノテク研究所
独立行政法人 日本原子力研究開発機構
兵庫県立大学 ニュースバル放射光施設

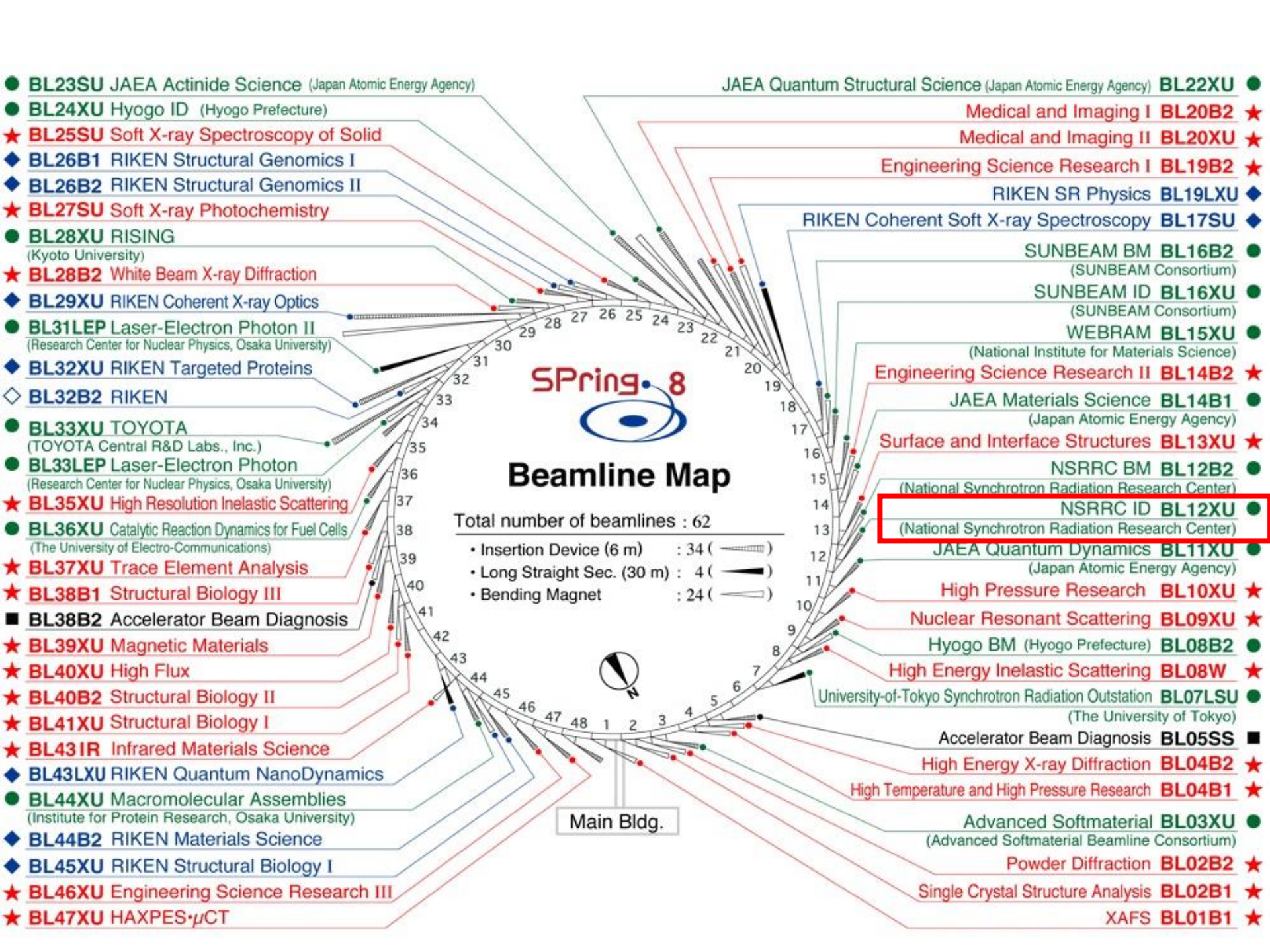
SPring-8
Beamline Map
Total number of beamlines : 62
• Insertion Device (6 m) : 34
• Long Straight Sec. (30 m) : 4
• Bending Magnet : 24
Main Bldg.
BL23SU JAEA Actinide Science (Japan Atomic Energy Agency)
BL24XU Hyogo ID (Hyogo Prefecture)
BL25SU Soft X-ray Spectroscopy of Solid
BL26B1 RIKEN Structural Genomics I
BL26B2 RIKEN Structural Genomics II
BL27SU Soft X-ray Photochemistry
BL28XU RISING (Kyoto University)
BL28B2 White Beam X-ray Diffraction
BL29XU RIKEN Coherent X-ray Optics
BL31LEP Laser-Electron Photon II (Research Center for Nuclear Physics, Osaka University)
BL32XU RIKEN Targeted Proteins
BL32B2 RIKEN
BL33XU TOYOTA (TOYOTA Central R&D Labs., Inc.)
BL33LEP Laser-Electron Photon (Research Center for Nuclear Physics, Osaka University)
BL35XU High Resolution Inelastic Scattering
BL36XU Catalytic Reaction Dynamics for Fuel Cells (The University of Electro-Communications)
BL37XU Trace Element Analysis
BL38B1 Structural Biology III
BL38B2 Accelerator Beam Diagnosis
BL39XU Magnetic Materials
BL40XU High Flux
BL40B2 Structural Biology II
BL41XU Structural Biology I
BL43IR Infrared Materials Science
BL43LXU RIKEN Quantum NanoDynamics
BL44XU Macromolecular Assemblies (Institute for Protein Research, Osaka University)
BL44B2 RIKEN Materials Science
BL45XU RIKEN Structural Biology I
BL46XU Engineering Science Research III
BL47XU HAXPES·μCT
JAEA Quantum Structural Science (Japan Atomic Energy Agency) BL22XU
Medical and Imaging I BL20B2
Medical and Imaging II BL20XU
Engineering Science Research I BL19B2
RIKEN SR Physics BL19LXU
RIKEN Coherent Soft X-ray Spectroscopy BL17SU
SUNBEAM BM BL16B2 (SUNBEAM Consortium)
SUNBEAM ID BL16XU (SUNBEAM Consortium)
WEBRAM BL15XU (National Institute for Materials Science)
Engineering Science Research II BL14B2
JAEA Materials Science BL14B1 (Japan Atomic Energy Agency)
Surface and Interface Structures BL13XU
NSRRC BM BL12B2 (National Synchrotron Radiation Research Center)
NSRRC ID BL12XU (National Synchrotron Radiation Research Center)
JAEA Quantum Dynamics BL11XU (Japan Atomic Energy Agency)
High Pressure Research BL10XU
Nuclear Resonant Scattering BL09XU
Hyogo BM (Hyogo Prefecture) BL08B2
High Energy Inelastic Scattering BL08W
University-of-Tokyo Synchrotron Radiation Outstation BL07LSU (The University of Tokyo)
Accelerator Beam Diagnosis BL05SS
High Energy X-ray Diffraction BL04B2
High Temperature and High Pressure Research BL04B1
Advanced Softmaterial BL03XU (Advanced Softmaterial Beamline Consortium)
Powder Diffraction BL02B2
Single Crystal Structure Analysis BL02B1
XAFS BL01B1

非弹性X射线散射的绝对化方法

$$\zeta_n(q^2)=\frac{1}{r_0^2}\frac{\omega_i}{\omega_f}\frac{1}{\cos^2\theta}\frac{N(q,\mathrm{d}\Omega)/\alpha}{N_0(q,\mathrm{d}\Omega)\cdot nl_{eff}}$$

➢引用He原子到2^1P态的激发过程作为归一化标准：

$$\frac{\zeta_n^S(q^2)}{\zeta_{He}(q'^2)}=\frac{\omega_f^{He}}{\omega_f^S}\frac{\cos^2\theta^{He}}{\cos^2\theta^S}\frac{N^S(q,\mathrm{d}\Omega)/\alpha^S}{N_0^S(q,\mathrm{d}\Omega)\cdot n^S l_{eff}^S}\Bigg/\frac{N_0^S(q,\mathrm{d}\Omega)\cdot n^S l_{eff}^S}{N^S(q,\mathrm{d}\Omega)/\alpha^S}$$

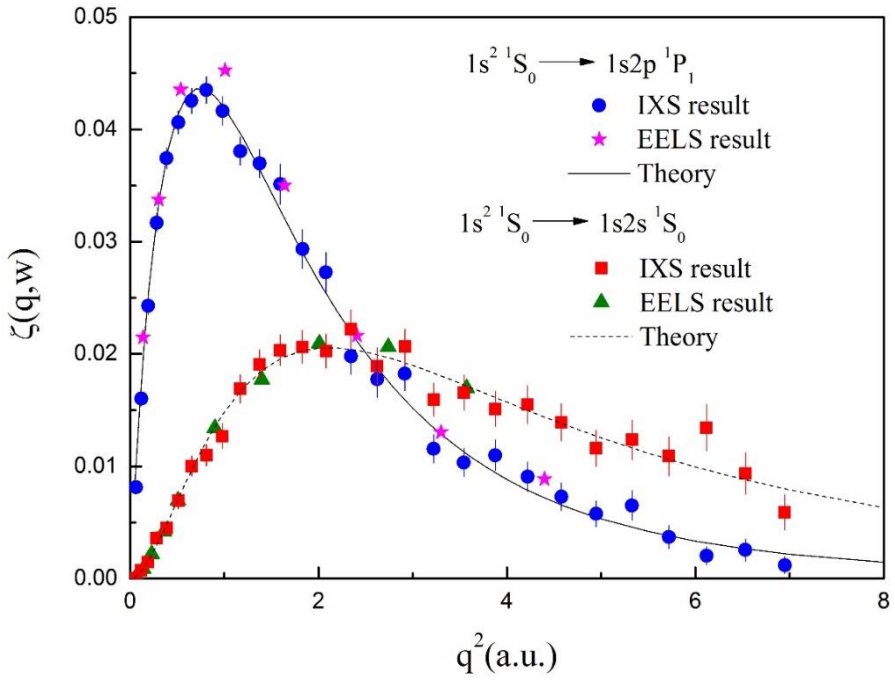

		误差大小
$N($		2%~10%
		<1%
$N_0($		<1%
		<0.6%
		受θ 影响
θ		<2%
$\zeta_n(q^2)$	最终结果	3%~10%

EELS:

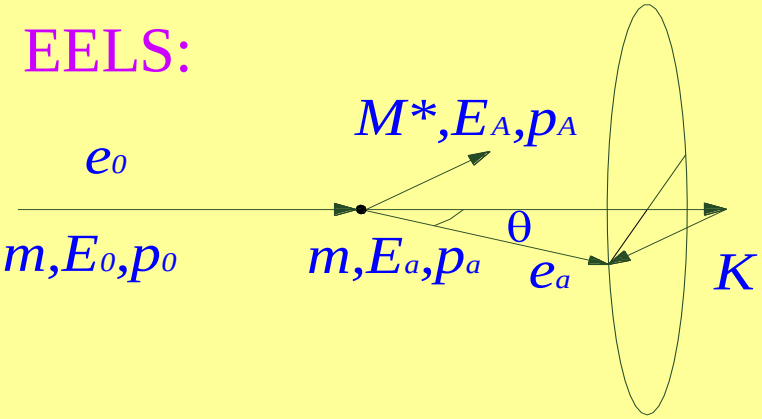

Schematics of EELS

Energy loss:

$$E_n = E_0 - E_a$$

Square of the momentum trans

$$K^2 = p_0^2 + p_a^2 - 2p_0p_a \cos$$

Differential Cross Section (DCS):

$$\frac{d\sigma_n^e(\theta)}{d\Omega} = \frac{2}{E_n}\frac{p_a}{p_0}\frac{1}{K^2} f_n\left(K^2\right) = \frac{4}{K^4}\frac{p_a}{p_0}\left|\left\langle \Psi_n \left| \sum_{j=1}^{N} e^{i\vec{K}\cdot\vec{r}_j} \right| \Psi_0 \right\rangle\right|^2$$

Generalized Oscillator Strength (GOS) :

$$f_n\left(K^2\right) = \frac{2E_n}{K^2}\left|\left\langle \Psi_n \left| \sum_{j=1}^{N} e^{i\vec{K}\cdot\vec{r}_j} \right| \Psi_0 \right\rangle\right|^2$$

IXS:

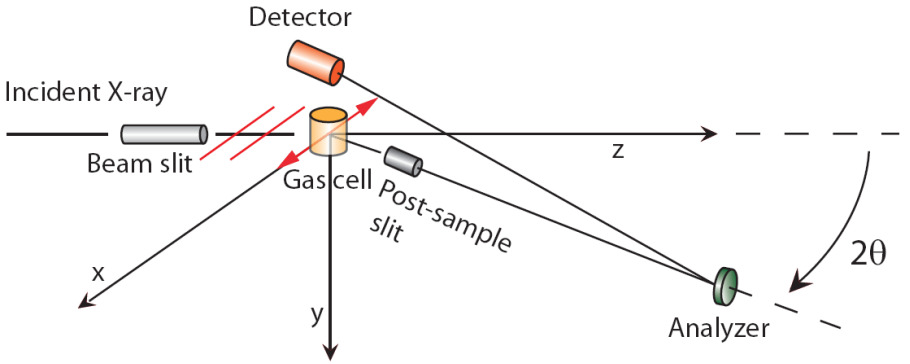

Energy loss:

$$E_n = \hbar\omega_i - \hbar\omega_f$$

ntum transfer:

$$k_f^{\,2} - 2k_ik_f\cos 2\theta$$

Differential Cross Section (DCS):

$$\frac{d\sigma_n^{\gamma}(\theta)}{d\Omega} = r_0^2\frac{\omega_f}{\omega_i}\left|\vec{\varepsilon}_i\cdot\vec{\varepsilon}_f^{\,*}\right|^2\left|\left\langle \Psi_n \left| \sum_{j=1}^{N} e^{i\vec{q}\cdot\vec{r}_j} \right| \Psi_0 \right\rangle\right|^2$$

Squared form factor :

$$\zeta\left(\vec{q},\omega_n\right) = \left|\left\langle \Psi_n \left| \sum_{j=1}^{N} e^{i\vec{q}\cdot\vec{r}_j} \right| \Psi_0 \right\rangle\right|^2$$

排除系统误差！

实验技术一：高能电子散射

实验装置：快电子散射谱仪

探针粒子：电子

入射粒子能量：1500 eV

样品气压：约10^{-2}Pa

测量角度：+5°到-15°

绝对化方法：相对流量技术

实验技术二：X射线散射

实验装置：X射线散射谱仪

探针粒子：光子

入射粒子能量：10 keV

样品气压：约10 atm

测量角度：5°到120°

绝对化方法：静态气压比

	准确	不准确
精确		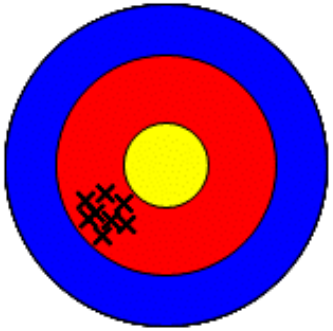
不精确		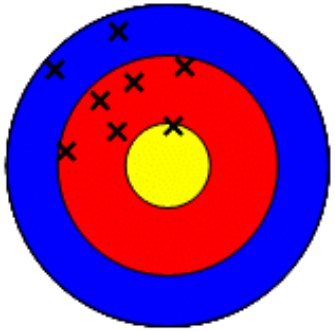

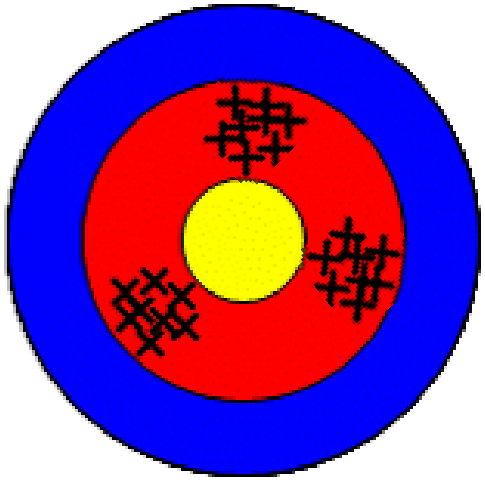

交叉检验：

- 不同研究组利用同一实验技术测量
- 用不同实验技术测量同一物理量

The measurement of Planck constant *h*

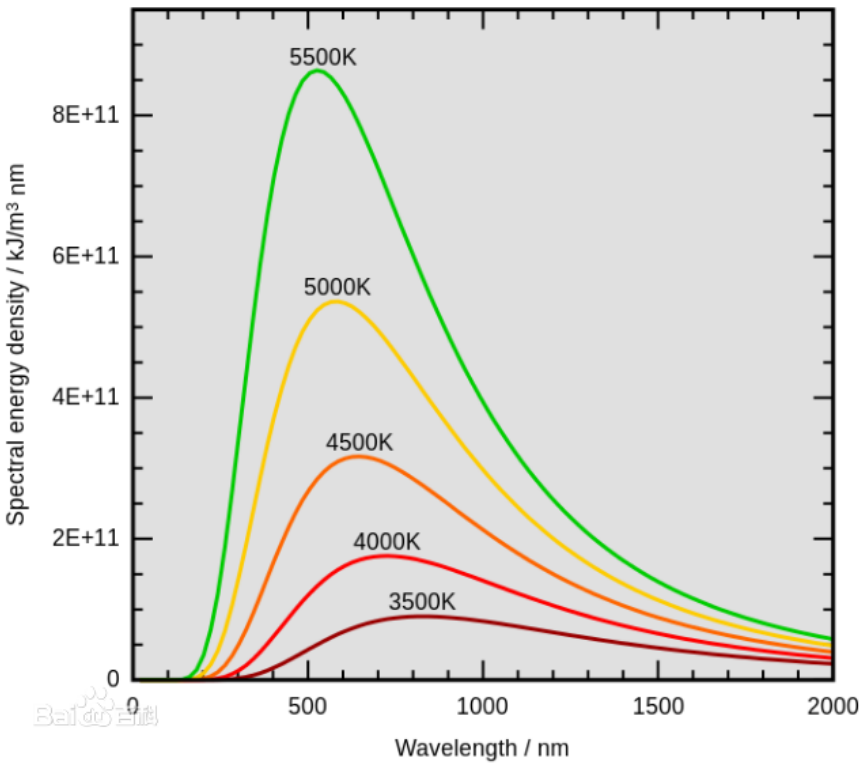

$$r_0(\lambda,T)=\frac{2\pi hc^2}{\lambda^5}\frac{1}{e^{hc/\lambda kT}-1}$$

Blackbody Radiation

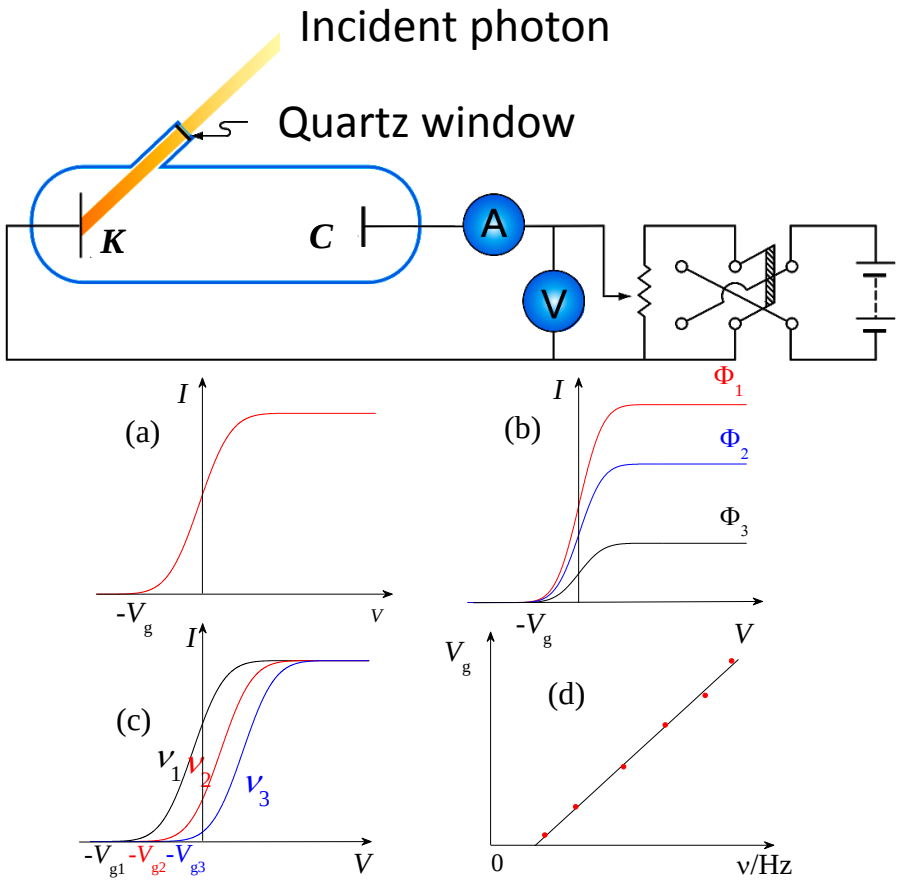

$$V_g=\frac{h}{e}\nu-\frac{\Phi}{e}$$

Photoelectric effect

Diffraction of polycrystal gold

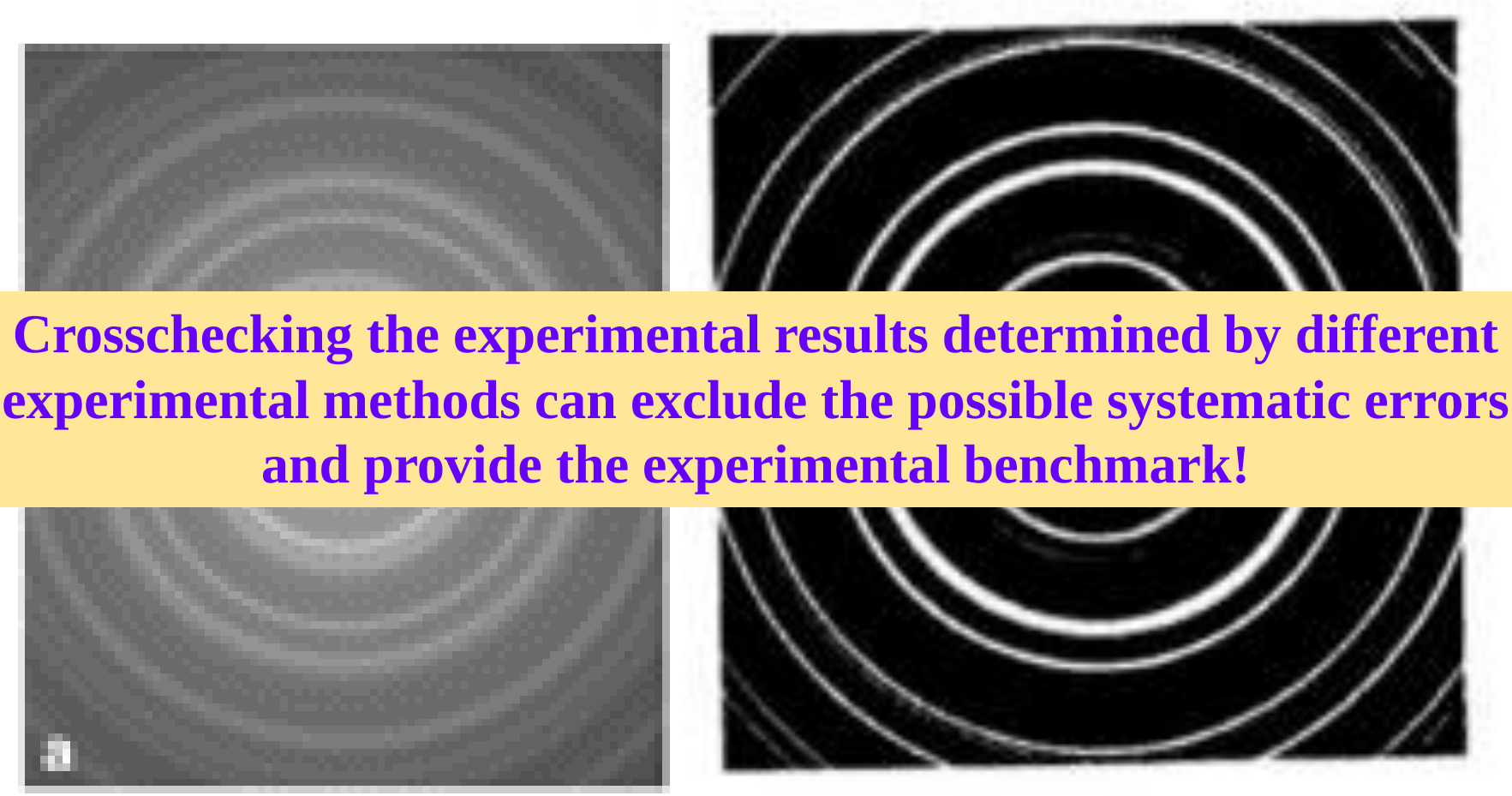

Crosschecking the experimental results determined by different experimental methods can exclude the possible systematic errors and provide the experimental benchmark!

High-energy electron diffraction **X-ray diffaction**

EELS:

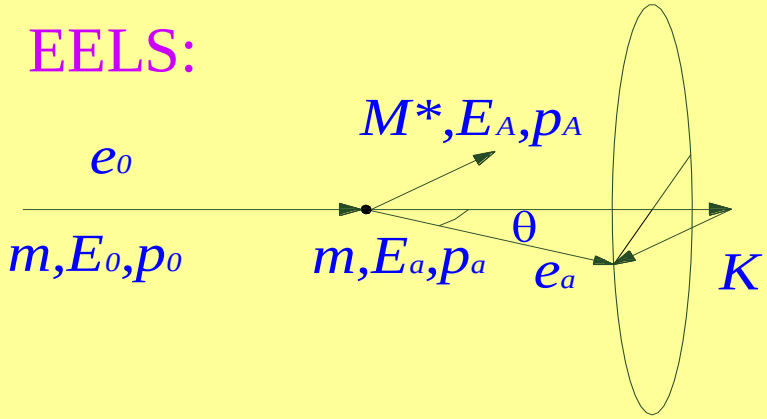

Schematics of EELS

Energy loss:

$$E_n = E_0 - E_a$$

Square of the momentum transfer:

$$K^2 = p_0^2 + p_a^2 - 2p_0 p_a \cos\theta$$

Differential Cross Section (DCS):

$$\frac{d\sigma_n^e(\theta)}{d\Omega} = \frac{2}{E_n}\frac{p_a}{p_0}\frac{1}{K^2} f_n\left(K^2\right) = \frac{4}{K^4}\frac{p_a}{p_0}\left|\left\langle \Psi_n \left| \sum_{j=1}^{N} e^{i\vec{K}\cdot\vec{r}_j} \right| \Psi_0 \right\rangle\right|^2$$

Generalized Oscillator Strength (GOS) :

$$f_n\left(K^2\right) = \frac{2E_n}{K^2}\left|\left\langle \Psi_n \left| \sum_{j=1}^{N} e^{i\vec{K}\cdot\vec{r}_j} \right| \Psi_0 \right\rangle\right|^2$$

IXS:

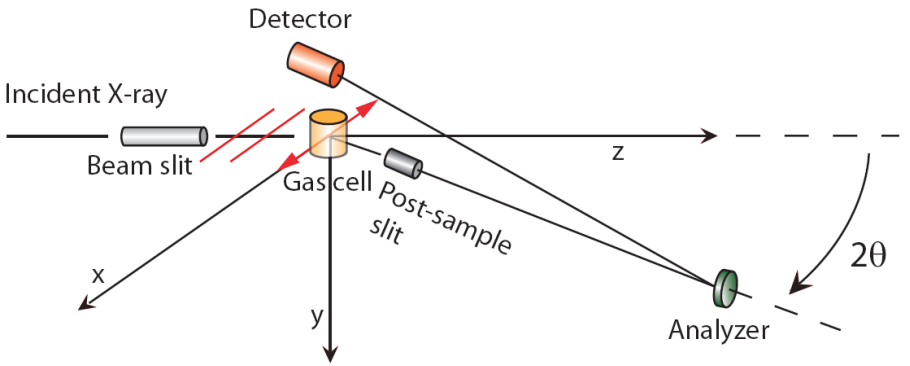

Energy loss:

$$E_n = \hbar\omega_i - \hbar\omega_f$$

Square of the momentum transfer:

$$q^2 = k_i^2 + k_f^{\,2} - 2k_i k_f \cos 2\theta$$

Differential Cross Section (DCS):

$$\frac{d\sigma_n^\gamma(\theta)}{d\Omega} = r_0^2 \frac{\omega_f}{\omega_i}\left|\vec{\varepsilon}_i \cdot \vec{\varepsilon}_f^{\,*}\right|^2 \left|\left\langle \Psi_n \left| \sum_{j=1}^{N} e^{i\vec{q}\cdot\vec{r}_j} \right| \Psi_0 \right\rangle\right|^2$$

Squared form factor :

$$\zeta\left(\vec{q},\omega_n\right) = \left|\left\langle \Psi_n \left| \sum_{j=1}^{N} e^{i\vec{q}\cdot\vec{r}_j} \right| \Psi_0 \right\rangle\right|^2$$

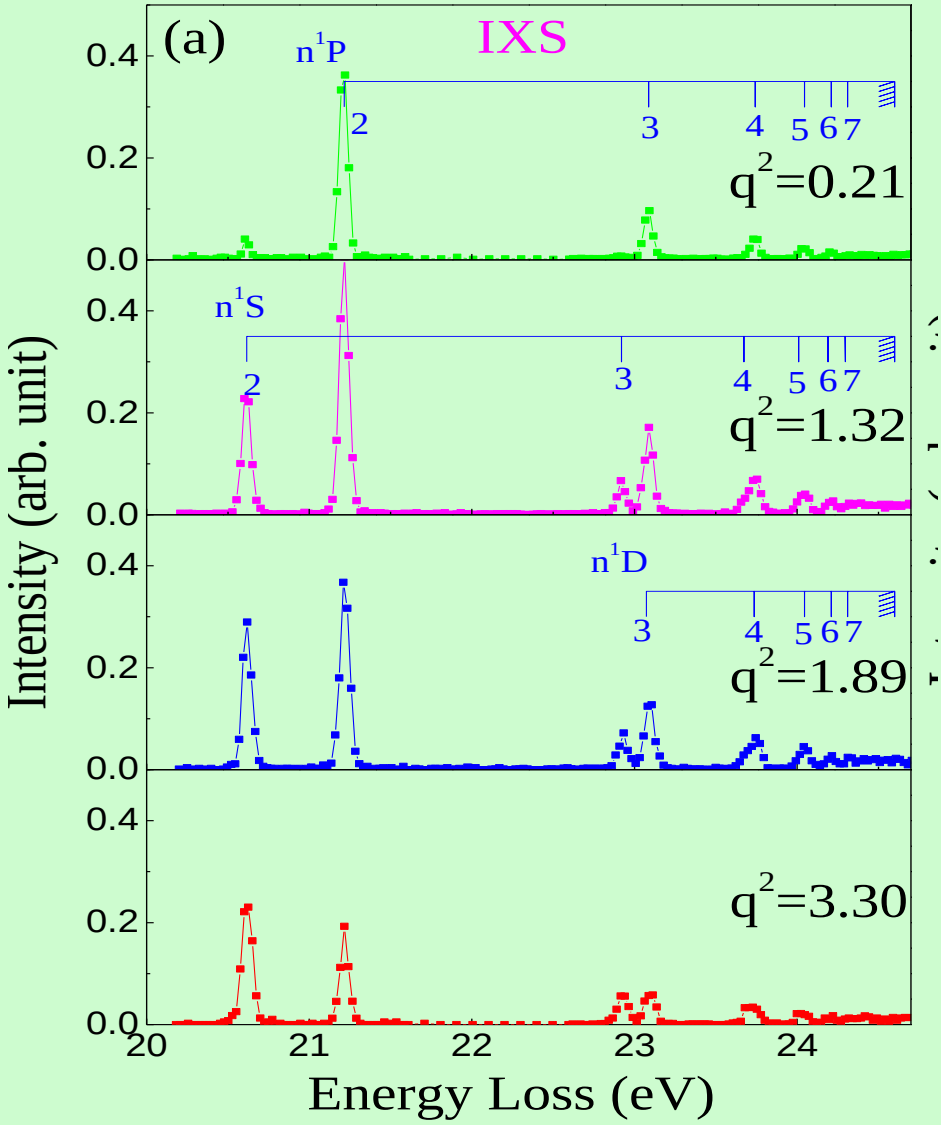

Inelastic X-ray scattering Spectra measured at an incident photon energy of 10 keV and energy resolutions of 70 meV.

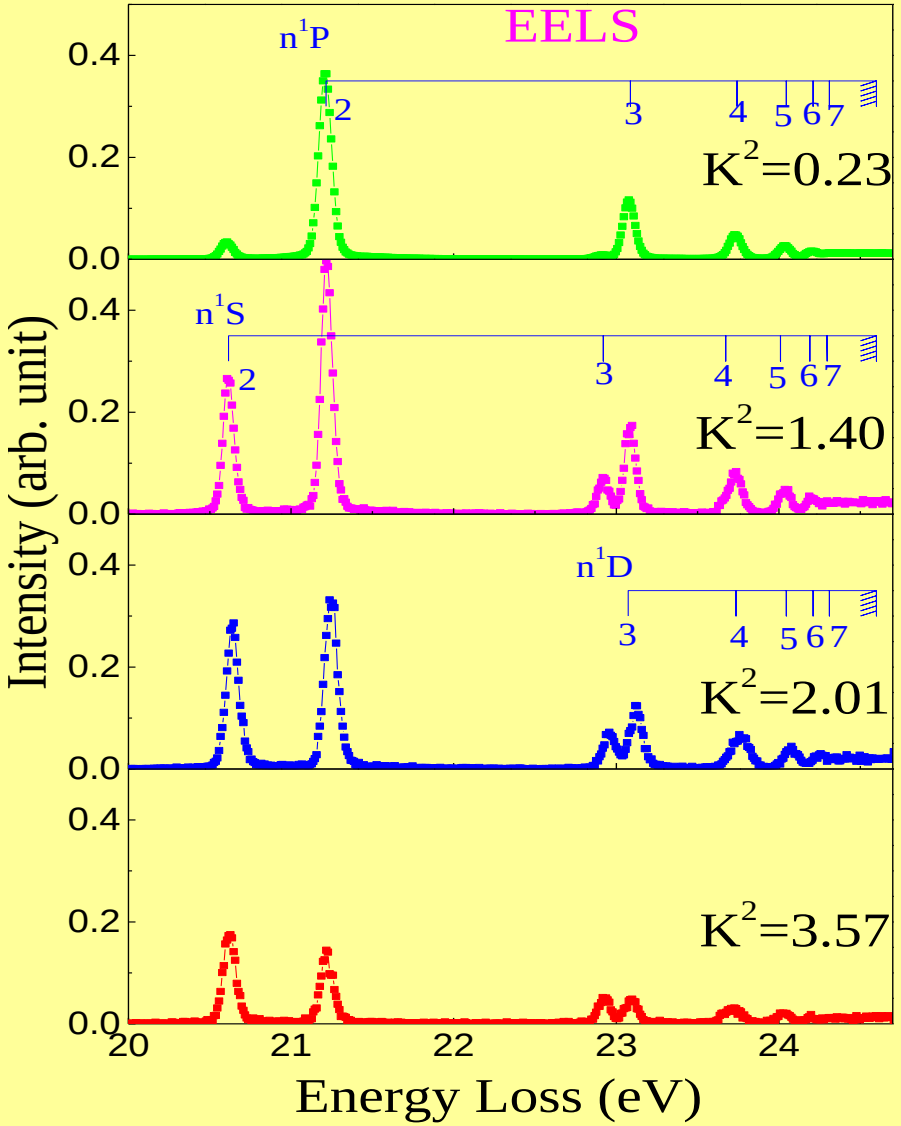

Electron Energy Loss Spectra (EELS) measured at an incident electron energy of 2.5 keV and an energy resolution of 80 meV.

排除系统误差！

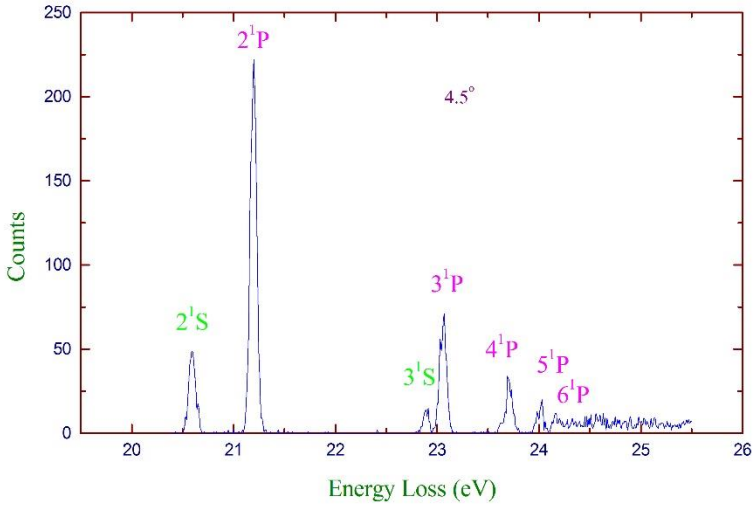

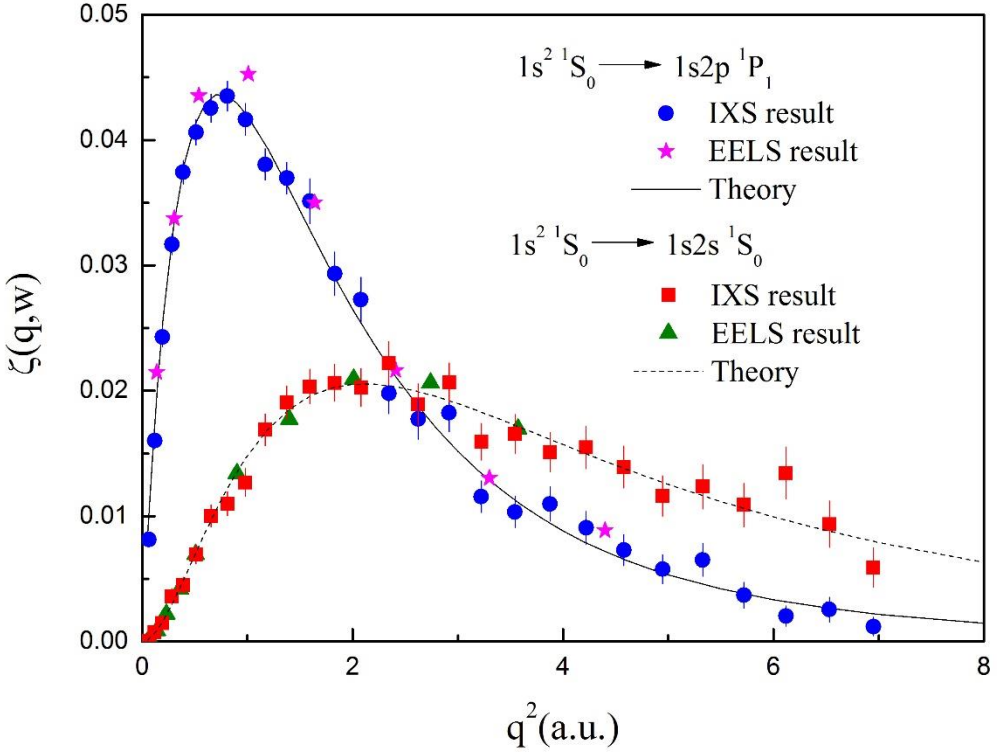

$$\zeta(\vec{q},\omega_n)=\left|\left\langle \Psi_n \left| \sum_{j=1}^{N} e^{i\vec{q}\cdot\vec{r}_j} \right| \Psi_0 \right\rangle\right|^2$$

B. P. Xie, L. F. Zhu,* K. Yang, B. Zhou, N. Hiraoka, Y. Q. Cai, Y. Yao, C. Q. Wu, E. L. Wang and D. L. Feng,* Phys. Rev. A 82, 032501(2010)

上海光源IXS装置

- 国际上的主要光源都有IXS谱仪
- 国内第一台IXS谱仪装置
- 可转角度0~110°

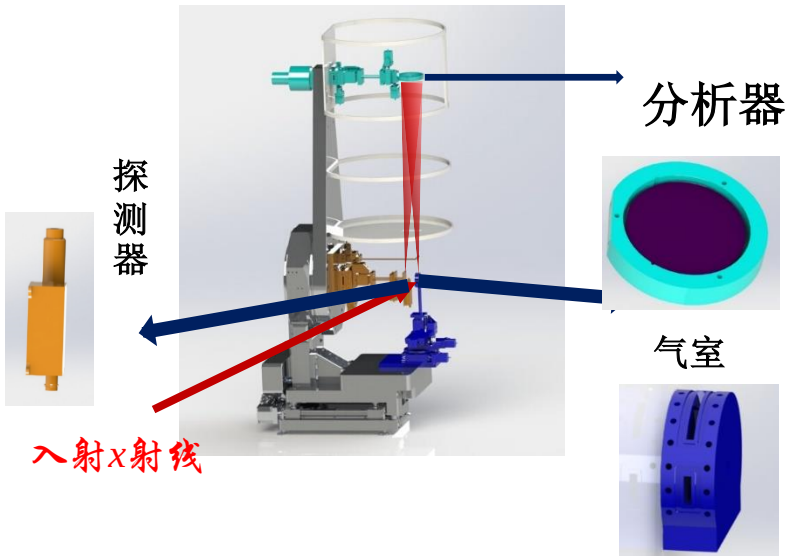

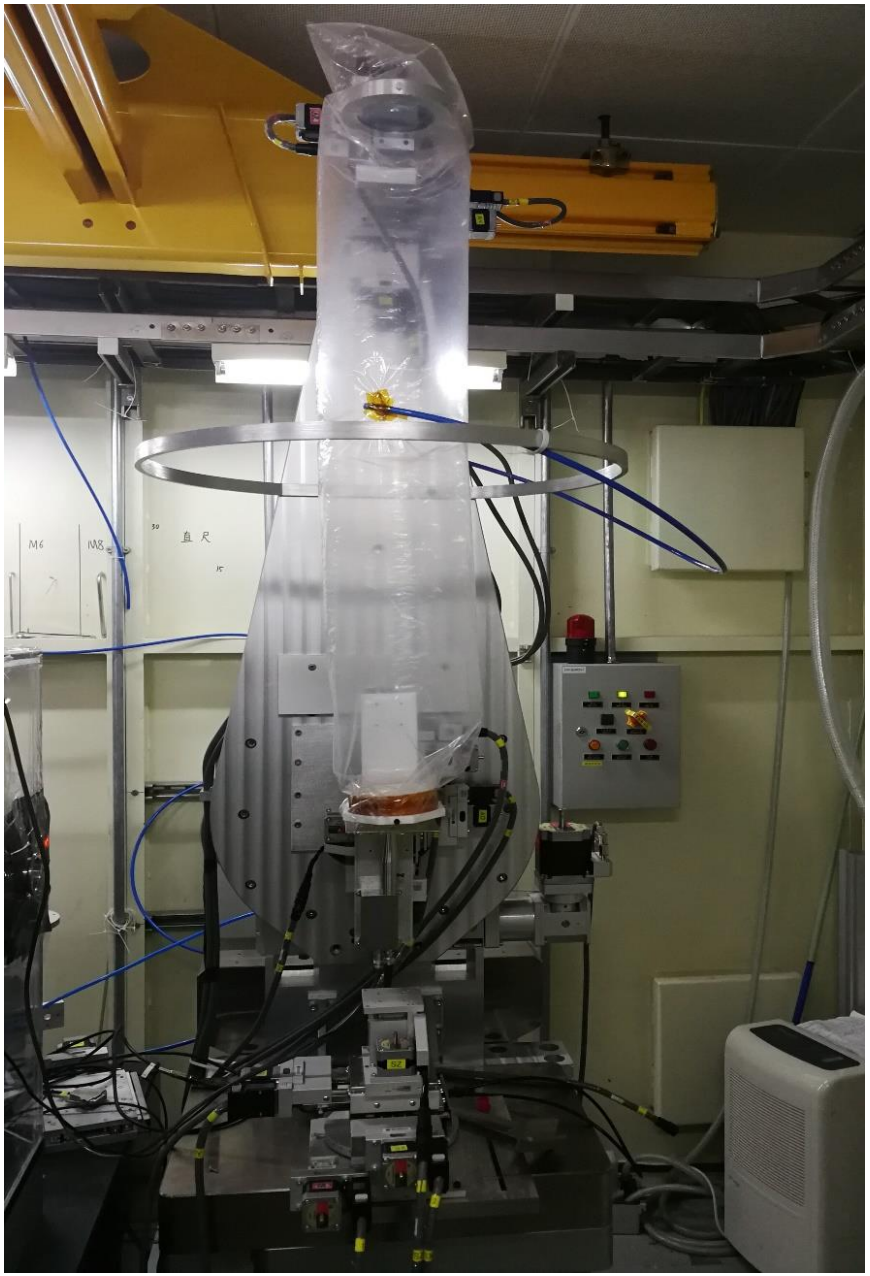

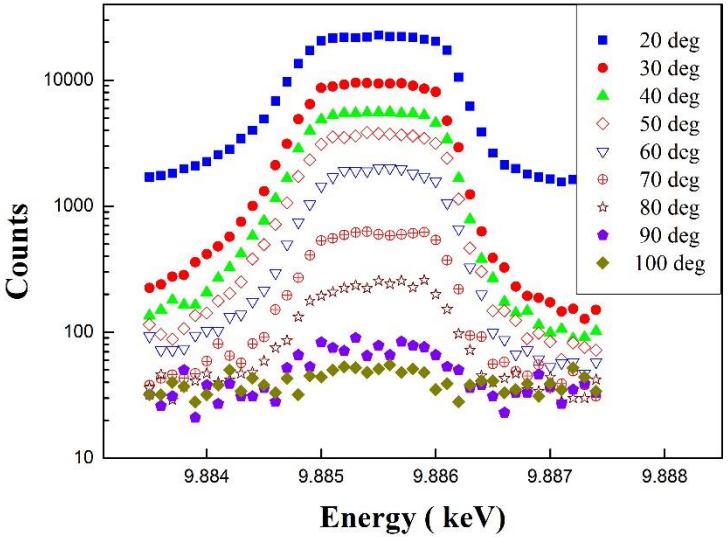

纤维丝弹性峰

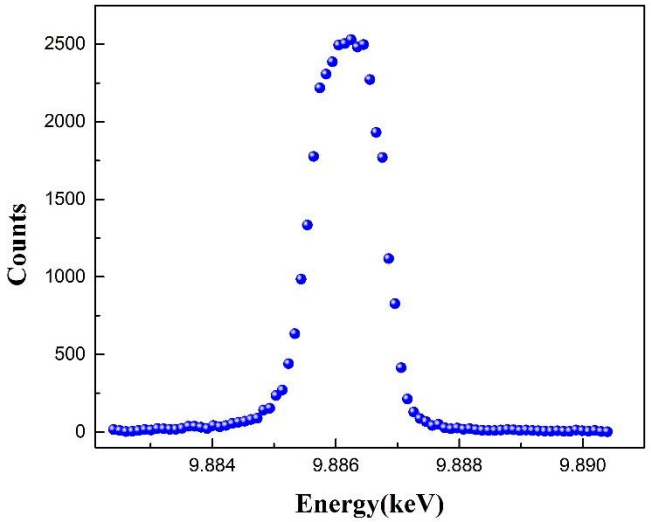

Elastic scattering for Helium @ 20 degree

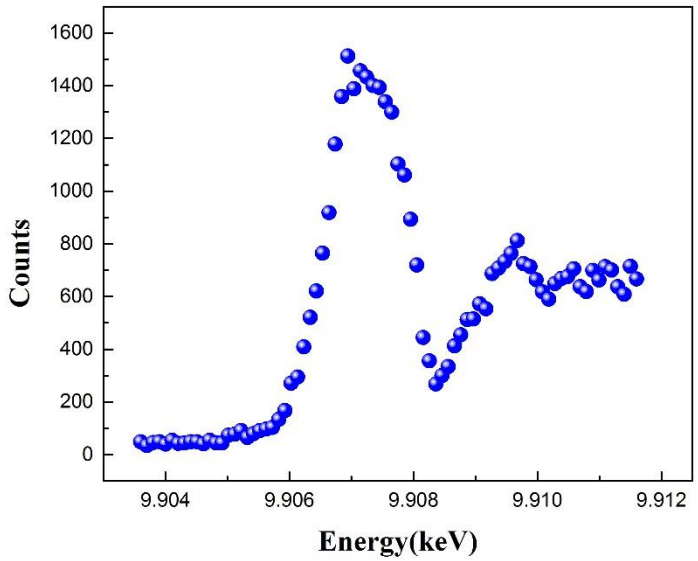

Inelastic scattering for Helium @ 20 degree

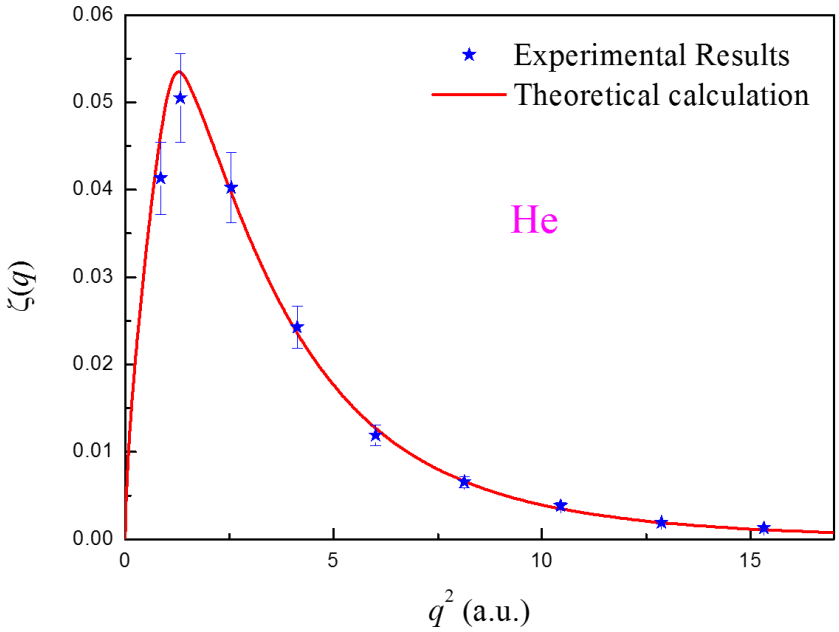

主要内容

- 背景
- 实验方法
- 现状
- 展望

一、原子分子价壳层激发态的电子结构问题

形状因子平方：

$$\zeta(\vec{q},\omega_n)=\left|\left\langle \Psi_n \left| \sum_{j=1}^{N} \exp(i\vec{q}\cdot\vec{r}_j) \right| \Psi_0 \right\rangle\right|^2$$

$$\zeta(\vec{q},\omega_n)=\left|\left\langle \Psi_n(\vec{p}+\vec{q}) \middle| \Psi_0(\vec{p}) \right\rangle\right|^2$$

I、He原子基态电子结构

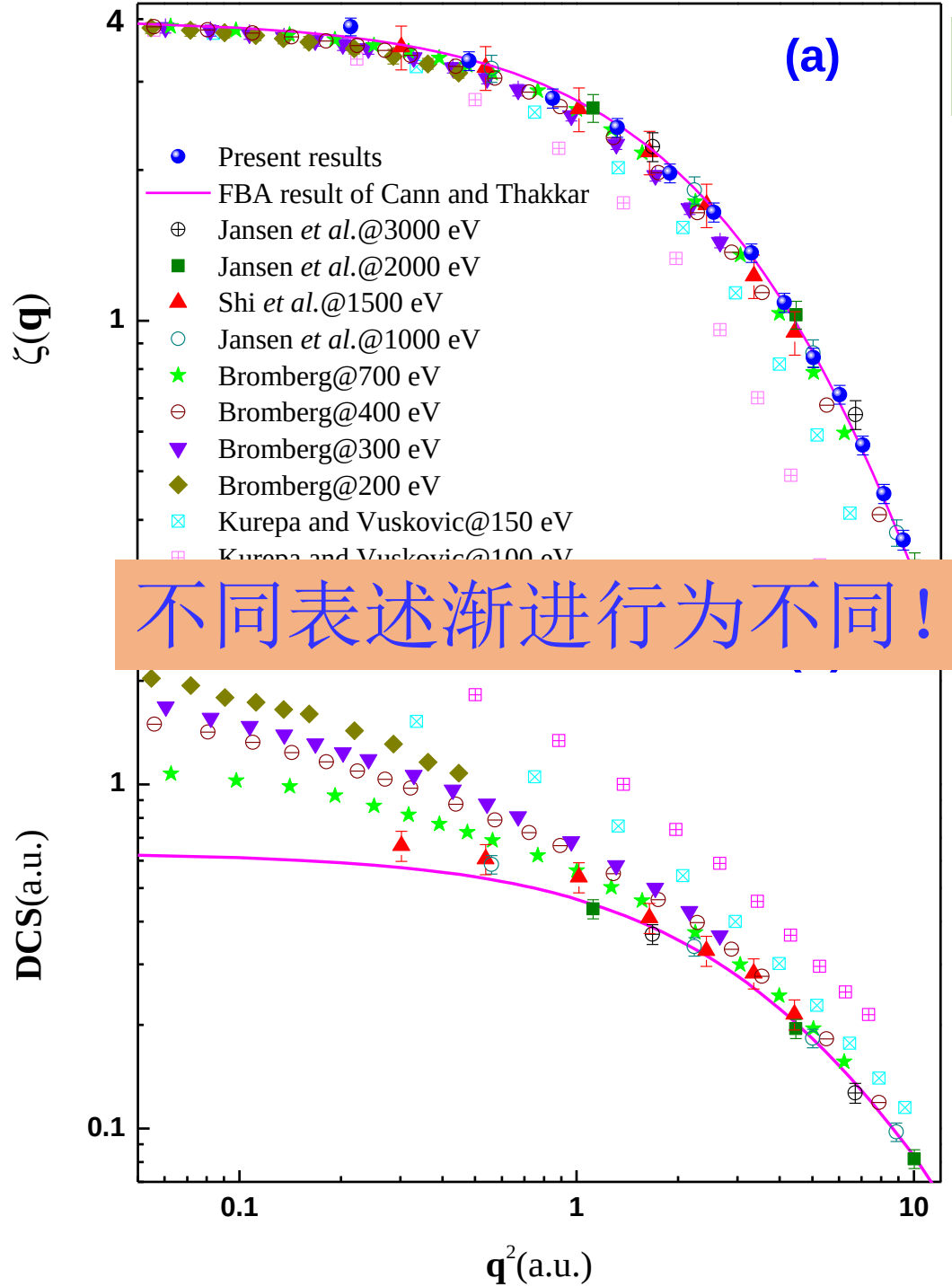

不同表述渐进行为不同！

$$\frac{d\sigma_n^{\gamma}(2\theta)}{d\Omega} = r_0^2 \left|\vec{\varepsilon}_i \cdot \vec{\varepsilon}_f^{\,*}\right|^2 \left|\left\langle \Psi_0 \left| \sum_{j=1}^{N} e^{i\vec{q}\cdot\vec{r}_j} \right| \Psi_0 \right\rangle\right|^2$$

$$\zeta(\vec{q}) = \left|\left\langle \Psi_0 \left| \sum_{j=1}^{N} e^{i\vec{K}\cdot\vec{r}_j} \right| \Psi_0 \right\rangle\right|^2$$

$$\left(\frac{d\sigma}{d\Omega}\right)_e^B = \frac{4}{K^4}\left|Z - \left\langle \Psi_0 \left| \sum_{j=1}^{N} e^{i\vec{K}\cdot\vec{r}_j} \right| \Psi_0 \right\rangle\right|^2$$

测试FBA的有效性

Y.W. Liu *et al.* **Phys. Rev. Lett.** (in revision)

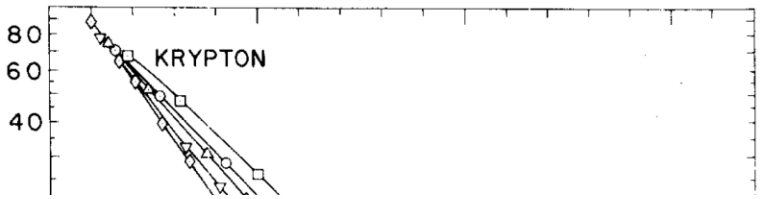

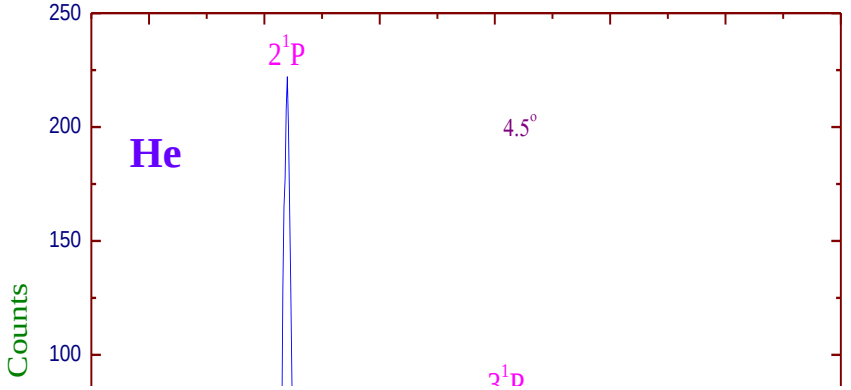

four gases Ne, Ar, Kr, and Xe, when the cross sections are plotted as a function of ΔP, the higher energy curves lie higher, and the curves tend to merge in the limit as ΔP approaches zero. We have previously pointed out[30] that this merging suggests that the Born approximation will hold in the limit of small ΔP and that in this limit the cross sections should be describable by a simple potential. Helium, however, presents an anomalous situation. Here the lower energy curves lie higher, and there is no merging of the curves in the limit as ΔP approaches zero, in contradistinction to what we have found for Hg,[30] N_2 and Co,[36] O_2 and CO_2,[38] and NH_3 and H_2O[37] in addition to the other inert gases presented here.

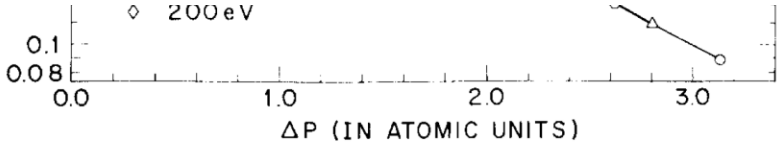

[12]R. H. J. Jansen and F. J. DeHeer, in Abstracts of Papers of the Eighth International Conference on the Physics of Electronic and Atomic Collisions (Institute of Physics, Belgrade, Yugoslavia, 1973), p. 269.
[13]M. V. Kurepa, L. Dj. Vuskovic, and S. D. Kalezic, Ref. 12, p. 267.
[14]J. Mehr, Z. Physik 198, 345 (1967).
[15]S. P. Khare and B. L. Moiseiwitsch, Proc. Phys. Soc. Lond. 85, 821 (1965).
[16]J. E. Purcell, R. A. Berg, and A. E. S. Green, Phys. Rev. A 2, 107 (1970).
[17]P. S. Ganas, S. K. Dutta, and A. E. S. Green, Phys. Rev. A 2, 111 (1970).
[18]R. W. LaBahn and J. Callaway, Phys. Rev. 180, 91 (1969); 188, 520 (1969).

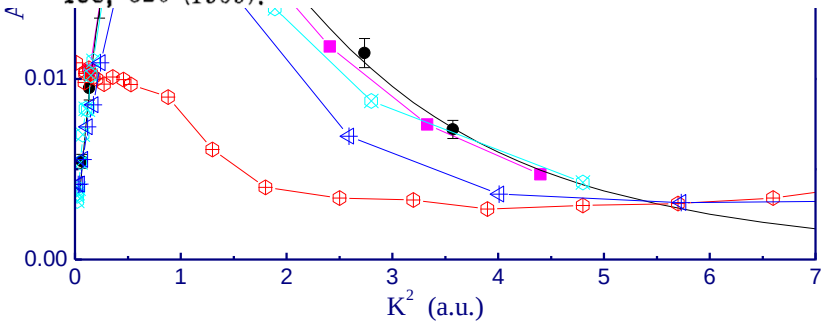

J. P. Brombergy, J. Chem. Phys. 61, 963(1974), B. P. Xie et a., Phys. Rev. A 82, 032501(2010)

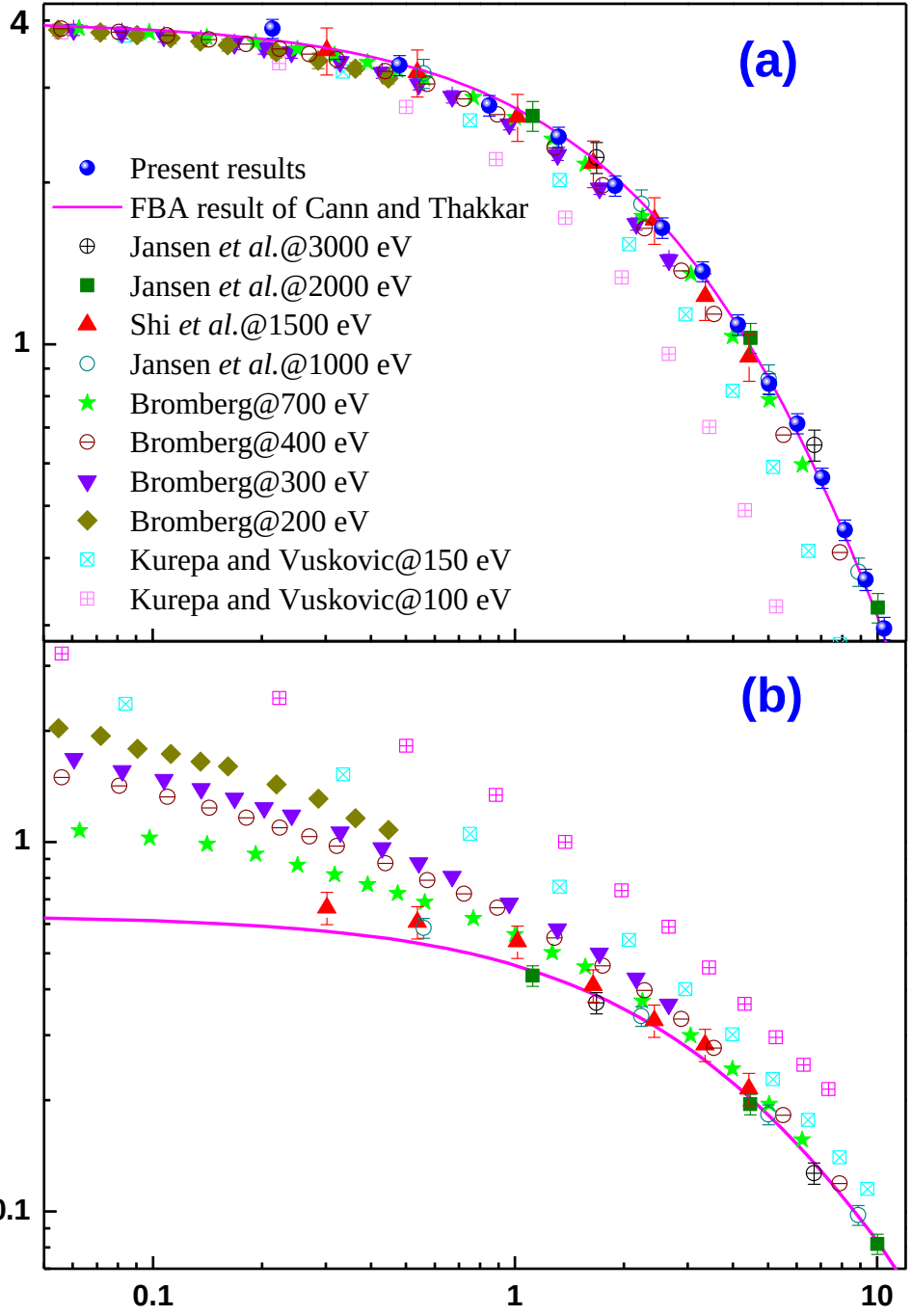

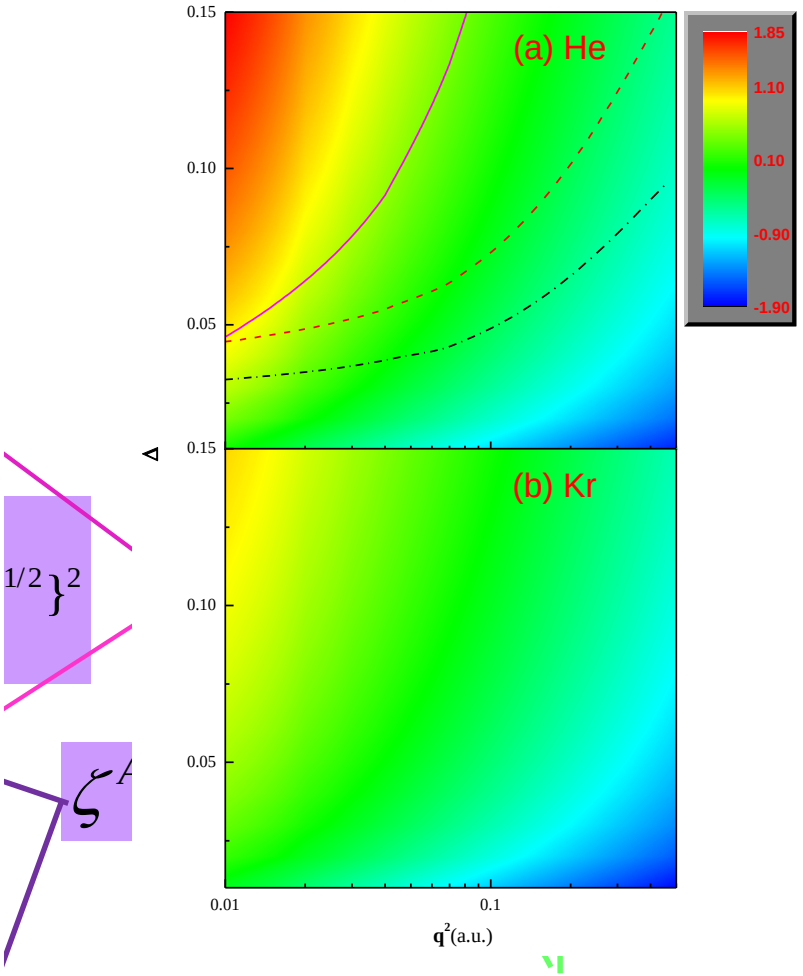

$$\delta = -\frac{4}{q^4}\Delta + \frac{8Z}{q^4}\left\{\zeta^{1/2}(q) - \left[\zeta(q) - \Delta\right]^{1/2}\right\}$$

Y.W. Liu *et al.* **Phys. Rev. Lett.** (in revision)

II、H_2分子基态的纯电子结构

Northey et al, JCP 145, 154304 (2016):

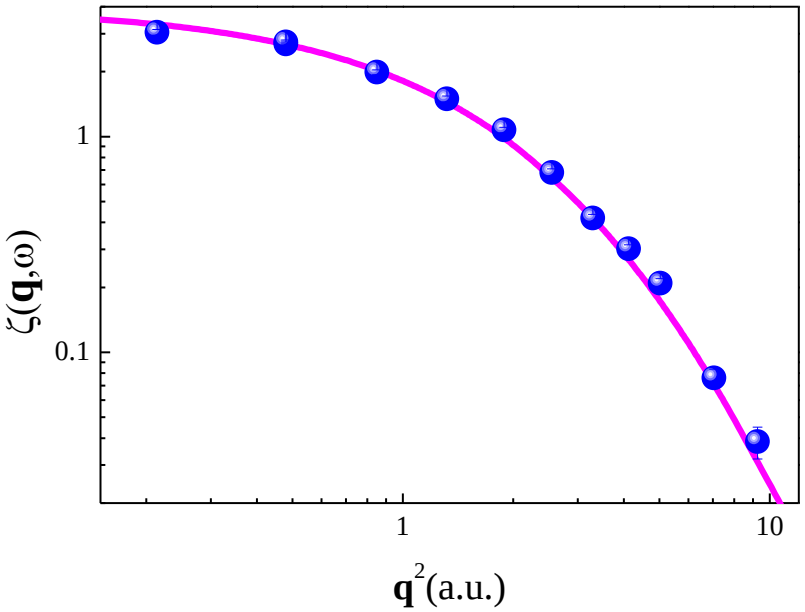

$$\left(\frac{d\sigma}{d\Omega}\right)_e = \frac{4}{K^4}\left|\langle\Psi_0\,|\,e^{i\vec{K}\cdot\vec{R}_a}+e^{i\vec{K}\cdot\vec{R}_b}-\sum_{i=1}^{2}e^{i\vec{K}\cdot\vec{r}_j}\,|\,\Psi_0\rangle\right|^2$$

$$\left(\frac{d\sigma}{d\Omega}\right)_\gamma = r_0^2\left|\vec{\varepsilon}_i\cdot\vec{\varepsilon}_f^{\,*}\right|^2\left|\left\langle\Psi_0\left|\sum_{j=1}^{N}e^{i\vec{q}\cdot\vec{r}_j}\right|\Psi_0\right\rangle\right|^2$$

在国际上首次获得分子基态纯电子结构

THE JOURNAL OF CHEMICAL PHYSICS **145**, 154304 (2016)

Elastic X-ray scattering from state-selected molecules

Thomas Northey,[1] Andrés Moreno Carrascosa,[1] Steffen Schäfer,[2] and Adam Kirrander[1,a)]
[1]*EaStCHEM, School of Chemistry, University of Edinburgh, David Brewster Road, EH9 3FJ Edinburgh, United Kingdom*
[2]*Aix-Marseille Université and Institut Matériaux Microélectronique Nanosciences de Provence (IM2NP), Marseille, France*

(Received 16 June 2016; accepted 24 August 2016; published online 19 October 2016)

The characterization of electronic, vibrational, and rotational states using elastic (coherent) X-ray scattering is considered. The scattering is calculated directly from complete active space self-consistent field level *ab initio* wavefunctions for H_2 molecules in the ground-state $X^1\Sigma_g^+$ and first-excited $EF^1\Sigma_g^+$ electronic states. The calculated scattering is compared to recent experimental measurements [Y.-W. Liu *et al.*, Phys. Rev. A **89**, 014502 (2014)], and the influence of vibrational and rotational states on the observed signal is examined. The scaling of the scattering calculations with basis set is quantified, and it is found that energy convergence of the *ab initio* calculations is a good indicator of the quality of the scattering calculations. *Published by AIP Publishing.* [http://dx.doi.org/10.1063/1.4962256]

High-precision measurement of the differential cross section of X-ray elastic scattering from H_2[13] provides a welcome opportunity to examine molecular form factors and an interesting route for the study of the electronic structure of atoms and molecules. The excellent agreement between the experimental measurements and the calculations presented in this article hold promise that this approach could be extended to a wider range of molecules.[28] In the future, the prospect of identifying electronic states in conjunction with time-dependent ultrafast X-ray scattering could enable complete characterization of reaction paths using X-ray scattering. Recent time-resolved experiments[18–20,67] combined with theory[28,66,68] constitute an important first step towards this goal.

Ya-Wei Liu et al, RRA 89, 014502, (2014);

二、原子分子价壳层激发态的基准动力学参数

I、氮分子价壳层激发态的积分截面

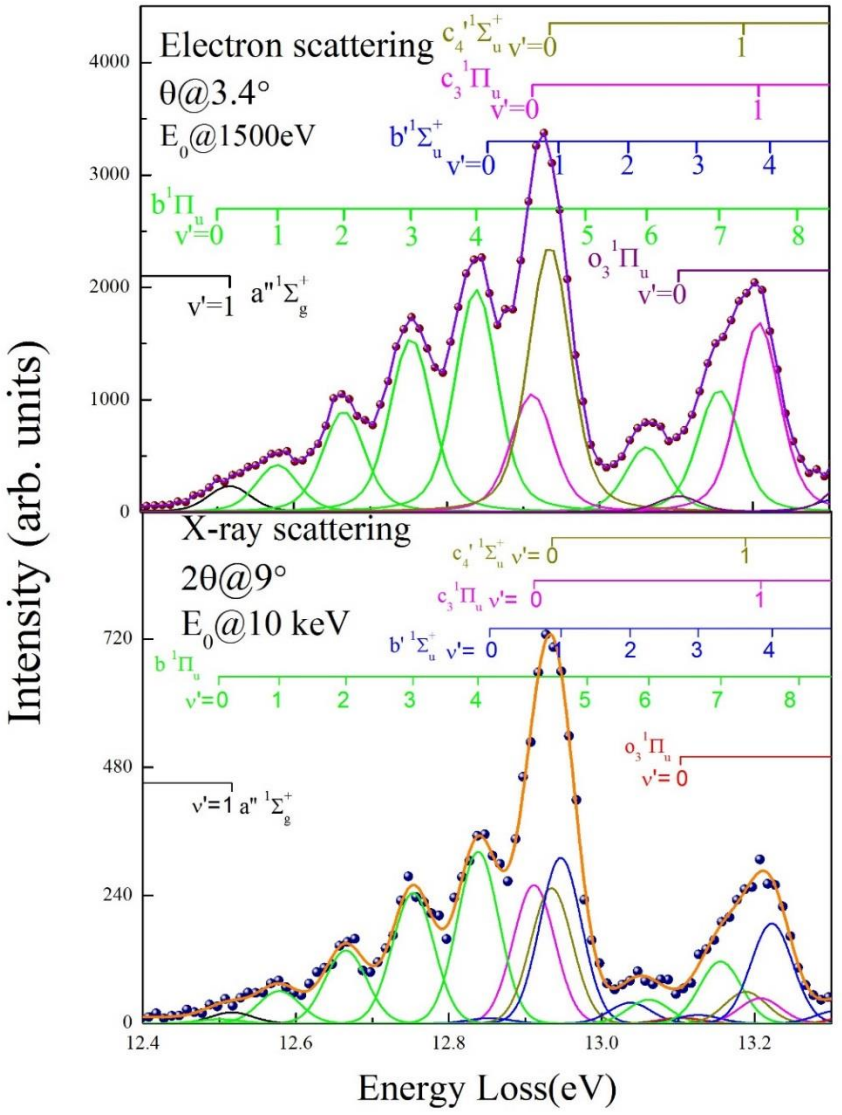

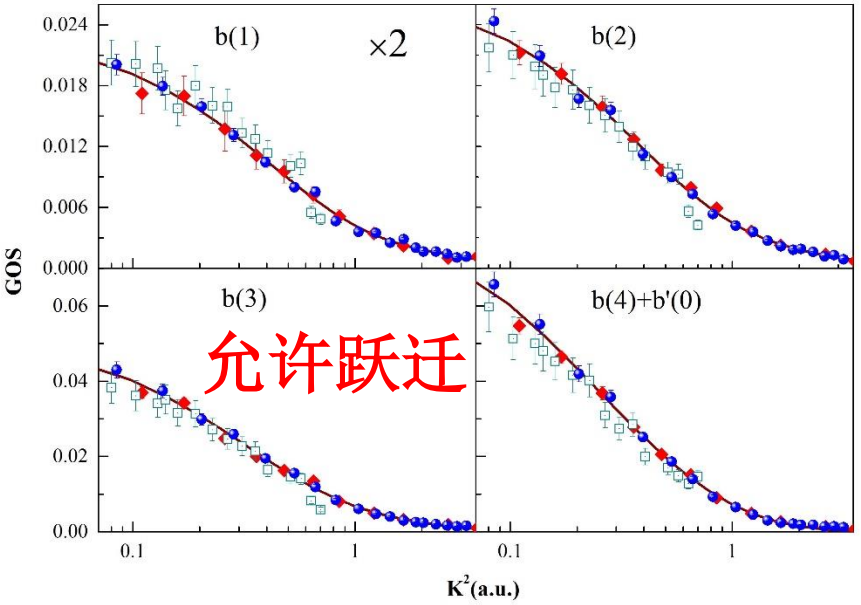

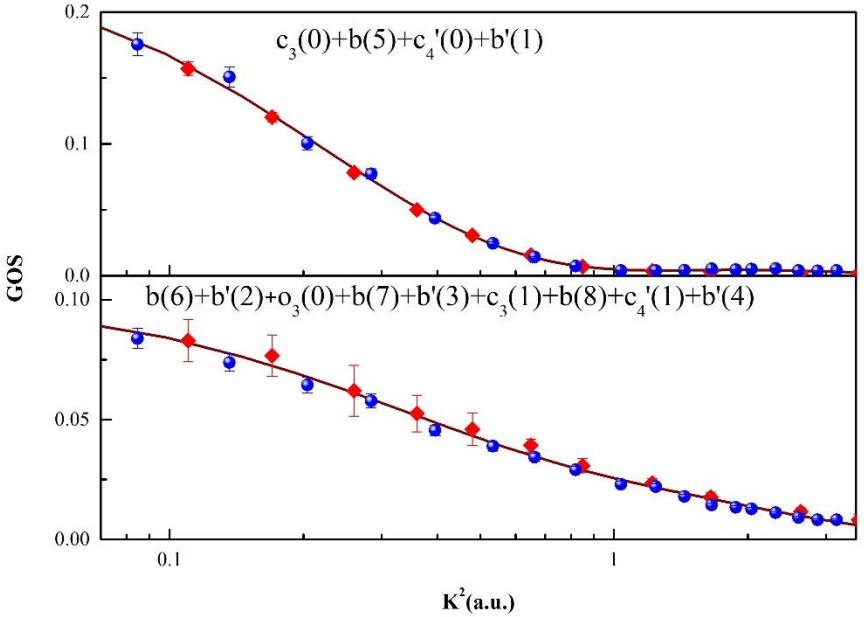

Y.W. Liu *et al.* **J. Geophys. Res. 122** 3459 (2017); Y.G. Peng *et al.* **Phys. Rev. A** 89,032512(2014)

积分截面

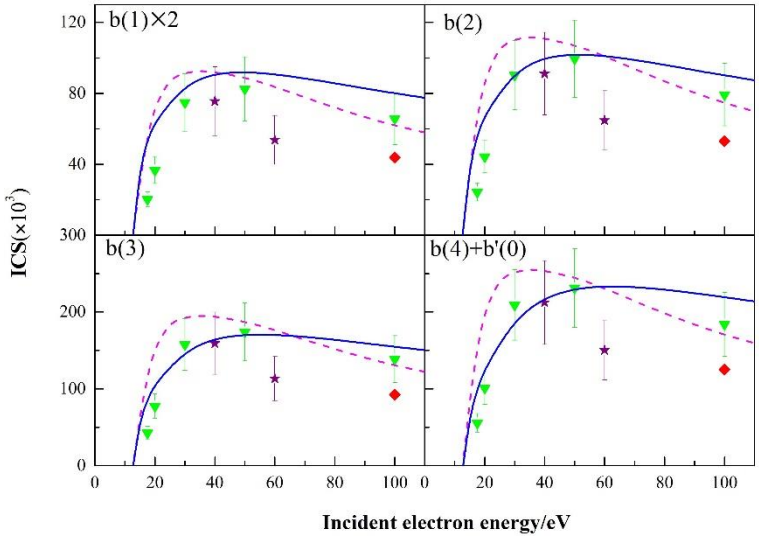

BE-scaling method

H. Tanaka et al., Rev. Mod Phys. 88, 025004(2016)

$$\sigma_{\mathrm{BE}}\left(E_0\right)=\frac{E_0}{E_0+B+E_n}\sigma_{\mathrm{Born}}\left(E_0\right)$$

Born积分截面：

$$\sigma_{\mathrm{Born}}\left(E_0\right)=\frac{\pi}{E_0E_n}\int_{K^2_{\mathrm{min}}}^{K^2_{\mathrm{max}}}\frac{f\left(K,E_n\right)}{K^2}\mathrm{d}K^2$$

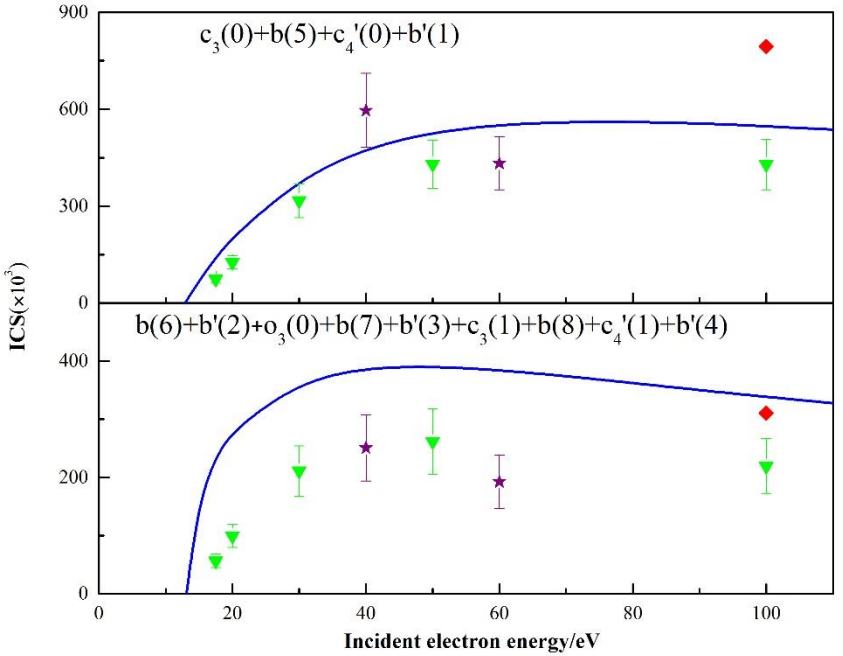

Y.W. Liu *et al.* **J. Geophys. Res. 122** 3459 (2017); Y.G. Peng *et al.* **Phys. Rev. A** 89,032512(2014)

II、其它类似工作：

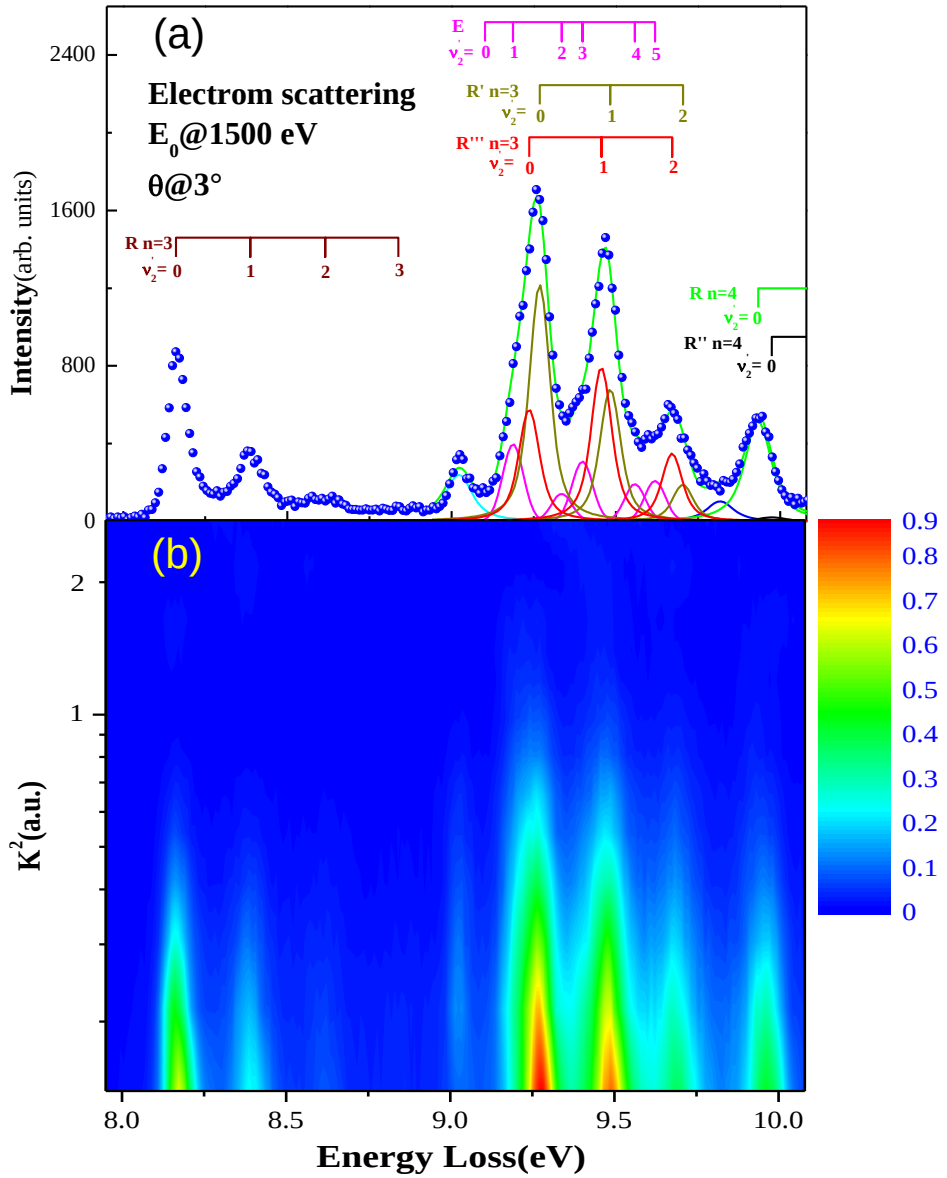

乙炔分子价壳层激发的能量损失谱

Y.W. Liu *et al.* **Astrophys. J. Suppl. 234:10 (2018)**

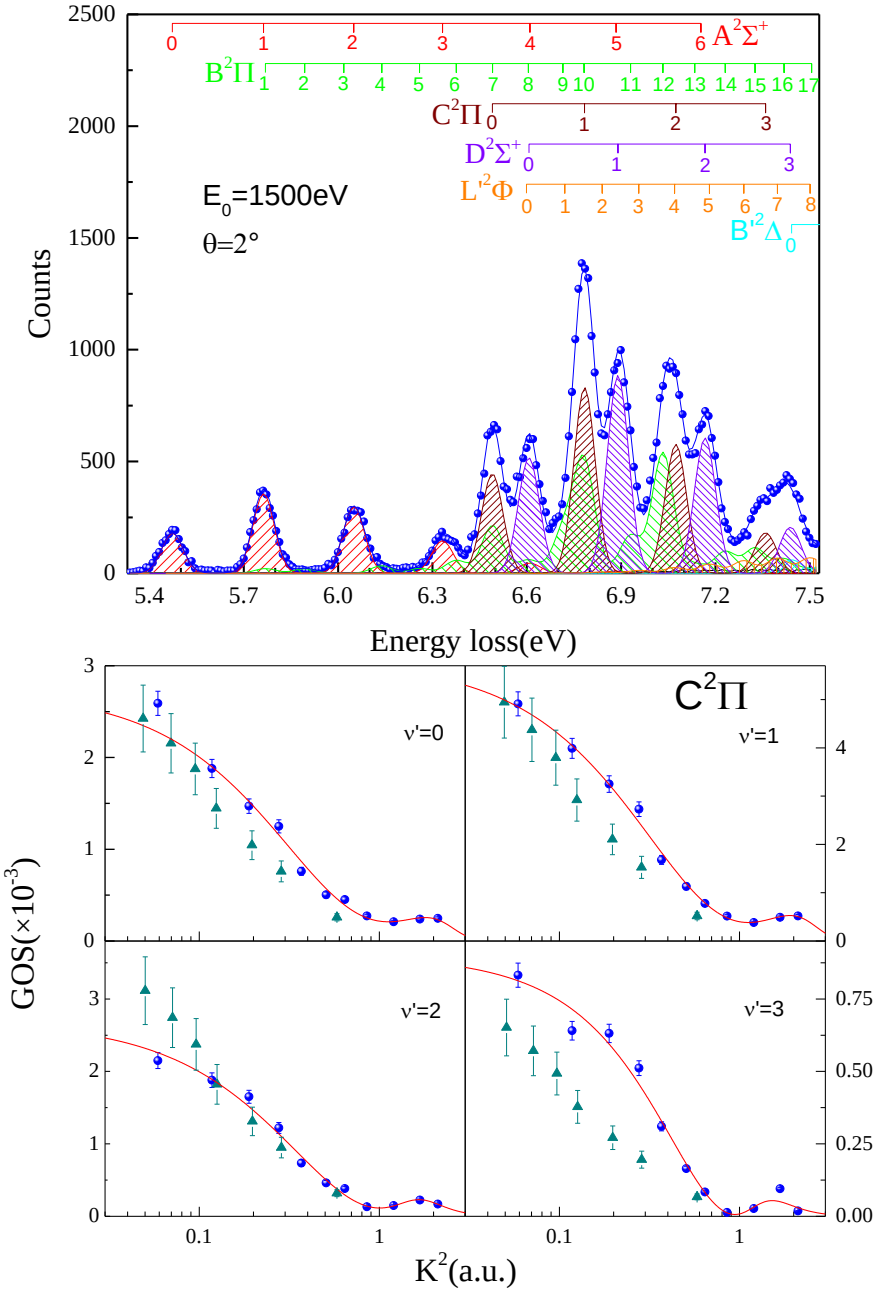

NO分子价壳层激发态的积分截面

X.Xu et al. J. Chem. Phys. 148, 044311 (2018).

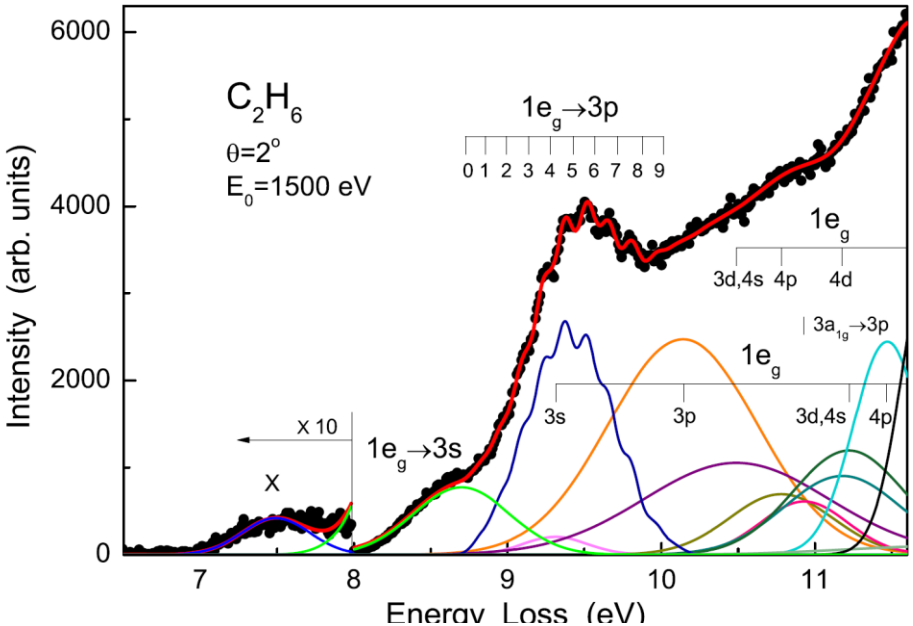

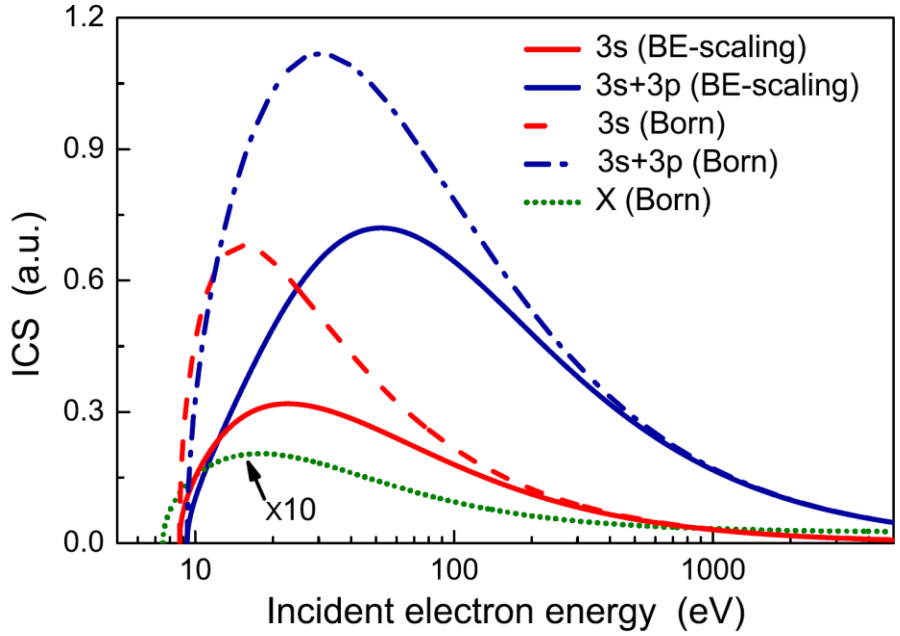

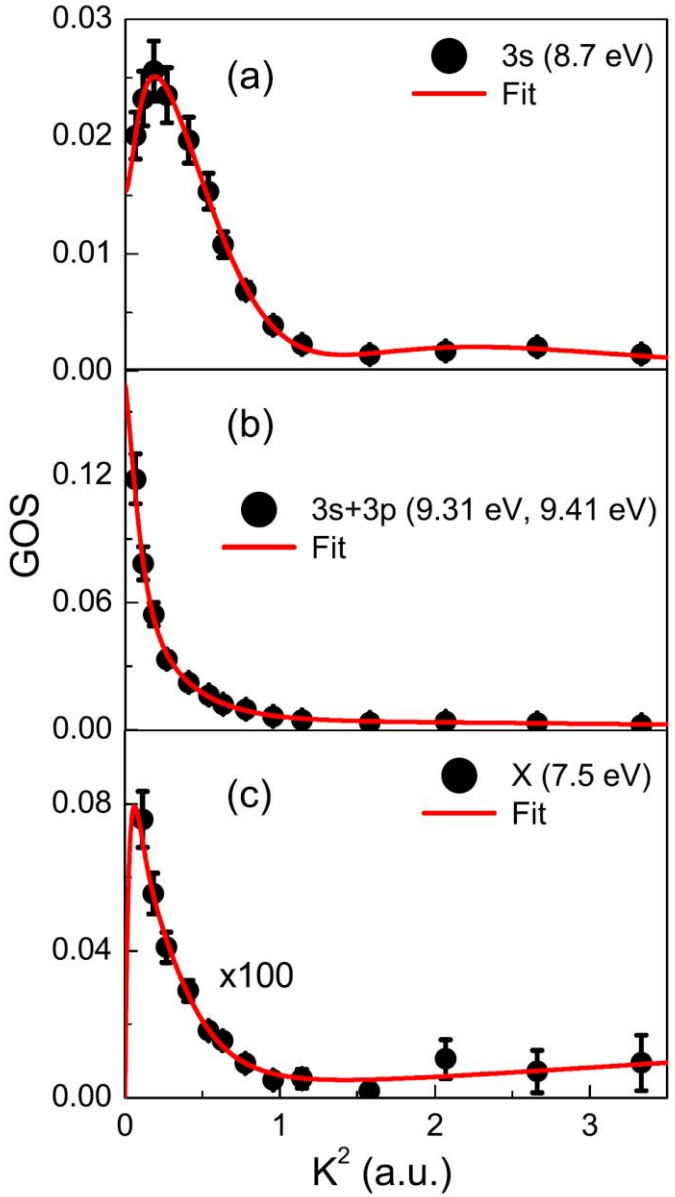

C_2H_6分子价壳层激发态的积分截面

W. Q. Xu et al. J. Chem. Phys. 148, 144313 (2018).

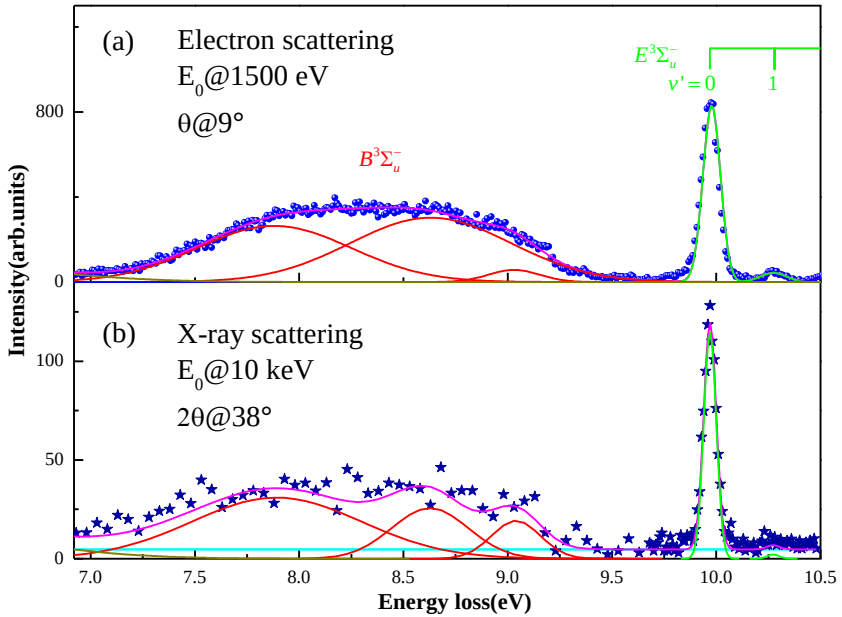

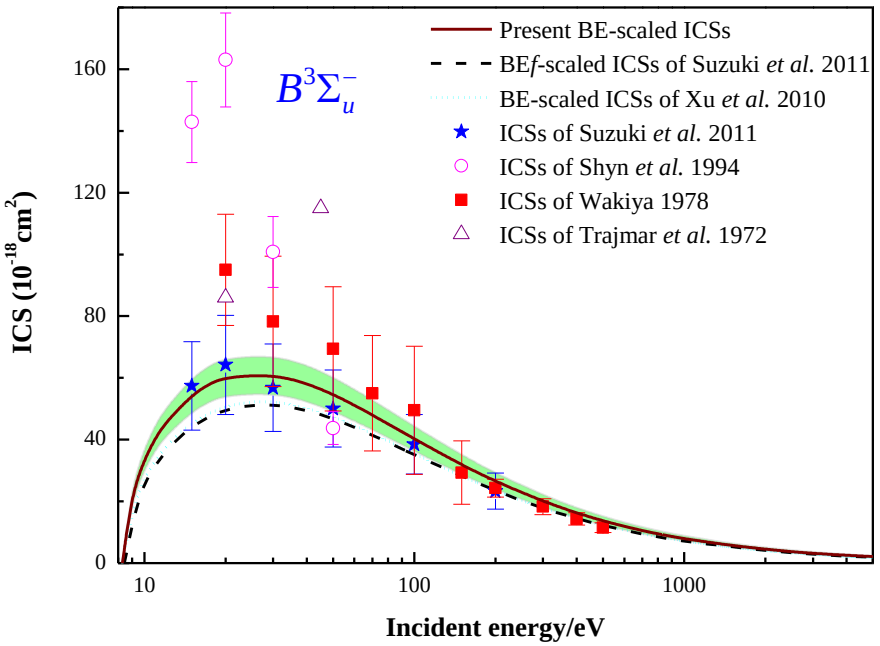

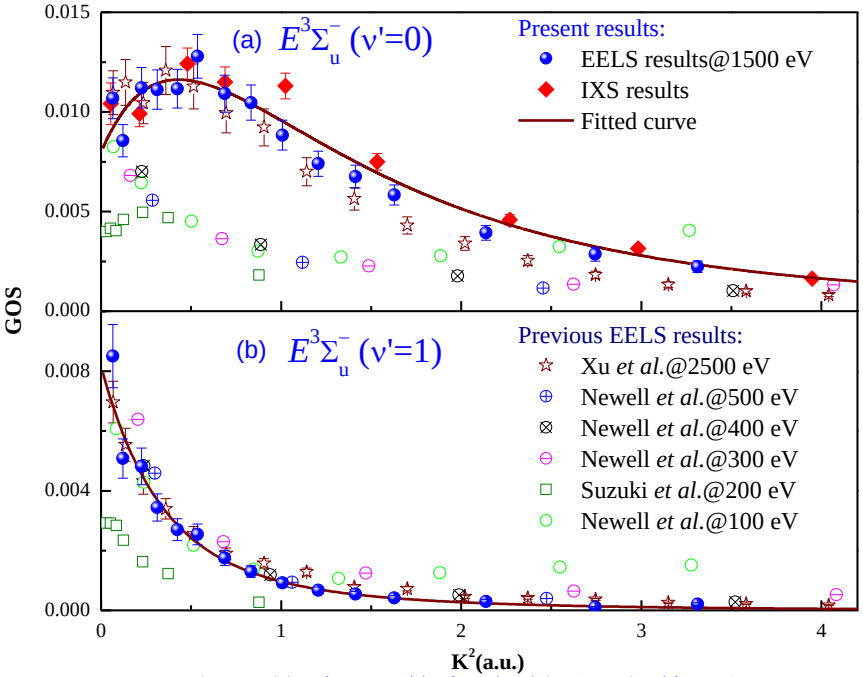

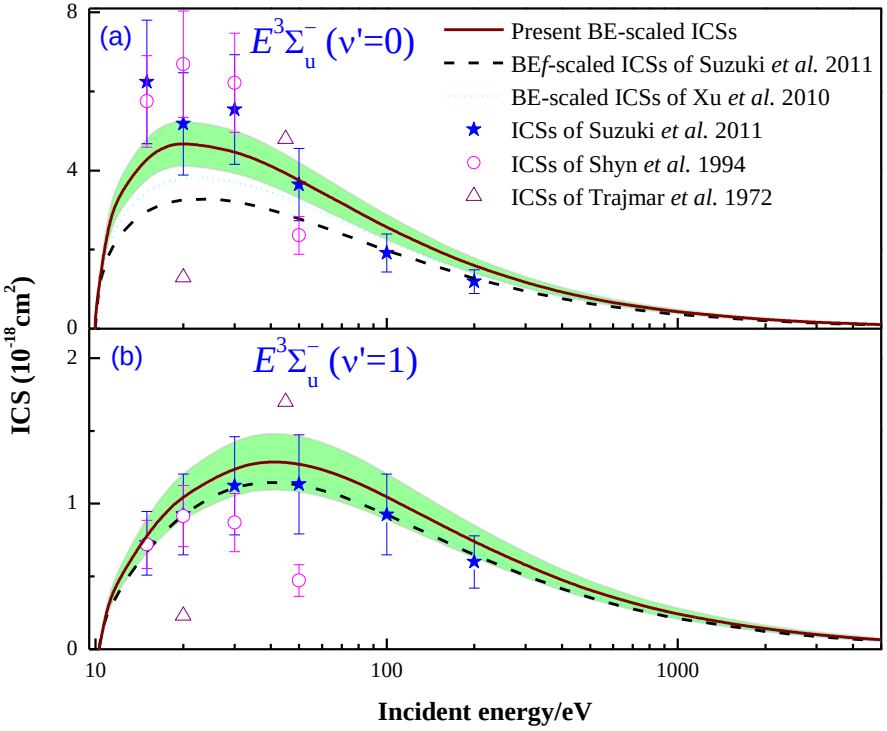

O_2分子价壳层激发态的积分截面

Y. W. Liu et al. Astrophys. J. Suppl. 238:26 (2018)

III、氢及其同位素分子价壳层激发态的动力学参数

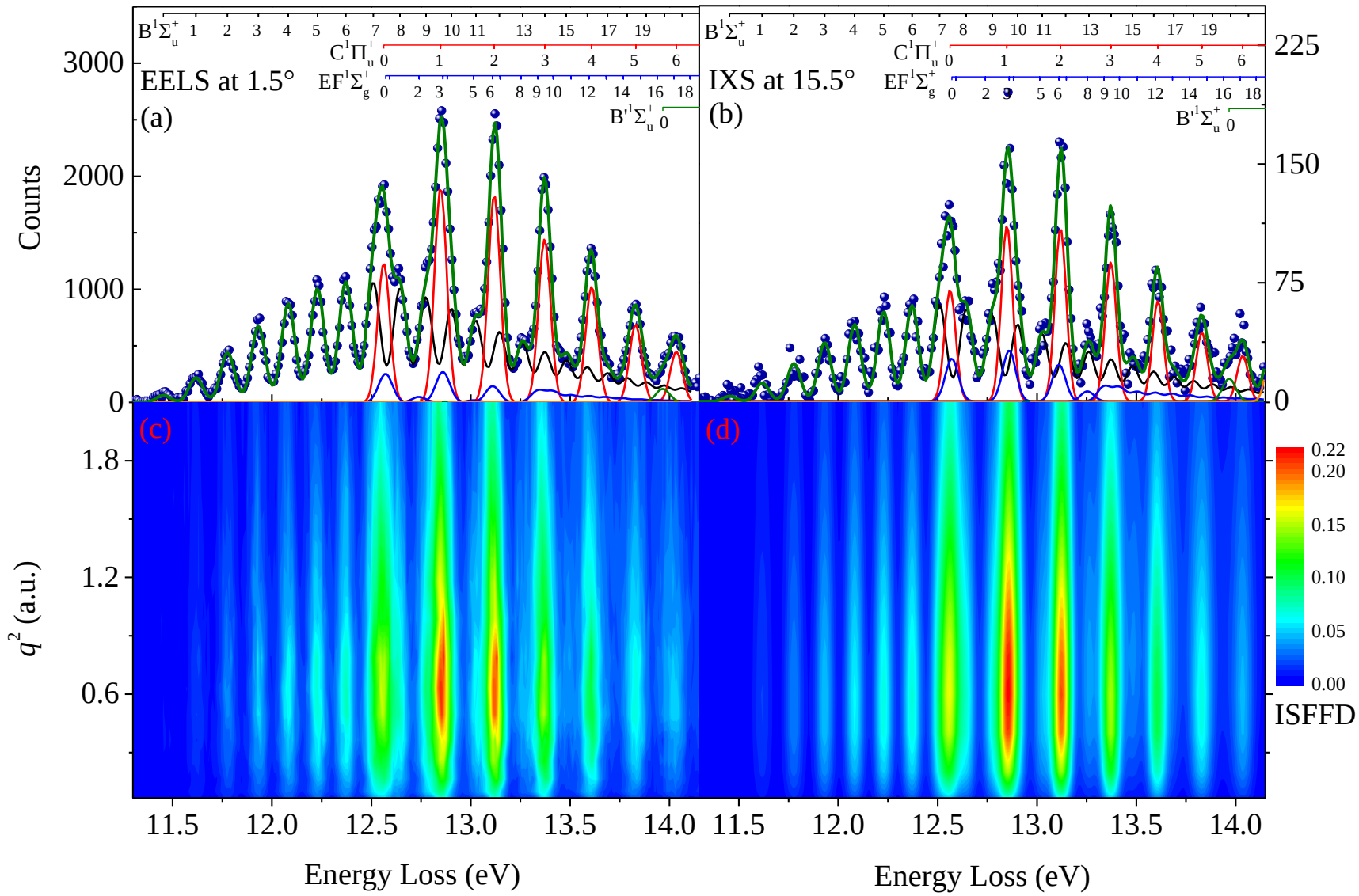

L. Q. Xu et al., **Phys. Rev. A** 97, 032503 (2018)
L. Q. Xu et al., **Phys. Rev. A** 98, 012502（2018）

ISFF density of H_2

H_2、HD和D_2的同位素效应

1. NRIXS@BL12XU, SPring-8

- **Energy resolution:70 meV**
- **Photon energy: ~10 keV**
- **Excitation energy region:11-22 eV**

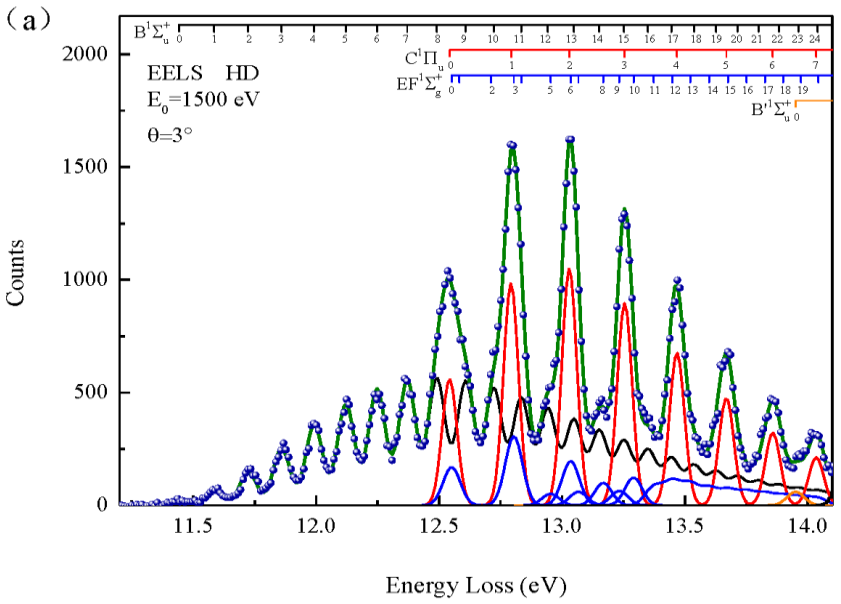

2. EELS@USTC, Hefei

- **Energy resolution: 70 meV**
- **Incident electron energy: 1.5 keV**
- **Excitation energy region: 11-22 eV**

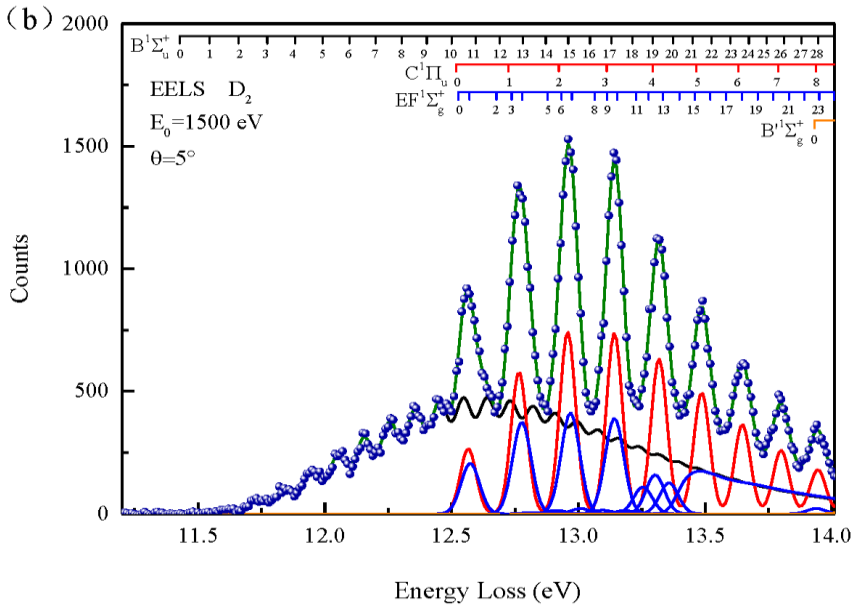

1. L. Q. Xu et al., **Phys. Rev. A** 97, 032503 (2018)
2. L. Q. Xu et al., **Phys. Rev. A** 98, 012502（2018）

H_2、HD和D_2的同位素效应

ISFF： $\zeta(\mathbf{q},\omega_n)=\left|\left\langle \Psi_n \left| \sum_{j=1}^{N} e^{i\vec{q}\cdot\vec{r}_j} \right| \Psi_0 \right\rangle\right|^2$

$2p\sigma_u\ B^1\Sigma_u^+ \leftarrow X^1\Sigma_g^+$

H_2

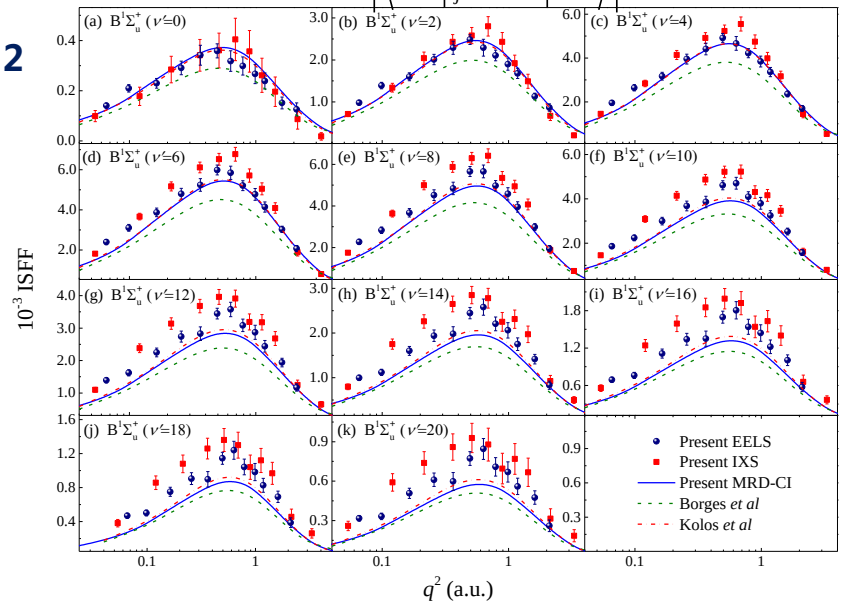

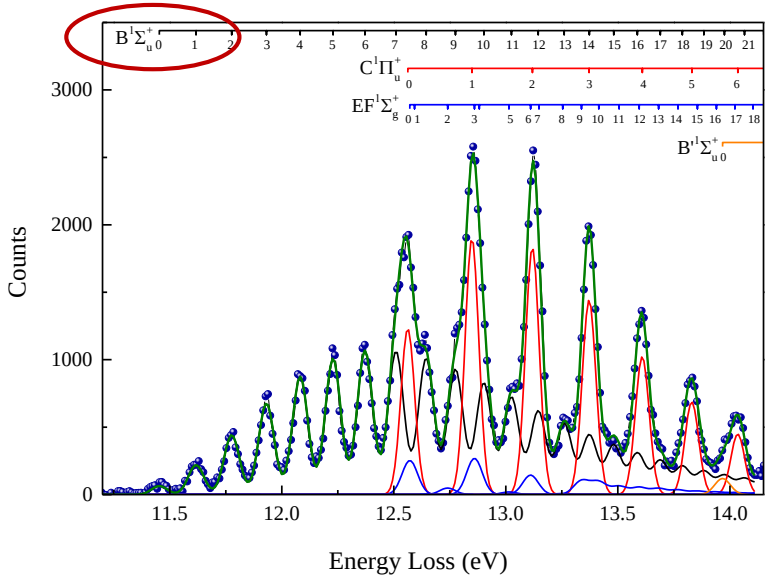

HD

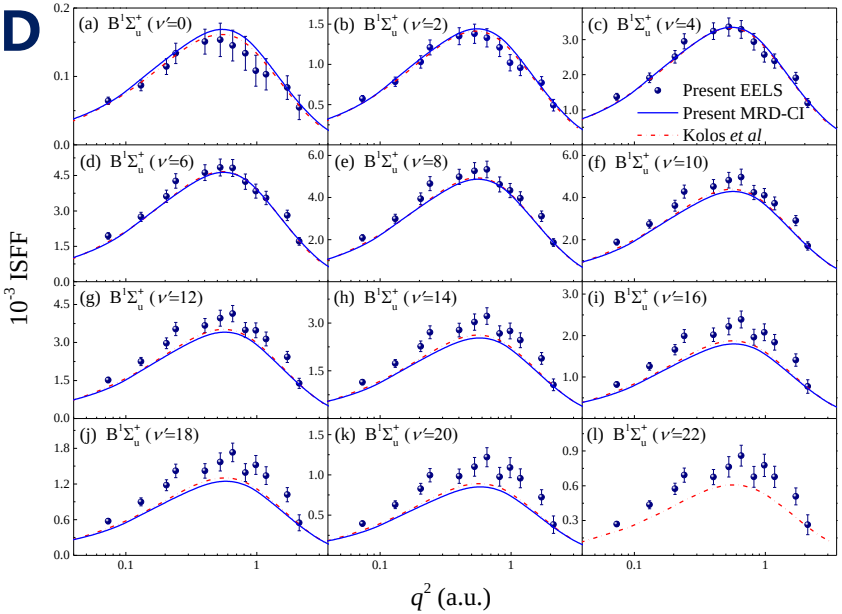

D_2

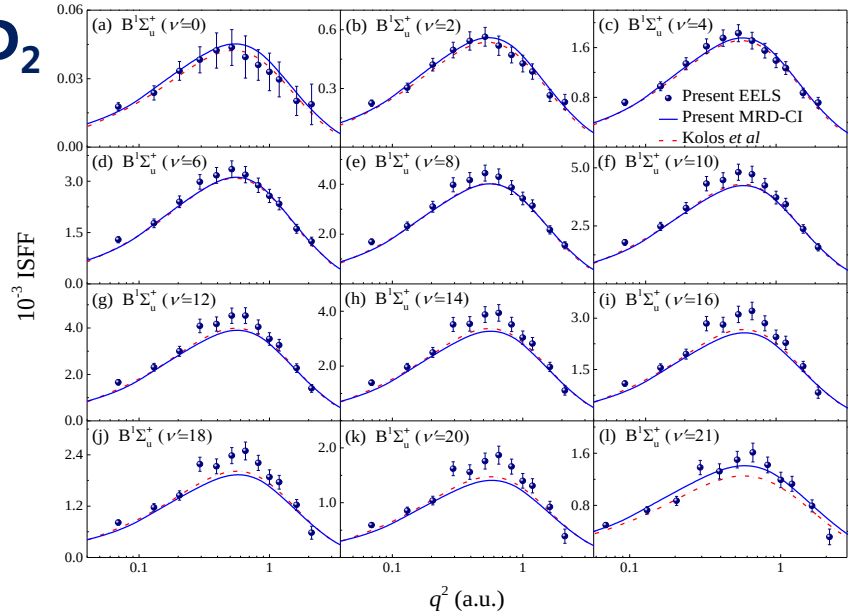

H_2、HD和D_2的同位素效应

H_2

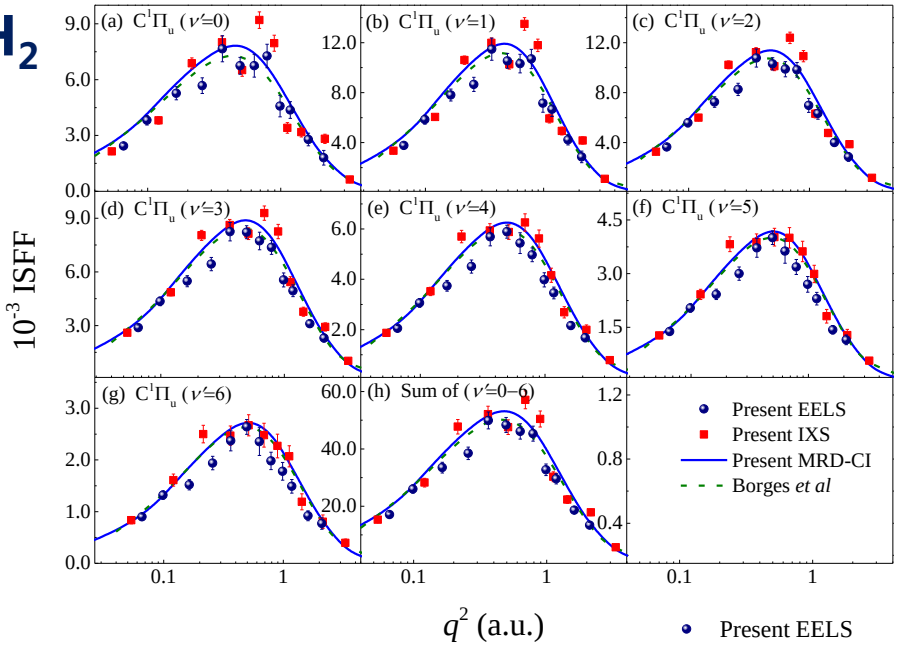

$2p\pi_u\ C^1\Pi_u \leftarrow X^1\Sigma_g^+$

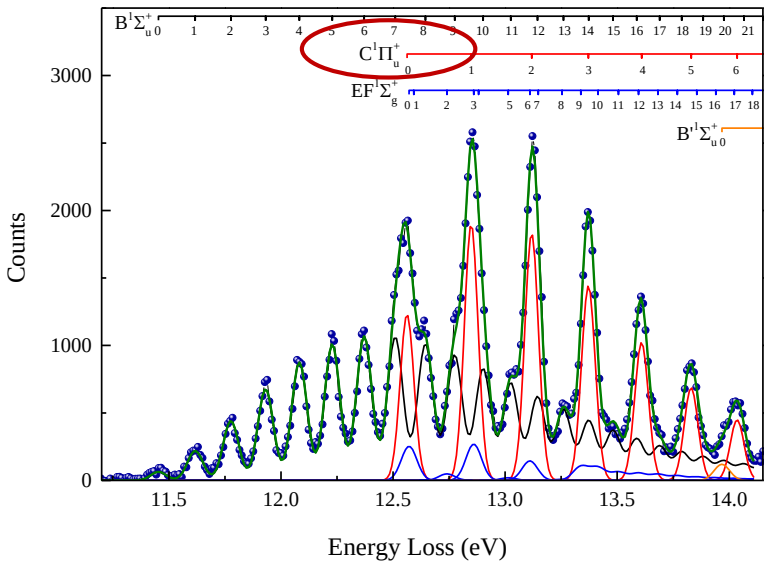

HD

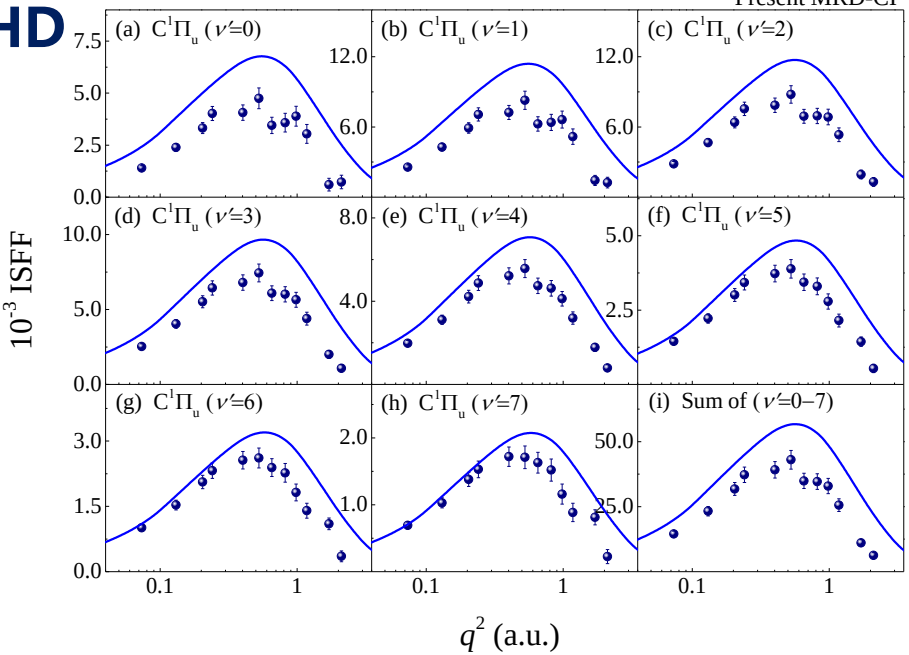

D_2

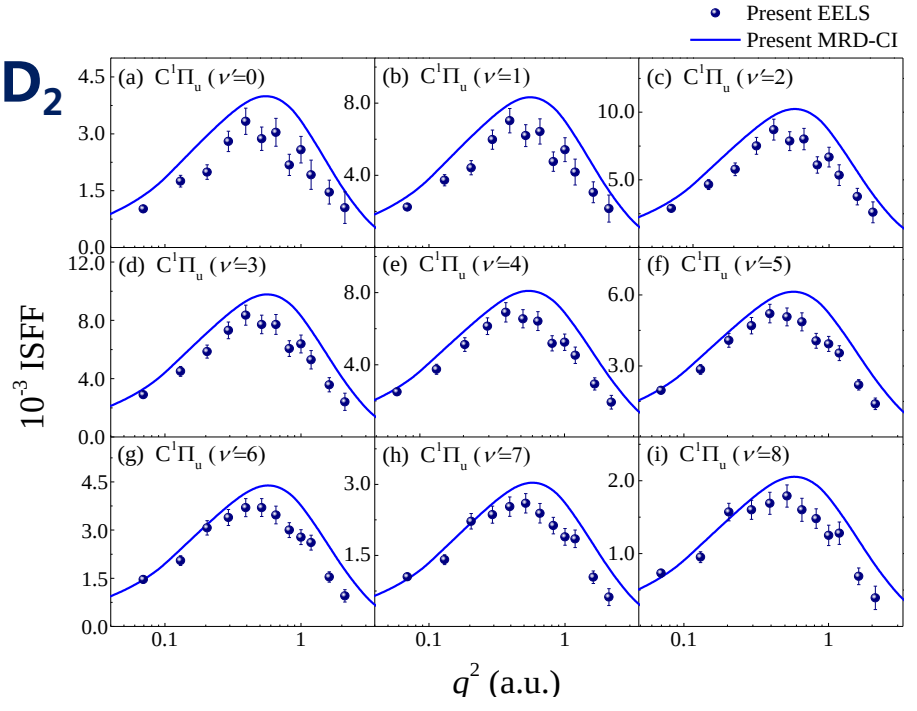

H_2、HD和D_2的同位素效应

$2s\sigma_g\ EF^1\Sigma_g^+ \leftarrow X^1\Sigma_g^+$

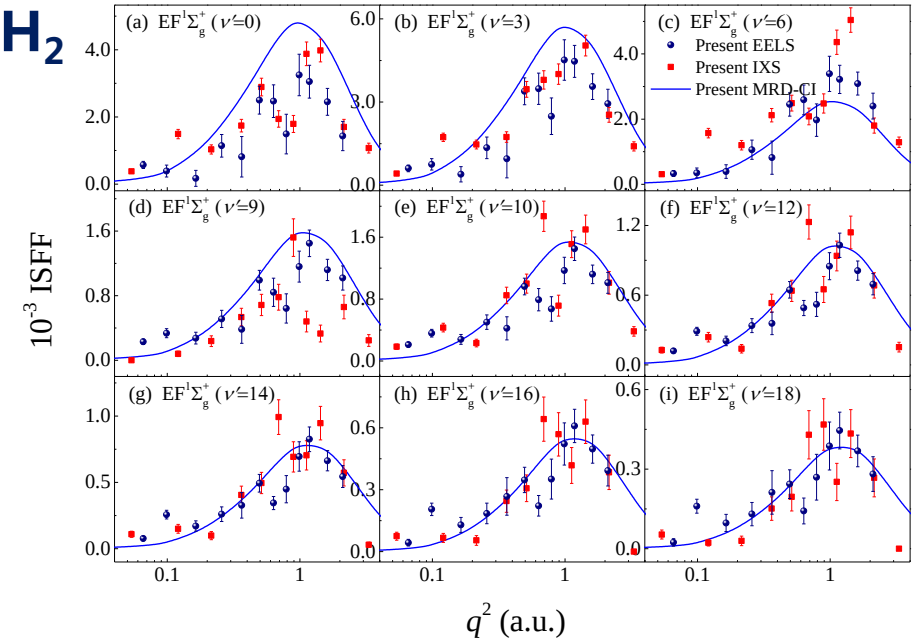

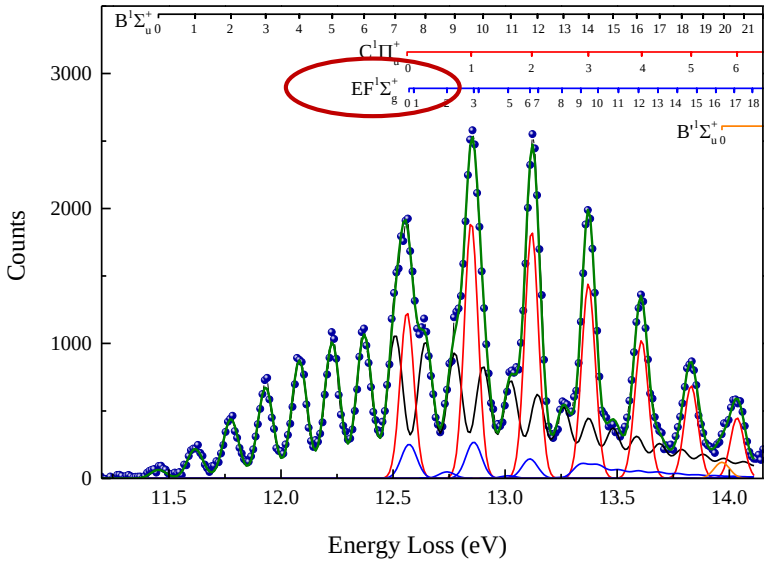

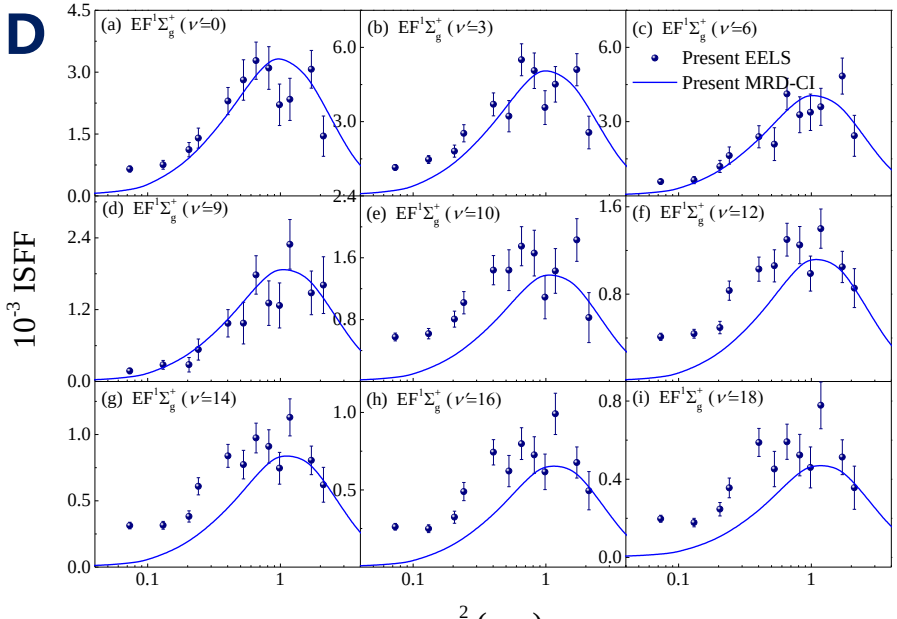

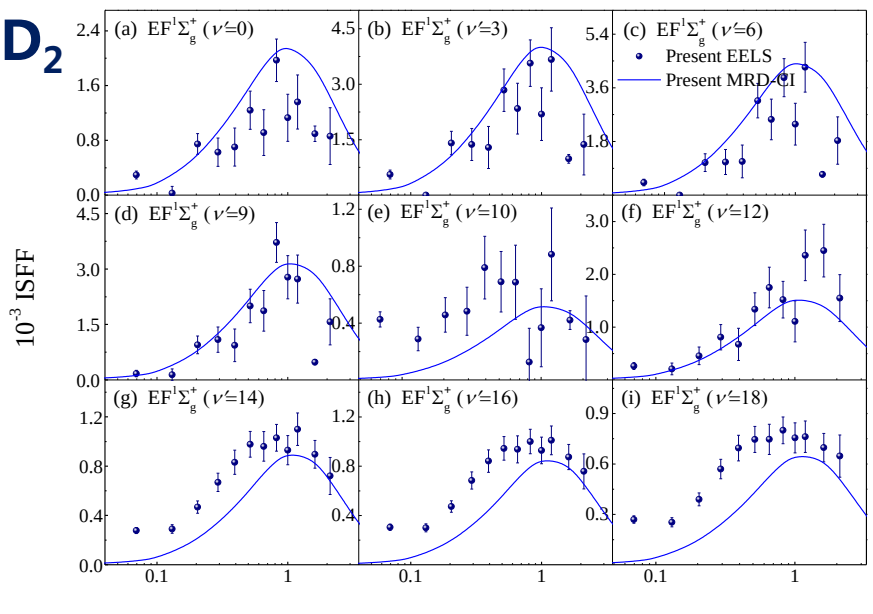

H_2、HD和D_2的同位素效应

ISFF：

$$\zeta(\mathbf{q},\omega_n)=\left|\left\langle \Psi_n \left| \sum_{j=1}^{N} e^{i\vec{q}\cdot\vec{r}_j} \right| \Psi_0 \right\rangle\right|^2$$

$C^1\Pi_u + EF^1\Sigma_g^+$

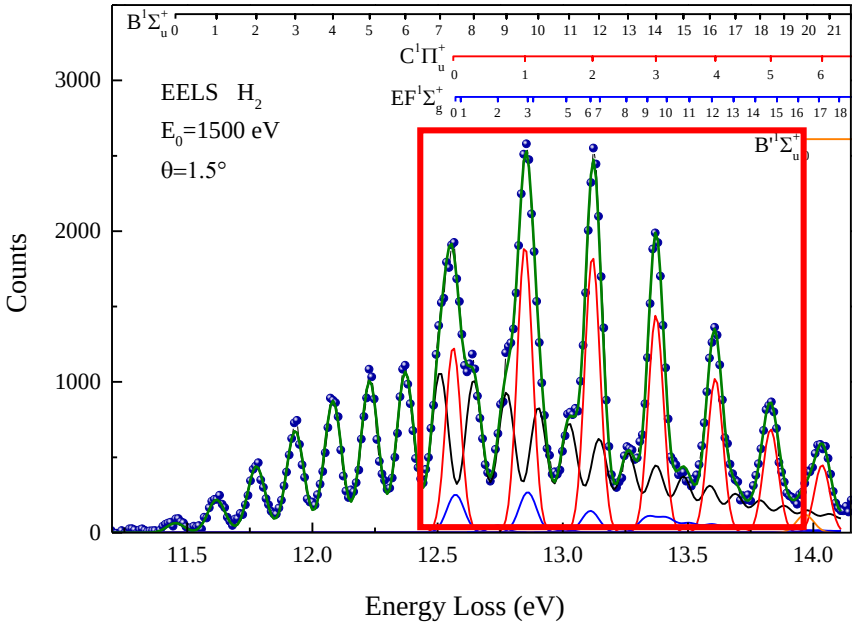

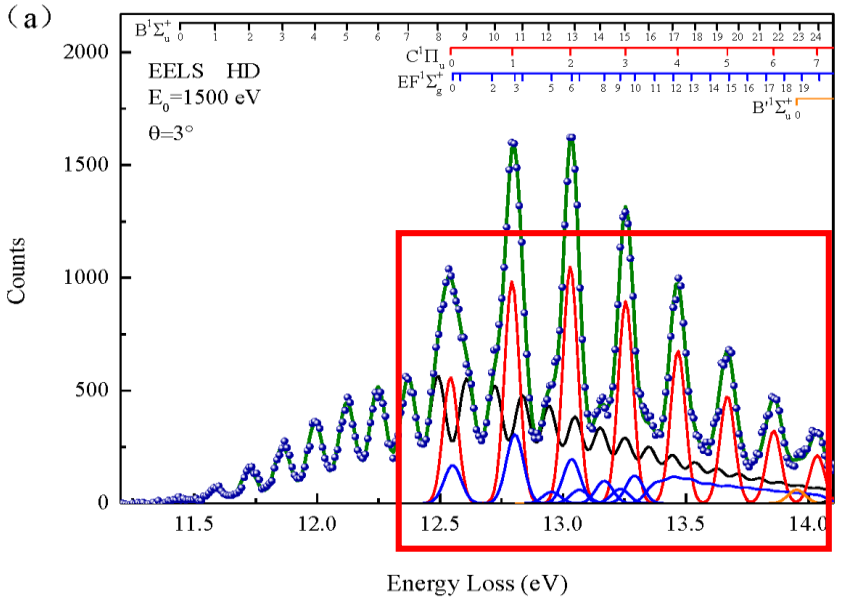

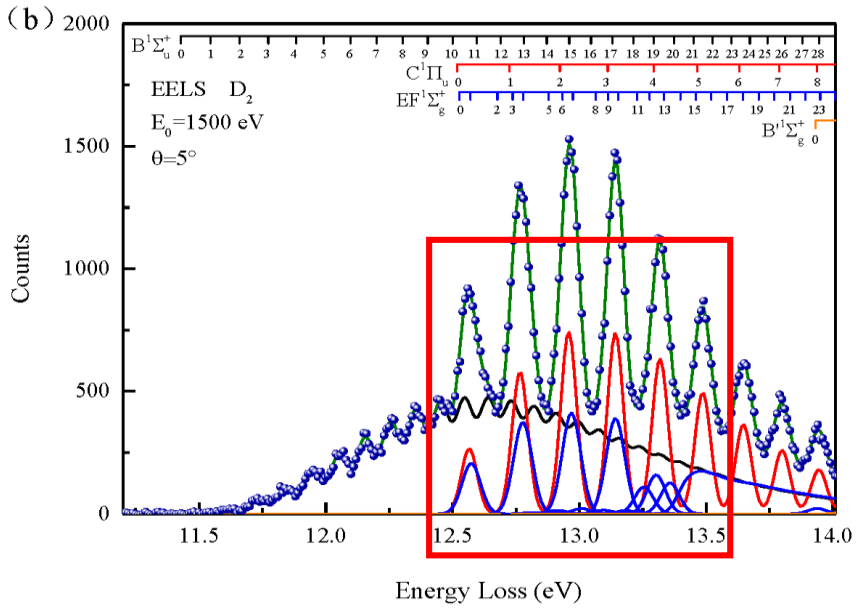

1. L. Q. Xu et al., **Phys. Rev. A** 97, 032503 (2018)
2. L. Q. Xu et al., **Phys. Rev. A** 98, 012502（2018）

H_2、HD和D_2的同位素效应

H_2

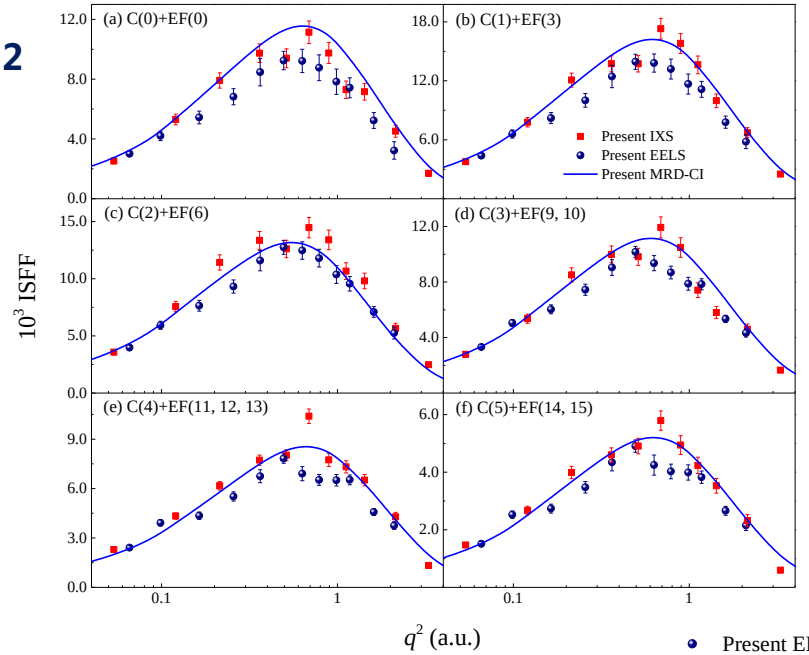

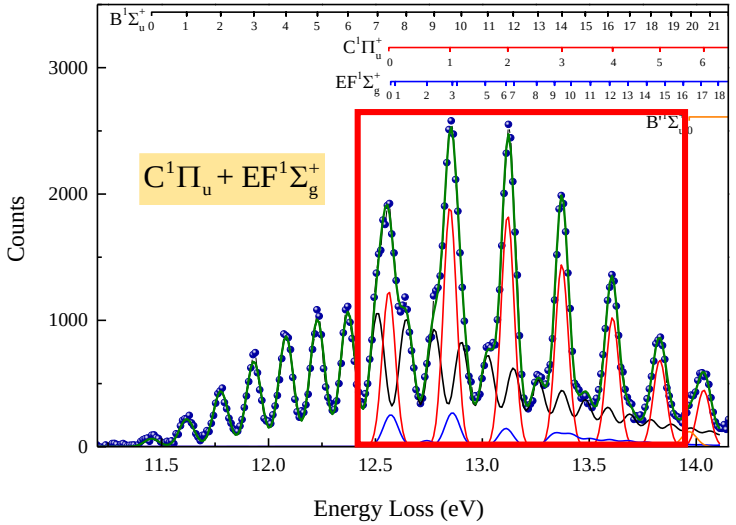

HD

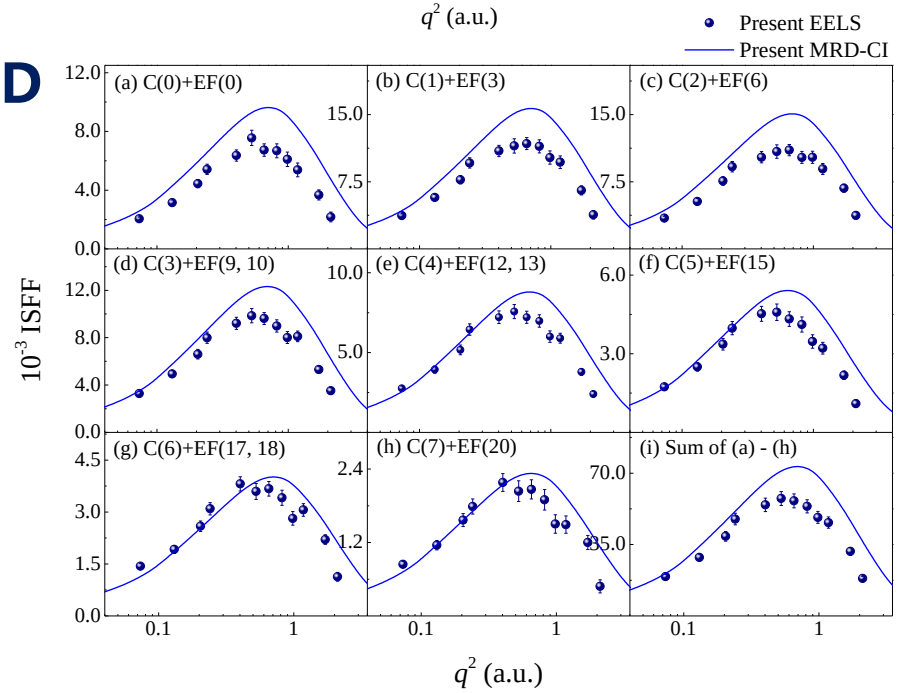

D_2

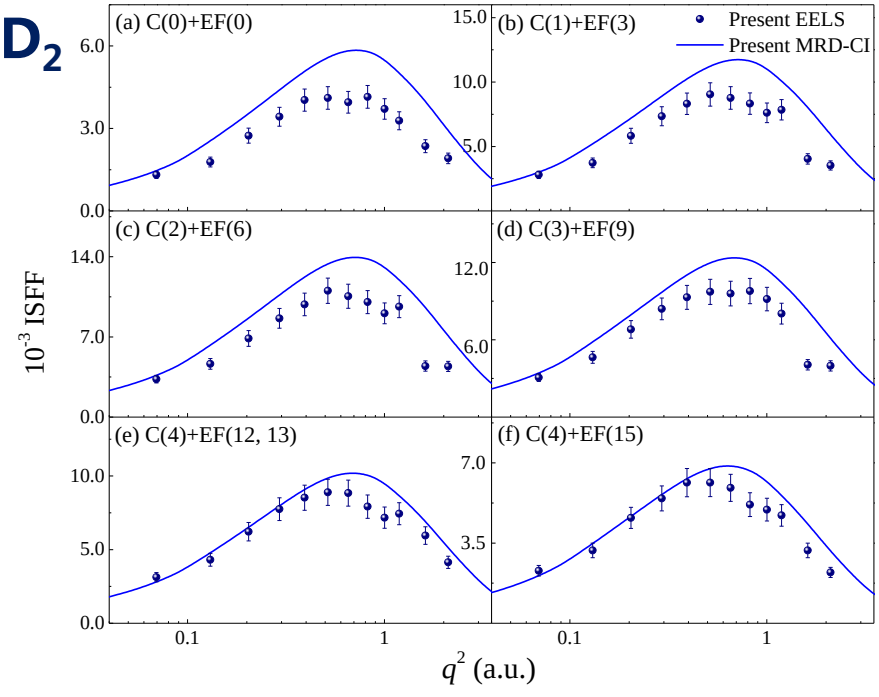

三、 Dipole (γ,γ)方法及光吸收截面测量

形状因子平方：

$$\zeta(\vec{q},\omega_n)=\left|\left\langle \Psi_n \left| \sum_{j=1}^{N} \exp(i\vec{q}\cdot\vec{r}_j) \right| \Psi_0 \right\rangle\right|^2$$

$$\lim_{q^2\to 0}\zeta(\mathbf{q},\omega_n)=\left|\left\langle \Psi_n \left| z \right| \Psi_0 \right\rangle\right|^2$$

L. Q. Xu et al, Eup. Phys. J. D 71, 183(2017)

二、 Dipole (γ,γ)方法及光吸收截面测量

小角度X射线散射模拟光吸收过程

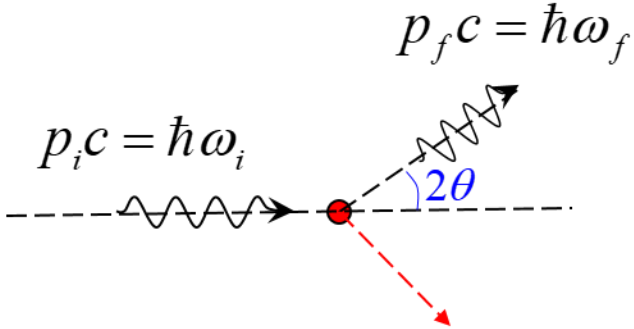

对于原子体系，在小动量转移处：

$$\langle\Psi_n|\sum_{j=1}^{N}\exp(iq\cdot z_j)|\Psi_0\rangle = \langle\Psi_n|\sum_{j=1}^{N}(1+qz_j+\frac{(qz_j)^2}{2!}+\frac{(qz_j)^3}{3!}+.....)|\Psi_0\rangle$$

考虑到初末态函数的正交性，上式右边第一项为零。

忽略高阶项后有：

$$\lim_{q\to 0}|\langle\Psi_n|\sum_{j=1}^{N}\exp(iq\cdot z_j)|\Psi_0\rangle| = q\cdot M_n$$

其中 $M_n = |\langle\Psi_n|\sum_{j=1}^{N} z_j|\Psi_0\rangle|$ 是电偶极跃迁矩阵元

Dipole (γ, γ) 方法

Measurement of OOSs of He

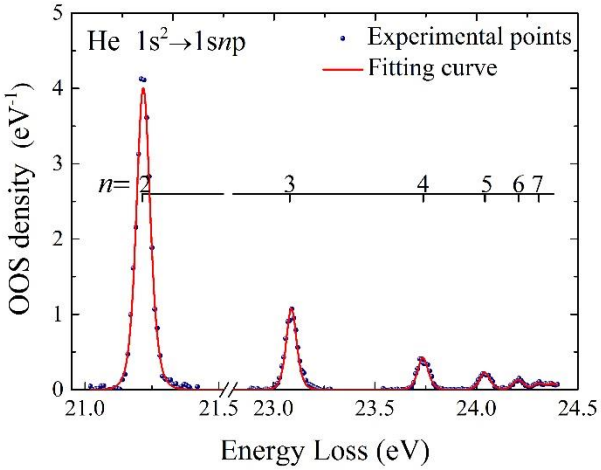

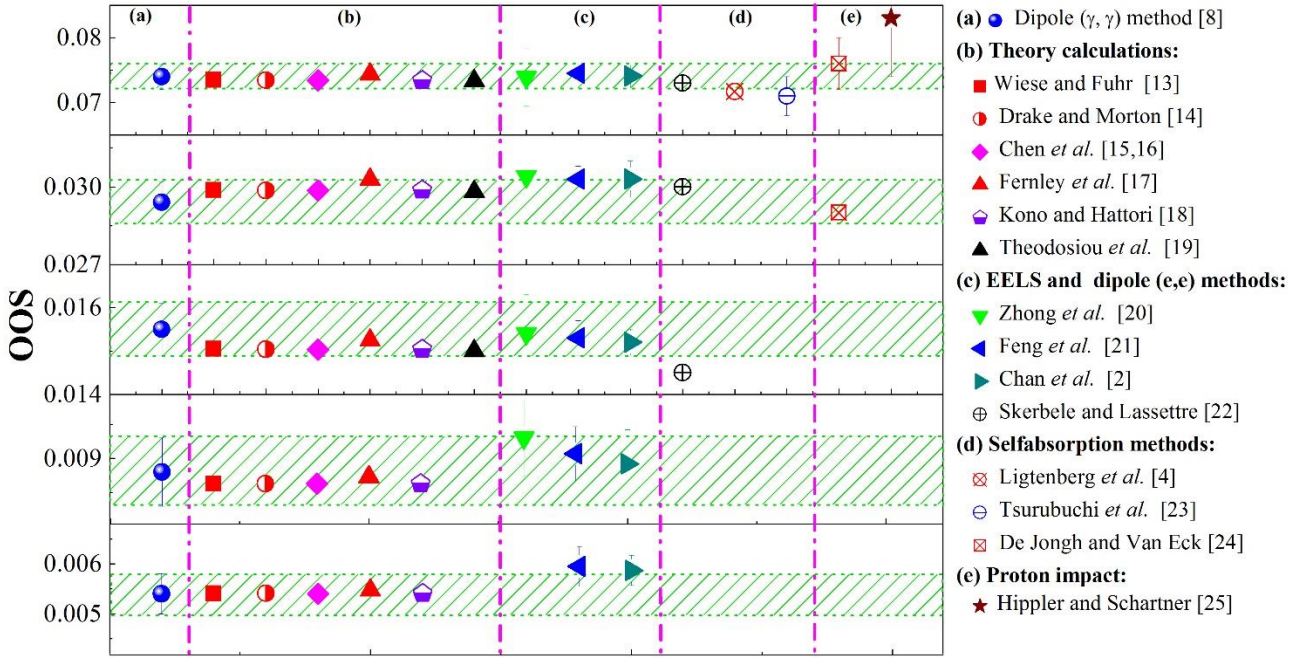

L.Q. Xu, Y.W. Liu *et al*, *Sci. Rep.* 5 18350(2015);

Measurement of OOSs of N_2

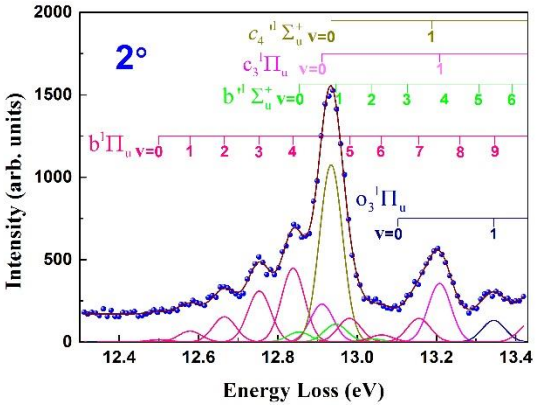

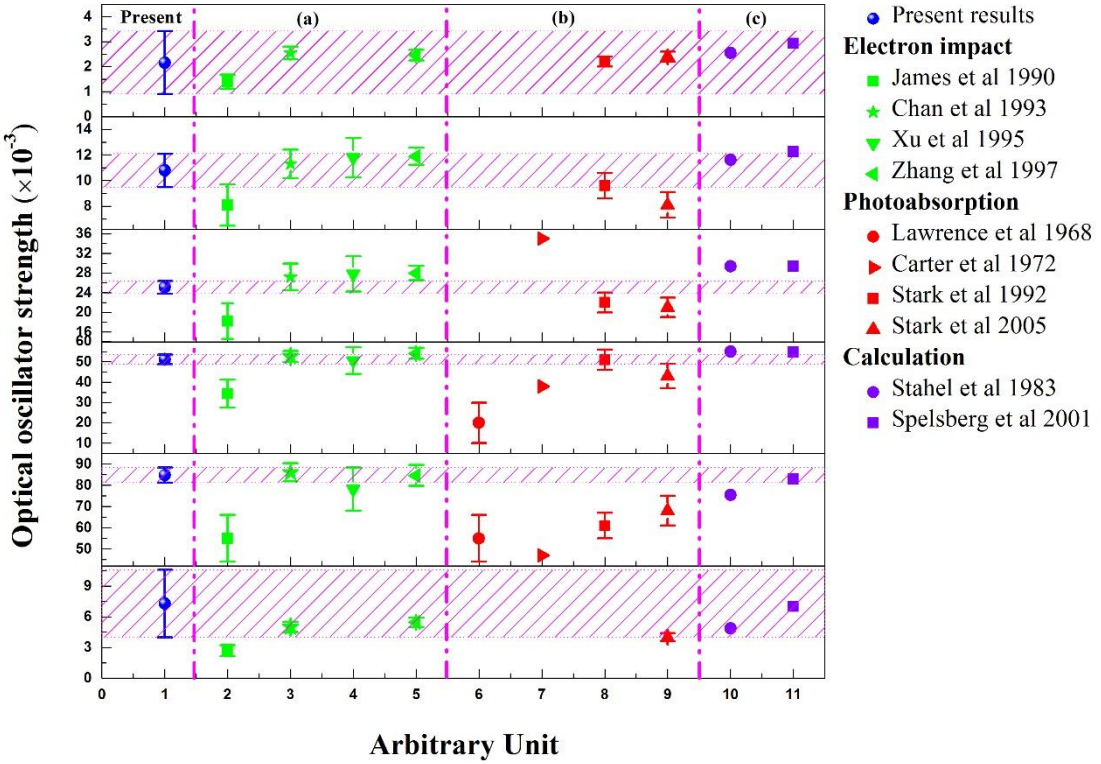

The OOSs of b(0 – 4, 6)from up to down

Y.W. Liu, X. Kang *et al*, *Astrophys. J.* 819:142(2016)

Measurement of OOSs of CO

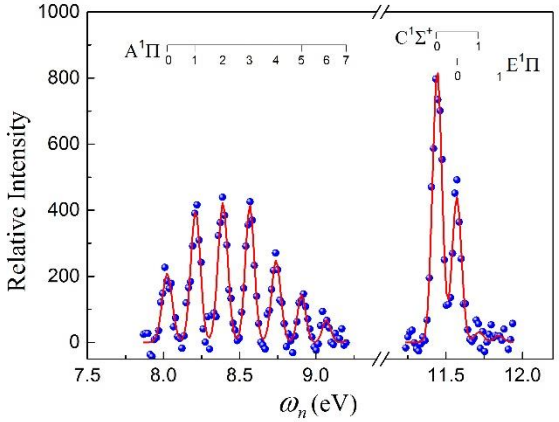

X-ray scattering Spectrum of CO

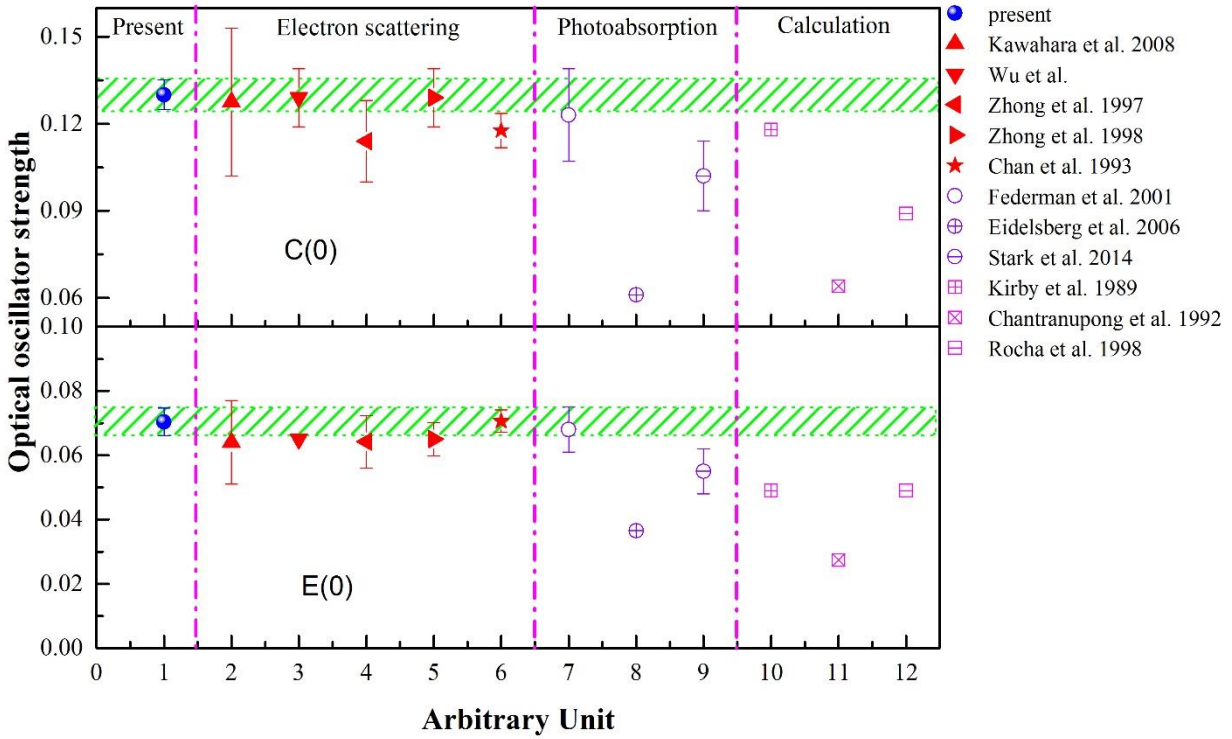

The OOSs of C(0)–X(0) and E(0)–X(0) of CO

X. Kang, Y.W. Liu *et al*, *Astrophys. J.* 807:96 (2015);

urement of OOSs of Ar

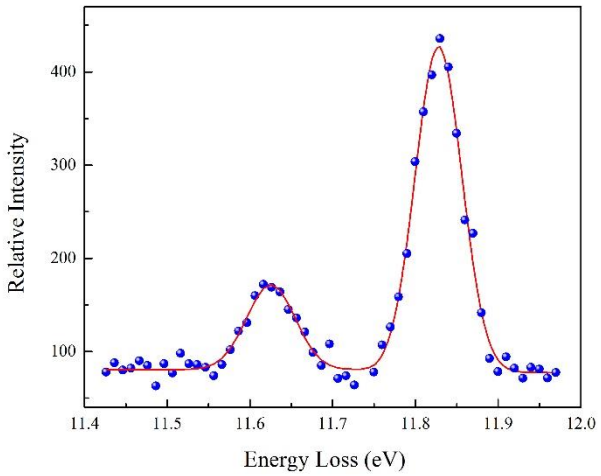

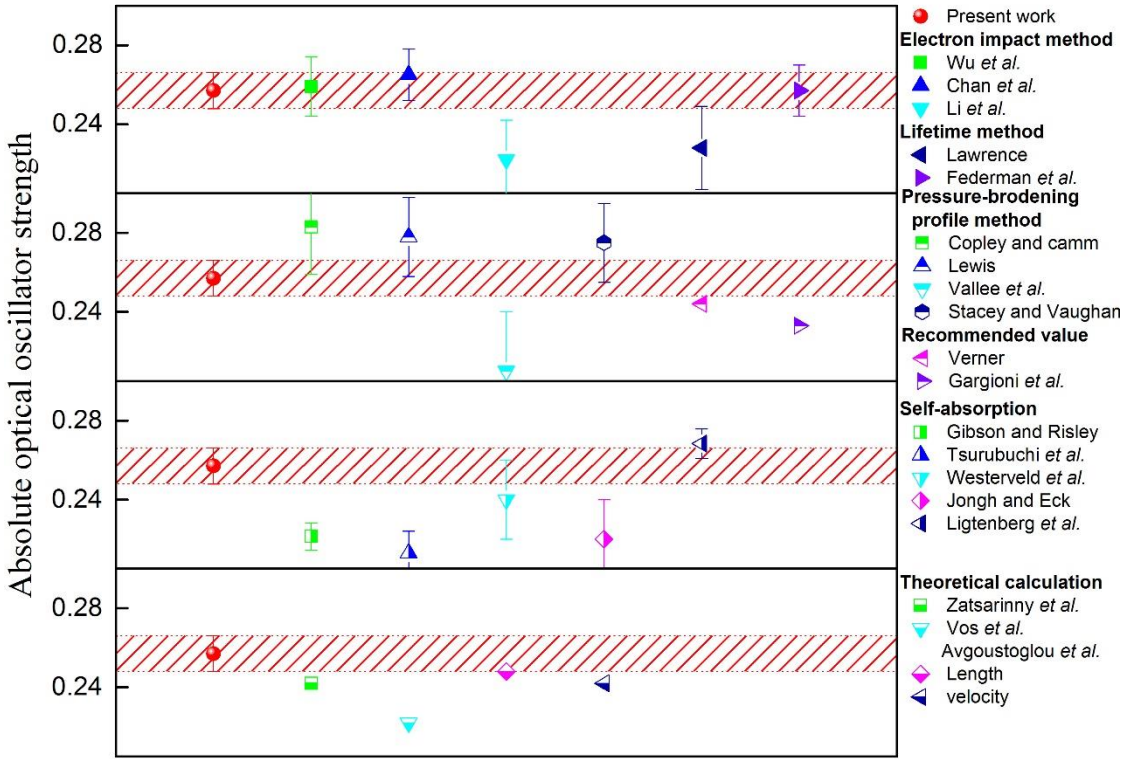

The OOS of $3p^5 4s'[3/2]_1$

X. Xu, D.D. Ni, X. Kang, Y.W. Liu *et al*, J. Phys. B. 49, 064010 (2016)

The comparison of three commonly used methods

	Photoabsorption method	Dipole(e,e) method	Dipole(γ, γ) method
Energy resolution	About 0.1meV	About 70meV	About 70meV
Line-saturation effect	Yes	No	No
B(E)		vary rapidly	vary slowly
Signal-to-noise Ratio	Good	Good	Good
Precision	Poor for strong transition	Moderate	Good

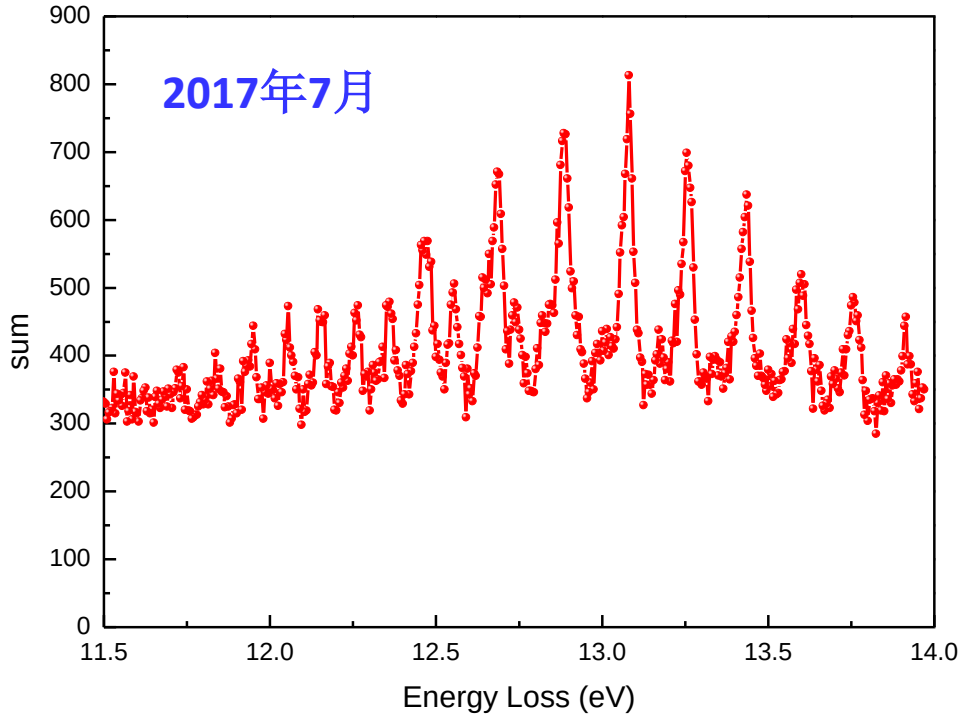

D_2

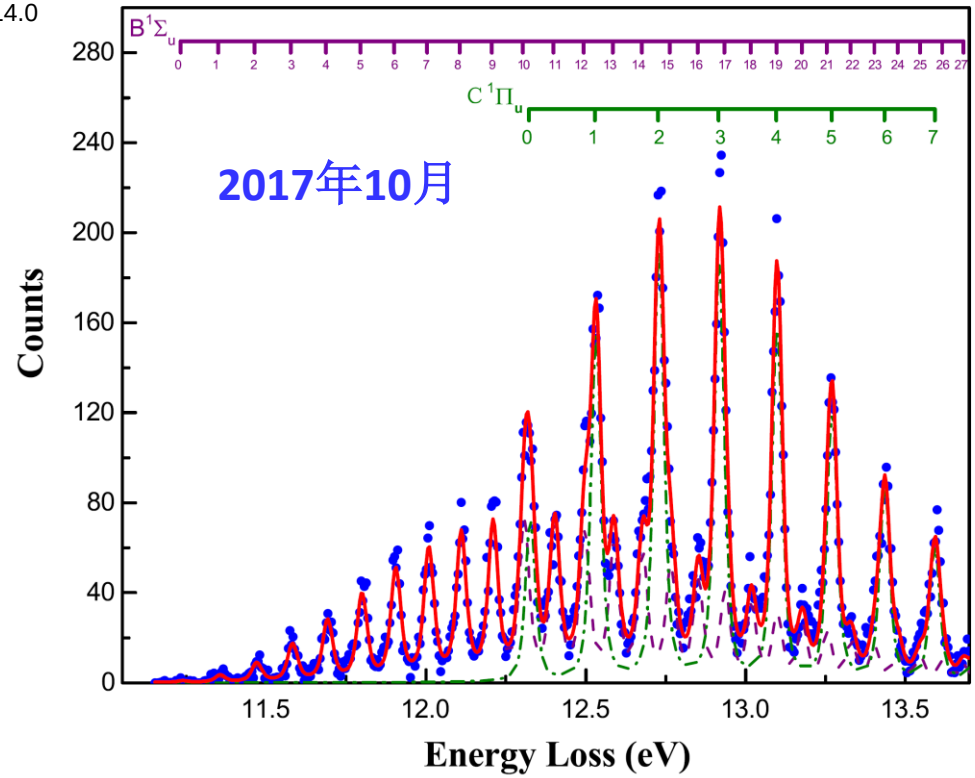

T. Xiong *et al*, Phys. Rev. A 98, 042509(2018)

主要内容

- 背景
- 实验方法
- 现状
- 展望

展望

1. 拓展非弹性γ射线散射技术于原子分子物理动力学三叔研究，提出、实现并命名了测量光吸收截面的dipole（γ，γ）方法

2. 利用高能电子散射和γ射线散射技术，在交叉检验的基础上，获得了一些对天体物理、大气物理非常重要的小分子的动力学参数

3. 非弹性γ射线散射方法在原子分子物理中的应用才刚刚开始，对今后的工作充满期待

谢谢！